DESIGN AND IMPLEMENTATION OF AN ECG FRONT END CIRCUIT

A THESIS SUBMITTED TO
THE GRADUATE SCHOOL OF NATURAL AND APPLIED SCIENCES
OF
MIDDLE EAST TECHNICAL UNIVERSITY

BY

MOHAMMADREZA ROBAEI

IN PARTIAL FULFILLMENT OF THE REQUIREMENTS
FOR
THE DEGREE OF MASTER OF SCIENCE
IN
ELECTRICAL AND ELECTRONICS ENGINEERING

FEBRUARY 2015

Approval of the thesis:

A CONCEPTUAL DESIGN AND EVALUATION OF A MULTICHANNEL ECG DATA ACQUISITION DEVICE

submitted by **MOHAMMADREZA ROBAEI** in partial fulfillment of the requirements for the degree of **Master of Science in Electrical and Electronics Engineering Department, Middle East Technical University** by,

Prof. Dr. Gülbin Dural Ünver ___________
Dean, Graduate School of **Natural and Applied Sciences**

Prof. Dr. Gönül Turhan Sayan ___________
Head of Department, **Electrical and Electronics Engineering**

Assoc. Prof. Dr. Yeşim Serinağaoğlu Doğrusöz ___________
Supervisor, **Electrical and Electronics Engineering Dept., METU**

Examining Committee Members

Prof. Dr. B. Murat Eyüboğlu ___________
Electrical and Electronics Engineering Dept., METU

Assoc. Prof. Dr. Yeşim Serinağaoğlu Doğrusöz ___________
Electrical and Electronics Engineering Dept., METU

Prof. Dr. Nevzat G. Gençer ___________
Electrical and Electronics Engineering Dept., METU

Prof. Dr. Haluk Külah ___________
Electrical and Electronics Engineering Dept., METU

Fikret Küçükdeveci, MSc. ___________
Project Manager, Kardiosis Ltd, METU Teknokent

Date: 02/06/2015

I hereby declare that all information in this document has been obtained and presented in accordance with academic rules and ethical conduct. I also declare that, as required by these rules and conduct, I have fully cited and referenced all material and results that are not original to this work.

Name, Last name	: Mohammadreza Robaei
Signature	:

ABSTRACT

DESIGN AND IMPLEMENTATION OF AN ECG FRONT END CIRCUIT

Robaei, Mohammadreza
M.S., Department of Electrical and Electronics Engineering
Assoc. Prof. Dr. Yeşim Serinağaoğlu Doğrusöz
February 2015, 90 pages

Since the first electrocardiogram (ECG) was recorded by Eindhoven in 1903, examination of the electrical activity of the heart using surface electrodes obtained great clinical significance over the years. According to annual report of World Health Organization in 2013, cardiovascular diseases are counted as one of the four major reasons of 80% of deaths in the world. Therefore, the ability to acquire high quality recordings of electrical activity of the heart from surface of the body would be highly beneficial for diagnosis. For this purpose, invasive and noninvasive methods are used. Standard 12-lead ECG as one of the noninvasive methods is commonly used in the world at hospitals and clinics. In addition, more sophisticated methods are developed to measure the electrical activity of the heart from the surface of the body, using larger numbers of electrodes known as Body Surface Potential Measurement (BSPM). Invasive methods are also used in special cases to make in vivo measurements. In comparison to non-invasive methods, such as conventional 12-lead system and BSPM, invasive methods require surgical operation to implement the proper electrode network in the desired location. Standard 12-lead system is commonly used in clinical applications for diagnosing and monitoring because of its simplicity in use but it suffers from low spatial resolution of the acquired data. In contrast, BSPM as non-invasive technique, acquires data using large number of electrodes attached to the surface of the body. As a result, the acquired data has better spatial resolution than the 12-lead system.

Data obtained from BSPM have significant importance in applications such as localization of the electrical sources in the heart.

In this study, we aim to build an analog front end unit to detect the electrical activity of the heart using 10 electrodes connected to the surface of the body. These ten electrodes are recording measurements from the right arm (RA), left arm (LA), and left leg (LL) electrodes, six chest electrodes (V1~V6), and one RLD electrode. Unipolar measurements are used for chest channels (V1~V6). Also, lead I and lead II are constructed via bipolar measurements between (LA, RA) and (LL, RA) pairs, respectively.

The analog front end proposed in this thesis is designed to be compatible with 24-bit Sigma Delta analog to digital converter (ADC), so we kept the channels as simple as possible to use the features recommended by the ADC. This unit can be used as the front end of any ECG recording device; it can be the first stage for a 12-lead ECG system, as well as for a BSPM system. Depending on the application requirements, either bipolar or unipolar measurements can be recorded.

Keywords: Electrocardiography (ECG), Body surface potential mapping, ECG front end, Right leg drive, Analog-to-digital conversion.

ÖZ

EKG FRONT END DEVRE TASARIMI VE GERÇEKLEMESİ

Robaei, Mohammadreza
Yüksek Lisans, Elektrik ve Elektronik Mühendisliği Bölümü
Tez Yöneticisi: Assoc. Prof. Dr. Yeşim Serinağaoğlu Doğrusöz
Şubat 2015, 90 sayfa

İlk elektrokardiyografi (EKG) 1903 yılında Eindhoven tarafından kaydedildiğinden beri, yüzey elektrotları kullanılarak kalbin elektriksel aktivitesinin incelenmesi büyük klinik önem kazanmıştır. Dünya Sağlık Örgütünün 2013'te yayınlanan yıllık raporuna göre, kardiyovasküler hastalıklar dünyadaki ölümlerin %80'inin dört ana nedenlerinden biri olarak sayılmıştır. Bu nedenle, kalbin elektriksel aktivitesini vücut yüzeyinden yüksek kalite ile ölçebilmek bu hastalıkların teşhisinde son derece yararlı olacaktır. Bu amaç için, invazif ve noninvazif yöntemler kullanılmaktadır. Standart 12-kanallı EKG bir noninvazif yöntem olarak genellikle hastanelerde ve kliniklerde kullanılmaktadır. Buna ek olarak, Vücut Yüzeyi Potansiyel Ölçümleri (VYPÖ) olarak bilinen, kalbin elektriksel aktivitesini vücut yüzeyinden çok sayıda elektrot kullanarak ölçebilen yöntemler geliştirilmiştir. Invazif yöntemler de in-vivo ölçümler yapmak için özel durumlarda kullanılmaktadır. Standart 12-kanallı ve VYPÖ gibi noninvazif yöntemlere kıyasla, invazif yöntemlerde elektrotları istenilen uygun yere sabitlemek için cerrahi operasyon gereklidir. Standart 12-kanallı sistem kullanım sadeliği nedeni ile yaygın olarak teşhis ve izleme için klinik uygulamalarda kullanılmaktadır, ancak elde edilen veriler düşük uzaysal çözünürlüğe sahiptir. Bunun aksine, VYPÖ noninvazif bir yöntem olarak, çok sayıda elektrot kullanarak vücut yüzeyinden veri almaktadır. Sonuç olarak, elde edilen veriler 12-kanallı sistemden daha iyi uzaysal çözünürlüğe sahiptir.

VYPÖ’den elde edilen veriler, kalpteki elektriksel kaynakların lokalizasyonu gibi uygulamalar için çok önem taşımaktadır.

Bu çalışmada, vücudun yüzeyine bağlı 10 elektrot kullanılarak kalbin elektriksel aktivitesini tespit etmek için bir analog front end birimi tasarladık. Bu on elektrot, sağ kol (RA), sol kol (LA), sol bacak (LL) elektrotları, altı göğüs elektrodu (V1 - V6) ve RLD’den oluşmaktadır. Göğüs elektrotları kullanılarak unipolar ölçümler yapılmaktadır. Ayrıca, Lead I ve Lead II bipolar kanalları sırasıyla (LA RA) ve (LL, RA) çiftleri arasında ölçülmektedir.

Bu tezde önerilen analog front end 24-bit Sigma Delta analog - dijital dönüştürücü ile uyumlu olacak şekilde tasarlanmıştır. Bu yüzden devre ADC’nin önerdiği özellikleri kullanmak için mümkün olduğunca basit tasarlanmıştır. Bu ünite, herhangi bir EKG kayıt cihazı için analog front end olarak kullanılabilir; bir 12-kanallı ECG sistemi ilk birim olabilceği gibi bir BSPM sistemi için de kullanılabilir. Uygulama gereklerine göre, bipolar veya unipolar ölçümler kaydedilebilir.

To My Family,

ACKNOWLEDGEMENTS

To my advisor, Assoc. Prof. Dr. Yeşim Serinağaoğlu Doğrusöz, for her suggestions, guidance, and support through the thesis without which this thesis would not have been possible.

I would also like to show gratitude to Fikret Küçükdeveci and Kardiosis A.Ş. which take the responsibility of PCB manufacturing and bill of material. I would thank Mehmet Cüvelek for PCB review and comments on PCB design. I would also want to thank Esra Öztürk for her magnificent PCB mountings.

I would like to thank to my lab mates Mir Mehdi, Cihan, Gizem, Uğur, Sasan, Ceren, Kemal, Mehdi, Görkem, Kerim, Duygu, Fourough, Ali Reza, and the others in the biomedical group for their support and motivations.

To my dear friend, Iknur, for her help and encouragements through the past two years.

To my family for their love, understanding, and support. Their patience always has been helped me whole my life.

Finally, to my mother without who this thesis would not be accomplished. She has not been just a mother, she has been also my best friend that I always have trusted.

TABLE OF CONTENTS

ABSTRACT v
ÖZ vii
ACKNOWLEDGEMENTS x
TABLE OF CONTENTS xi
LIST OF TABLES xiv
LIST OF FIGURES xv
ABBREVIATIONS xviii

CHAPTERS

1. INTRODUCTION 1
  1.1 Motivation 1
  1.2 Scope of the Thesis 2
  1.3 Outline of the Thesis 2
2. LITERATURE SURVEY 5
  2.1 Brief History of Electrocardiography 5
  2.2 Electromechanical Characteristics of the Heart 6
    2.2.1 Anatomy of the Heart 6
    2.2.2 Electrophysiology of the Heart 8
  2.3 Conventional 12-lead ECG 9
  2.4 Body Surface Potential Mapping (BSPM) 12
  2.5 Invasive Imaging of the Heart’s Electrical Activity 14
  2.6 Electrocardiographic Imaging 15
  2.7 Amplifier for ECG Measurement 17
  2.8 Other Systems 19

2.8.1 ADS129x 20

2.8.2 ADS119x 20

2.8.3 ADAS1000-x 21

2.8.4 HM301D 21

2.8.5 Design Characteristics and Comparison of Commercial Front End Circuits 21

3. DESIGN OF THE ECG FRONT END CIRCUIT 23

3.1 Introduction 23

3.2 Bio-potential Electrodes 26

3.3 Unipolar vs. Bipolar Measurement 28

3.4 DC Coupling vs. AC Coupling 29

3.5 Noise in the ECG Analog Front-End Unit 30

3.6 Common Mode Rejection and RLD 32

3.7 Safety Standards and Requirements 34

3.8 General Topology of the Design 36

3.9 Design Approach 37

3.9.1 Analog Path Design 37

3.9.2 Wilson Central Terminal 45

3.9.3 Right Leg Drive 46

3.10 Conclusion and Improvements 47

4. EXPERIMENTAL RESULTS 49

4.1 Input Impedance 50

4.2 Differential Mode Gain 51

4.3 Common Mode Gain 59

4.4 Common Mode Rejection Ratio 65

4.5 ECG Analog Front End Noise Floor 67

4.6 Crosstalk between Channels 69
4.7 Experimental Results from ECG Simulator 72
4.8 Measurement from Human Subject 75
5. CONCLUSION 77
5.1 Summary of the Thesis 77
5.2 Future Works 80
REFERENCES 81

APPENDICES

A. SCHEMATIC 87
B. LAYOUTS 89

LIST OF TABLES

TABLES

TABLE 2-1: GENERAL PROPERTIES OF COMMERCIAL ECG FRONT-ENDS. 20

TABLE 2-2: SUMMARIZED FEATURES OF COMMERCIAL ANALOG FRONT-ENDS DISCUSSED. 21

TABLE 3-1: SUMMARY OF ECG PERFORMANCE REQUIREMENTS [45]. 25

TABLE 3-2: CMOS VS. BJT 40

TABLE 3-3: OP-AMP SELECTION CRITERIA. 41

TABLE 3-4: INSTRUMENTATION AMPLIFIER SELECTION CRITERIA. 43

TABLE 4-1: MEASURED INPUT IMPEDANCE. 51

TABLE 4-2: DIFFERENTIAL MODE AMPLITUDE AND PHASE MEASUREMENTS. 54

TABLE 4-3: MEASURED -3DB CUTOFF FREQUENCIES. 57

TABLE 4-4: COMMON MODE AMPLITUDE MEASUREMENTS FOR UNIPOLAR CHANNELS V1 TO V6. 63

TABLE 4-5: CMRR MEASURED AT 50HZ…………………………………………....66

LIST OF FIGURES

FIGURES

FIGURE 2-1: ANATOMY OF THE HEART [5] 7

FIGURE 2-2: ACTION POTENTIAL PROPAGATION OF THE HEART [4] 8

FIGURE 2-3: EINTHOVEN TRIANGLE [7]. 9

FIGURE 2-4: WILSON CENTRAL TERMINAL (CT) FORMED BY AVERAGING OF LIMB ELECTRODES [4]. 10

FIGURE 2-5: GOLDBERGER AUGMENTED LEADS [4]……………………………….. 11

FIGURE 2-6: ECGI PROCEDURE [9]. 15

FIGURE 2-7: TWO ECG FRONT END DESIGN APPROACHES, (A) LOW NOISE AMPLIFIER WITH HIGH GAIN. (B) LOW GAIN APPROACH [40]..……………….................18

FIGURE 2-8: SIGNAL CHAIN FOR HIGH GAIN AND LOW GAIN APPROACHES, (A) TYPICAL SIGNAL CHAIN FOR LOW NOISE AMPLIFIER HIGH GAIN APPROACH, (B) TYPICAL SIGNAL CHAIN FOR LOW GAIN APPROACH [40], [41]…………………………...18

FIGURE 3-1: ELECTRODE ARRAY USED FOR BSPM. (A) ANTERIOR AND POSTERIOR VIEWS OF THE ELECTRODE ARRAY ATTACHED ON THE BLUE STRING. (B) LOCATION OF ELECTRODE ON THE SURFACE OF THE BODY [46]………………..28

FIGURE 3-2: ELECTRODE SKIN CONTACT INTERFACE RECOMMENDED BY AAMI........31

FIGURE 3-3: ECG SYSTEM AND EMI INTERFERENCE……………………………..33

FIGURE 3-4: TYPICAL V/I CURVE OF VARISTOR. 35

FIGURE 3-5: PROTECTION CIRCUIT. 36

FIGURE 3-6: BLOCK DIAGRAM OF THE ANALOG UNIT, (A) POWER UNIT, (B) ECG FRONT-END. 37

FIGURE 3-7: ECG ANALOG FRONT-END SIGNAL PATHS, (A) UNIPOLAR CHANNELS V1 TO V6, (B) BIPOLAR LEADS I AND II. 38

FIGURE 3-8: LOW PASS FILTER, (A) 2ND ORDER LINEAR PHASE 0.05 SALLEN-KEY LOW PASS FILTER, (B) BODE PLOT OF THE LOW PASS FILTER WITH TRANSFER FUNCTION GIVEN IN EQUATION (3-6) 44

FIGURE 3-9: WILSON CENTRAL TERMINAL (WCT)... 45

Figure 3-10: RLD 46
Figure 4-1: Analog front-end and Power supply. 49
Figure 4-2: Setup used for input impedance measurement. 50
Figure 4-3: Configurations used for differential mode frequency response, (a) setup to measure frequency response of unipolar channels, (b) setup used to measure frequency response of bipolar channels 52
Figure 4-4: The oscillogram of differential mode gain responses. Yellow signal is the differential 100mVp-p input signal, turquois is the signal amplified by factor of 14 by instrumentation amplifier, and the pink signal is the output of the low pass filter, (a) channel V1 responses for 10Hz input, (b) channel V4 responses for 500Hz input, (c) bipolar Lead I responses for 50Hz input, (d) bipolar Lead II responses for 1000Hz input. 53
Figure 4-5: Bode plot of the frequency response of the unipolar channels V1 to V6 plus bipolar Lead I and Lead II. 56
Figure 4-6: Differential gain linearity at 10Hz. 58
Figure 4-7: Differential gain linearity at 500Hz. 58
Figure 4-8: Post-amplifiers for high CMRR measurement using (a) non-inverter configuration using op-amp, (b) instrumentation amplifier. 60
Figure 4-9: Configurations used for common mode gain measurement. 62
Figure 4-10: Common mode gain measurements. Yellow signal is the common mode 3.3V input signal, turquois signal the signal reference electrode WCT, pink signal shows the voltage on RLD electrode, and the blue signal is the output of the low pass filter. 64
Figure 4-11: Common mode gain vs. frequency. 65
Figure 4-12: CMRR vs. frequency characteristics of LT1167 [54]. 65
Figure 4-13: Common mode rejection ratio. 66
Figure 4-14: Configuration used for noise level measurement of ECG analog front-end. 67
Figure 4-15: Measured peak to peak noise floor for ECG analog front-end. 68

FIGURE 4-16: FFT OF THE MEASURED ECG ANALOG FRONT-END NOISE FLOOR. 50HZ NETWORK FREQUENCY AND ITS HARMONICS ARE OBVIOUS IN THE NOISE SPECTRUM. 69

FIGURE 4-17: CROSSTALK AS RESULT OF MUTUAL INDUCTIVE AND CAPACITIVE COUPLINGS OF PROPAGATING SIGNAL IN AGGRESSOR TRACE (A-B) ON VICTIM TRACE (C_D)... 70

FIGURE 4-18: CONFIGURATION USED TO MEASURE CROSSTALK. CHANNEL V1 IS AGGRESSOR TRACE CARRYING 700MVP-P SINUSOIDAL SIGNAL WHILE TERMINATED AT THE OTHER END. REMAINING CHANNELS ARE TERMINATED AT THE BOTH END ACTING AS VICTIM CHANNELS.......................................71

FIGURE 4-19: CROSSTALK MEASURED FROM NEAR END AND FAR END FOR A GIVEN 700MV 100HZ SINUSOIDAL INPUT. THE FIGURE AT THE TOP SHOWS THE MEASUREMENT TAKEN FROM NEAR END AND THE ONE IN BENEATH ILLUSTRATES THE FAR END MEASUREMENT... 71

FIGURE 4-20: SETUP USED FOR RECORDINGS FROM ECG SIMULATOR.................. 72

FIGURE 4-21: ECG MEASUREMENTS FROM REAL PERSON 74

FIGURE 4- 22: ECG RECORDING FROM REAL PERSON USING 10 ELECTRODES …......... 75

FIGURE 4- 23: ECG MEASUREMENTS FROM REAL PERSON.............................. 76

FIGURE A-1: SCHEMATICS OF THE POWER UNIT AND ECG FRONT-END 87

FIGURE B-1: TOP LAYER LAYOUT...89

FIGURE B-2: BOTTOM LAYER LAYOUT 90

ABBREVIATIONS

AD	Analog Devices
AAMI	Advancement of Medical Instrumentation
AHA	American Heart Association
ADC	Analog to digital converter
AED	Automated External Defibrillator
ANSI	American National Standard Institute
BEM	Boundary Element Method
BSPM	Body Surface Potential Mapping
CMRR	Common Mode Rejection Ratio
CT	Computed Tomography
ECG	Electrocardiography
ECGI	Electrocardiographic Imaging
FEM	Finite Element Method
GBP	Gain Bandwidth Product
HPF	High pass filter
HRV	Heart Rate Variability
IP	Inverse Problem
LHV	left ventricular hypertrophyn
LPF	Low pass filter
LT	Linear Technology
MRI	Magnetic Resonance Imaging
RF	Radio Frequency
RLD	Right Leg Driven
PCB	Printed Circuit Board
TI	Texas Instrument
WCT	Wilson Central Terminal

CHAPTER 1

INTRODUCTION

1.1 Motivation

Since the first 12-lead electrocardiogram was recorded by Eindhoven, examining of electrical activity of the heart using surface electrodes obtained great clinical significance over the years. According to annual report of World Health Organization in 2013, cardiovascular disease is counted as one of the four major reasons of 80% of deaths in the world [1]. Therefore, the ability to acquire high quality recordings of electrical activity of the heart would be highly beneficial for the diagnosis of these diseases. For this purpose, invasive and noninvasive methods are used. Standard 12-lead ECG as one of the noninvasive methods is commonly used all over the world at hospitals and clinics. In addition, more sophisticated methods are developed to measure the electrical activity of the heart from surface of the body using larger numbers of electrodes known as Body Surface Potential Measurement or briefly BSPM. Invasive methods are also used in special cases to make in vivo measurements.

In this study, we aim to build an analog front end circuit to record the electrical activity of the heart using 10 electrodes connected to the surface of the body. These ten electrodes are used for recording measurements from the right arm (RA), left arm (LA), and left leg (LL) electrodes, six chest electrodes (V1~V6), and one RLD electrode. Unipolar measurements are used for chest channels (V1~V6). Also, lead I and lead II are constructed by bipolar measurements between (LA, RA) and (LL, RA) pairs respectively.

The analog front end proposed in this thesis is designed to be compatible with 24-bit Sigma Delta analog to digital converter (ADC), so we kept the channels as simple as possible to use the features that the ADC recommends. Since the front end circuit for 12-lead ECG recording device and multi-channel BSPM system are the same, the circuit designed in this thesis can be used as part of any body surface ECG recording system after adding ADCs and microcontrollers after the front end stage to transfer data to the computer.

1.2 Scope of the Thesis

Since this recording unit was designed to be used as part of a recording system containing Sigma Delta converter as analog to digital converter, signals paths were tried to be kept as simple as possible. Each channel consisted of three stages: (a) input, (b) amplification, and (c) low passer filter stages. At the first step, single channel had been tested on bread board using different components mentioned in Table 3-3 and Table 3-4. During these tests, various combinations of op-amps and instrumentation amplifiers were considered and finally according to the requirements, proper components were selected. After that, a sample channel was tested on pertinax to ensure the feasibility of the design. Finally, PCB layout was designed and mounted. After that, performance tests were done and experimental results from ECG simulator and from the body surface were recorded.

1.3 Outline of the Thesis

This thesis presents detailed documentation of design, implementation and assessment of an ECG front end circuit. Chapter 1 gives the summary of the thesis, motivation behind thesis, and the scope of the thesis. Chapter 2 is allocated to review the literature on different techniques of detecting the electrical activity of the heart, either invasive or non-invasive. In this chapter a brief description of invasive methods are given, and the non-invasive methods such ECG, BSPM, and ECGI is explained. Chapter 3 explains the hardware requirements of the system and criteria that have to be met in such a device. Chapter 4 goes through the performance evaluations of the analog front end. In this chapter, experimental results from ECG simulator and from the body surface are also given. Chapter 5 is the dedicated to conclusion and future works. Finally, in appendix A and appendix B, schematic and PCB layouts of the designed ECG front end are given.

CHAPTER 2

LITERATURE SURVEY

In this chapter, first a brief review of history of the electrocardiography is given. In the following, anatomy and electromechanical properties of the heart will be described. A short literature review about the invasive and non-invasive methods of recording of the electrical activity of the heart is given. The merits and downsides of each are explained and limitations of the 12-lead system will discussed. Body Surface Potential Mapping (BSPM) as an alternative method for conventional 12-lead ECG will be set out. Finally Inverse Problem (IP) and Electrocardiographic Imaging as applications of BSPM will be explained.

2.1 Brief History of Electrocardiography

In 1662, the works of French philosopher, Rene Descrates, were published after his death. In his works, Descrates had explained the human movements as complex interactions of mechanical phenomena plus "animal spirit" as spiritual cause of movement. A few years after that, in 1664, a Dutch scientist, Jan Swammerdam refuted the "animal spirit" theory of Descrates by showing the possibility of muscle movement without connection to the brain. After about a century, in 1769, Edward Bancroft, an American Scientist, found out that the shock from Torpedo fish has an electrical nature. It took a long time from this investigation to the first recording of the electrical activity of the heart by British physiologist, Augustus D. Waller. In 1887, in London he demonstrated the first recording of the electrocardiogram using his dog "Jimmy". And finally, in 1893, a Dutch physiologist Willem Einthoven made the big breakthrough by asserting the term electrocardiogram into medical associations; however, he himself claimed that it was Waller who had used the term the first time. In following, in 1897, Einthoven developed amplification system for his device after he was inspired by the invention of Clement Ader's amplification system for marine telegraph lines. After that, for more than 25 years, Einthoven continued to work in this area, and in 1924 he won the Nobel Prize for the invention of electrocardiogram. The invention of sting galvanometer electrocardiogram by Einthoven was extremely important, since after that many other scientists all over the world used his method and device working on the electrical nature of the heart, and by this way many further steps were taken in the field. In 1931, Frank Norman Wilson and colleagues defined unipolar potential measurement using reference node known as the Wilson Central Terminal (WCT). In 1944, Wilson introduced six chest leads to the ECG and the well-known 12-lead ECG was established. For additional information about ECG time line refer to reference [2].

Since the string galvanometer of Einthoven, a lot of works have been done to improve the method of recording potential from the surface of the body, such as Body Surface Laplacian ECG Mapping by Cohen and He [3], but still the principle has not changed much since the era of Einthoven.

2.2 Electromechanical Characteristics of the Heart

The human heart is a biological electromechanical pump responsible for blood circulation through the body. It weighs approximately 250-300g and located between the lungs behind the sternum [4] and at each beat, it pumps out 70 millimeter of blood toward the body which equals to 5.6L/min [5]. In the following section, brief anatomy, electrophysiology, and diseases of heart will be discussed.

2.2.1 Anatomy of the Heart

The heart consists of four chambers and four valves supported with veins and arteries responsible for blood circulation in the body. The blood is distributed and collected from the body through the circulation system. This circulation system consists of two circuits: (1) pulmonary circulation, and (2) systemic circulation [5].

The former brings deoxygenated blood from the right ventricle to the lungs through pulmonary arteries and brings back oxygenated blood to left atrium by pulmonary veins. The latter ejects blood from the left ventricle to the whole body by aorta and collects CO_2 saturated blood from the body and brings it back to the right atrium. The right atrium is a small chamber that pumps deoxygenated blood to the right ventricle through tricuspid valve, and the right ventricle pumps the received blood to pulmonary arteries via pulmonary valve. Then left atrium receives O_2-rich blood from the lungs and sends it to the left ventricle from mitral valve. Finally the blood is pumped out to the aorta via aortic valve (Figure2-1). In addition to the arteries carrying the blood to the organs, heart's myocardial cells also require oxygenated blood to function. This is done by coronary vessels and any problem in this circulation may cause a myocardial infarction commonly known as heart attack [5].

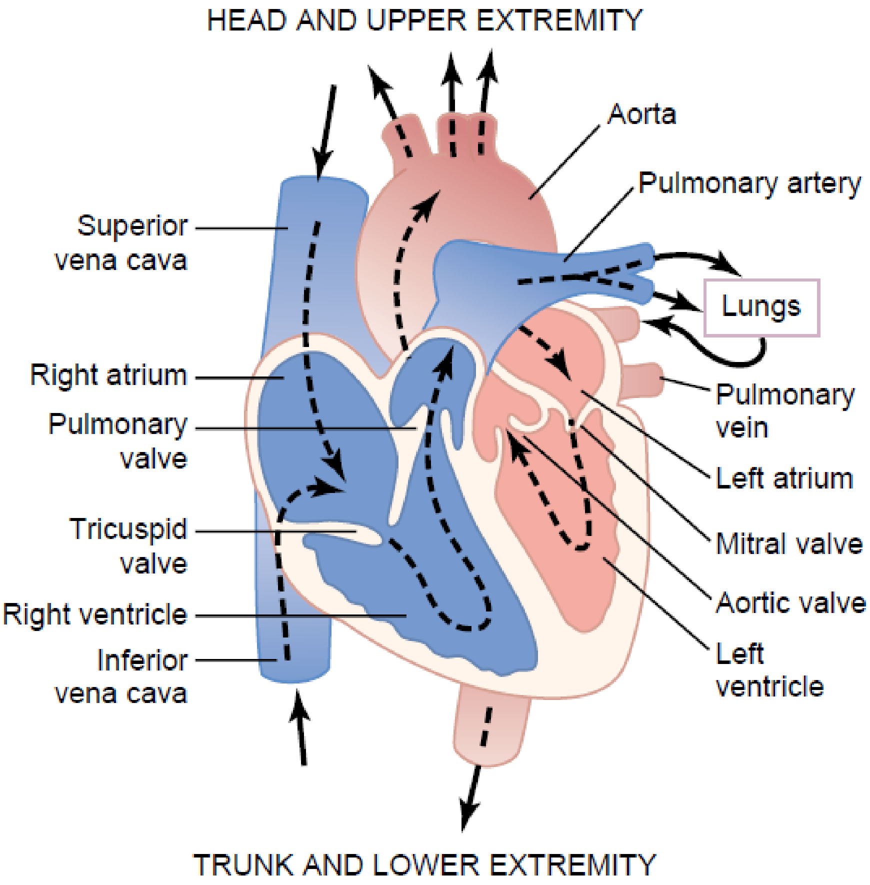
HEAD AND UPPER EXTREMITY
Aorta
Pulmonary artery
Superior vena cava
Lungs
Right atrium
Pulmonary vein
Pulmonary valve
Left atrium
Tricuspid valve
Mitral valve
Aortic valve
Right ventricle
Left ventricle
Inferior vena cava
TRUNK AND LOWER EXTREMITY

Figure 2-1: Anatomy of the heart [5]

2.2.2 Electrophysiology of the Heart

The electrical activity of the heart is originated at the right atrium from a point called the sinoatrial node (SA node) [4]. SA node is the natural pacemaker of the heart stimulating at a rate of 70 beats/min and regulates the heart working frequency. Then, activation continues to propagate through the atriums toward the atrioventricular node (AV node). The activation passes from the AV node to the bundle of His [4]. Then, it propagates to the right and left ventricles via right and left bundle branches. Then, it continues to the endocardial walls of both ventricles through the Purkinje fibers. Finally from endocardium of right and left ventricles simultaneous propagation occurs toward the epicardium by cell-to-cell activation passing through the myocardium. Figure 2-2 depicts the waveforms generated during the propagation of the electrical activity of the heart from beginning in the SA node to the end in ventricles. The superimposition of action potentials in each domain gives the well-known ECG signal [4].

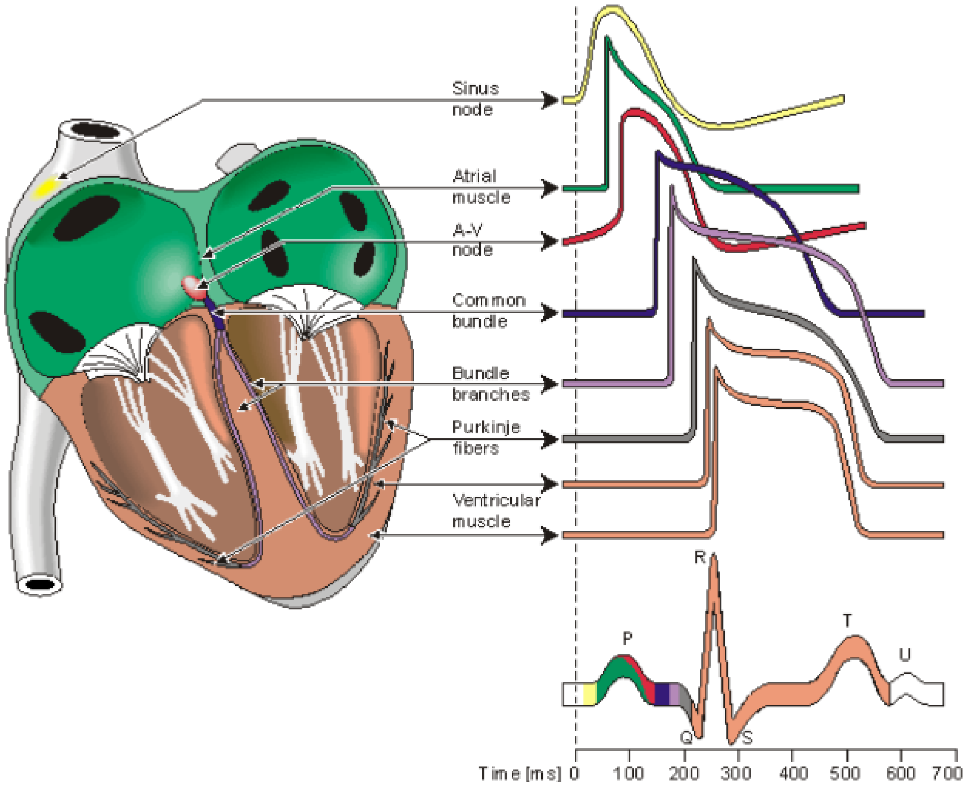
Sinus node
Atrial muscle
A-V node
Common bundle
Bundle branches
Purkinje fibers
Ventricular muscle
R
P
T
U
Q
S
Time [ms] 0
100
200
300
400
500
600
700

Figure 2- 2: Action potential propagation of the heart [4]

2.3 Conventional 12-lead ECG

The goal of the electrical imaging of the heart is the extraction and presentation of the electrical activity of the heart. This can be done either invasively using catheters, or non-invasively using surface electrodes attached to the surface of the body. Both of these data have to be recorded by the external device responsible for collecting and storing the data. This process of recording the electrical activity of the heart is called Electrocardiography (ECG).

To describe the electrical activity of the heart at least three leads are required [6]. These leads are derived from the difference of 3 electrodes attached to the right arm (RA), left arm (LA), and left leg (LL). These leads are Lead I from LA to RA, lead II from LL to RA, and lead III from LL to LA. AS shown in Figure 2-3, Leads I, II, and III build a triangle called the Einthoven's triangle to honor the legacy of Wilhelm Einthoven, who first introduced it in 1903.

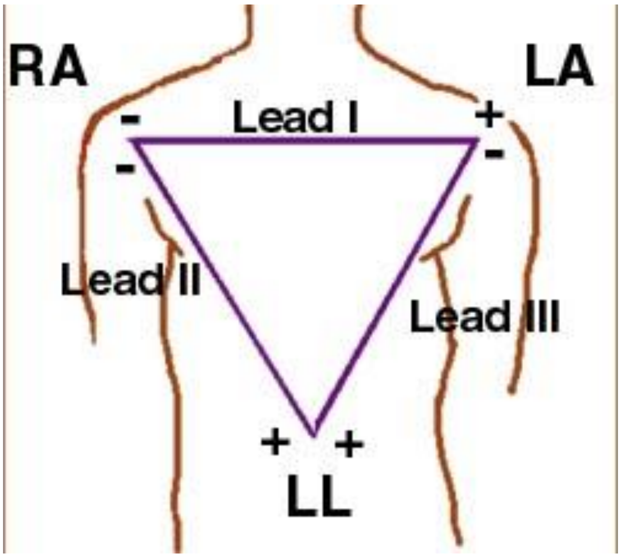

Figure 2- 3: Einthoven Triangle [7]

In addition to leads I to III, unipolar measurements of RA, LA, and LL with respect to a reference point gives unipolar measurements from these electrodes known as VR, VL, and VF respectively. The reference point is generally called the Wilson Central Terminal (WCT). WCT is built by averaging VR VL, and VF as shown in Figure 2-4.

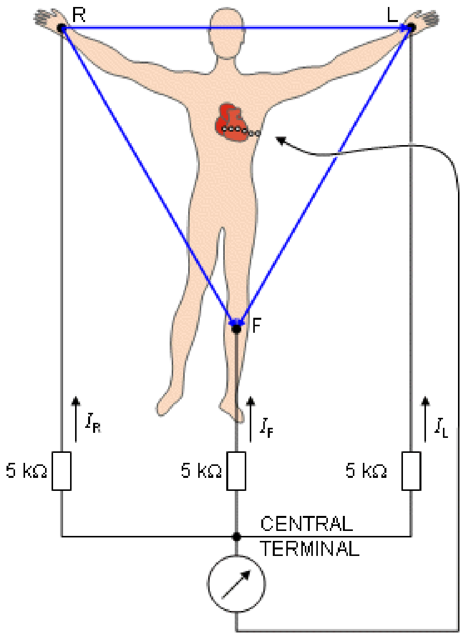

Figure 2- 4: Wilson central terminal (CT) formed by averaging of limb electrodes [4]

It is possible to increase the magnitude of the measured unipolar signals by 50% by omitting the resistance of the corresponding lead. Figure 2-4 illustrates this idea. New leads are called augmented leads and shown as aVL, aVR, and aVF. Equations (2-1) through (2-3) provides mathematical view over the measurements and why the new leads are 50% larger than the previous ones.

$$aVR = VR - \frac{VL + VF}{2} = \frac{2VR - VL - VF}{2}$$

$$= \frac{3VR - VL - VF - VR}{2} = \frac{3VR - WCT}{2} = \frac{3VR}{2} \qquad (2\text{-}1)$$

$$VL = \frac{3VL}{2} \qquad (2\text{-}2)$$

$$VF = \frac{3VF}{2} \qquad (2\text{-}3)$$

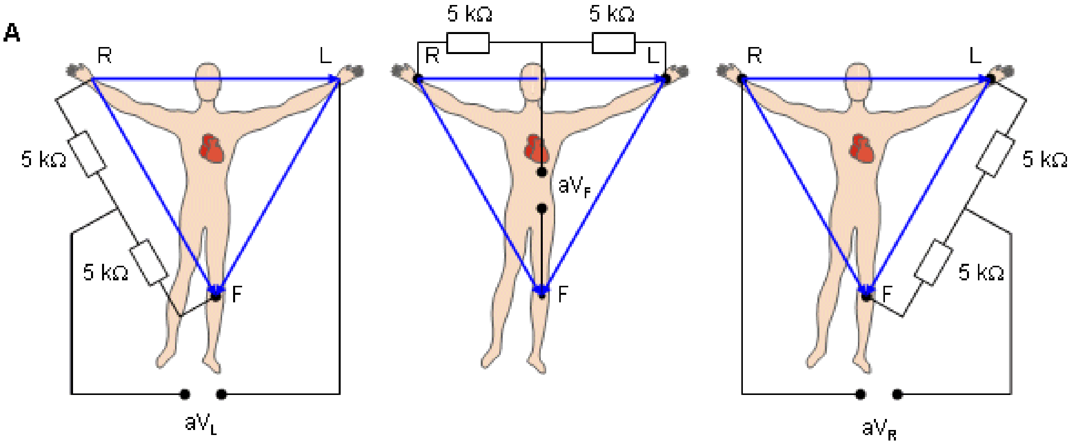

Figure 2- 5: Goldberger augmented leads [4]

Finally, six additional chest electrodes V1 to V6 are added to the system. These limb electrodes are also unipolar and measured with respect to WCT. These electrodes provide additional information about the electrical activity of the heart and its distribution. The 10th electrode known as the right leg drive (RLD) is also connected to the right leg (RL) for common mode signal cancelation. In this way, conventional 12-lead system is constructed using 10 electrodes.

The main advantage that makes the standard 12-lead ECG the dominant methodology in electrocardiography is the simplicity and effectiveness of the method. As mentioned above, just using a few number of electrodes, it is possible to provide data that have significant clinical and diagnostic applications. This method is fast enough to be used in situations that require prompt action such as at the clinics and hospitals. Indeed, it is very easy to prepare the patient to record the ECG and obtain results immediately.

Although, conventional 12-lead ECG is extremely efficient, it has its own restrictions which force the researchers to look for other methods or at least improvements. First of all, low spatial resolution of this system gives inadequate information about the distribution of the potential both on the body surface and on the heart. For this reason, this method strongly depends on interpretation via pattern matching on the surface of the body that leads to large error values in localization and inverse problem of electrocardiography. In addition, because the measurements have been taken from a small number of leads, it would be difficult to detect small variations in electrical activity of the heart from surface of the body. As a result it would be difficult to relate the ECG signals measured on the body surface back to the ones on the heart. For this purpose, other techniques that collect data using larger number of electrodes are recommended, such as Body Surface Potential or briefly BSPM.

2.4 Body Surface Potential Mapping (BSPM)

As explained in section 2.3, one of the main drawbacks of standard 12-lead system is the lack of information since just six electrodes are incorporated. The locations of these six electrodes were chosen by Wilson to fulfil the requirement for the unique standard. In that section, invasive methods were discussed and it was described that these methods are extremely invasive and indeed not practical most of the time. In this section, a non-invasive system will be explained as a more feasible substitution for invasive mechanisms. Body Surface Potential Mapping (BSPM) is a technique that includes 32-256 electrodes attached to both the anterior and posterior of the torso providing a greater number of spatial samples [8], [9]. In this way, the information missed by the conventional 12-lead system can be compensated. In other words, each additional electrode, presents a different aspect of the electrical activity of the heart. Nevertheless, potentials measured from surface of the body are influenced by the filtering effect of the torso, similar to the 12-lead ECG.

As a summary, the goals of this method can be summarized as:

- Improve the basic knowledge of the normal and abnormal electrical activity of the heart.
- Develop medical devices to apply new knowledge to diagnosis, monitoring and therapy.

In BSPM, unipolar or bipolar potential of heartbeats are collected from the electrodes on flexible strips and arranged in columns and rows, with the highest density at the left anterior. The recordings are taken with a sampling period of 1 to 2 milliseconds between each frame. Therefore, to show the complete cardiac cycle, 400 to 800 frames are required.

The data gathered from these additional sites can be used to make a map of distribution of potentials on the torso, called Body Surface Map. The advantages of this method is the ability to provide large amount of useful data from electrical activity of the heart, but their difficulty of implementation preclude their utilization as a replacement for the conventional ECG in the clinical applications [10]. However; there are growing significance and desire in clinical applications and research of such a modality. As an example of clinical application, for acute inferior-wall left ventricular infraction additional recordings from right side precordial portion of the torso is recommended [10]. Or in diagnosis with which ST analysis are used, such as myocardial infraction, the recording from additional sites are recommended. [10] In addition, the works of group of Dutch scientists have used BSPM analysis in localizing pathophysiological reasons related with type 1 ECG in the diagnosis of Brugada Syndrome (BrS) [11]. There are many other articles emphasizing in the efficiency of using body surface potential mapping in diagnosis such as localizing post-infraction ventricular tachycardia [12], and detection of right ventricular infraction using isopotential BSPM [13]. In addition to the cases mentioned above, BSPM has been used for cases such as pulmonary embolism, acute coronary syndromes, aortic dissection, ventricular hypertrophy, and localizing the BT in WPW syndrome[1] [14].

There are two main methods for representation of data obtained from BSPM. One of the most straightforward method is “Direct Interpretation”. In this representation, using interpolation and pattern matching techniques, data mapped onto the geometry or projection of the torso. The obtained potential map represents the potential distribution on a specific geometry at a given time. The required image processing techniques are interpolation, contour generation, scaling and color mapping [15]. On the downside, direct interpretation doesn’t give any temporal information. This can be overcome displaying sequence of maps representing the potential distribution in time order. It is also possible to integrate signal over a period in order to produce integrated signal, called Indirect Integral Mapping. The period can contain QRS, QRST, or ST- section of the ECG data. This method reduces the amount of data significantly; nevertheless, it also suffers from lack of temporal information [15].

---

[1] Wolf-Parkinson-White.

The recorded data displayed as sequence of contours give pictorial information about superimposed isochronous electrical activities of the heart in 2D or 3D dimensions. These data can also be used for validation of forward solution of the heart. During the comparison, the accuracy of the model used to simulate the torso and lung effects on the potential measured from the surface of the heart can be assessed.

Although BSPM has impressive diagnostic superiority over 12-lead ECG, its complexity precludes its approval in clinical applications. Therefore, there are works to optimize the number and position of recording sites to make the BSPM simpler and effective that can be used in clinical diagnostic requests [14], [16]. As a conclusion, both 12-lead ECG and BSPM suffers from the remote measurement in which signals are open to intervening mediums such as lungs and torso [17]; nevertheless, their non-invasiveness is a major reason of their dominance in many of the applications.

2.5 Invasive Imaging of the Heart's Electrical Activity

Recordings from conventional 12-lead ECG suffers from low spatial resolution, and attenuation and smoothing within the torso. One of the solutions to this problem is invasive measurements taken from points close to the heart. During invasive measurements, endocardial and epicardial potential distributions can be recorded with electrodes placed either in the chambers of the heart, from outer surface of the heart, or from intermediate wall of the heart. There are different types of techniques to make invasive measurements from the heart which are discussed in the following.

One of the invasive methods used to measure the epicardial potentials is using electrode socks. A sock contains multiple stainless steel electrodes aligned in specific spacing and records the potential distribution over the epicardium [18], [19]. To make the measurements from the myocardium, an array of plunge electrodes can be used [20].

To make the measurements from the endocardium, intravenous contact or non-contact catheters are required. In contact catheters, tip of the catheter measures the potential at the specific point determined by fluoroscopy. There are two main disadvantages for this method: (1) the number of measurement points is restricted, since each catheter contains one tip, (2) determining the position of the tip by fluoroscopy is time consuming and unrepeatable [21]. To overcome this problem, contact catheter basket is developed capable of simultaneous multiple detections [22] [23]. Far field detection techniques using non-contact catheter also have been used to measure endocardial potentials [24], [25].

As a summary, the ability to have direct in-vivo measurements from the epicardium, myocardium, and endocardium with high accuracy is an advantage of these methods; however, invasive nature of them is a big difficulty. Surgery is required to put the electrodes in a desired location. From this point of view, non-invasive methods have great superiority over the invasive methods.

2.6 Electrocardiographic Imaging

In addition to applications mentioned above, data gathered from BSPM have another importance in solving the inverse problem of the heart which is ultimately used to map the potential distribution on the heart surface. This is done via a non-invasive imaging modality called Electrocardiographic Imaging (ECGI). ECGI provides information similar to the one gathered invasively form the epicardial surface using socks electrode [17]. The process is shown in Figure 2-4.

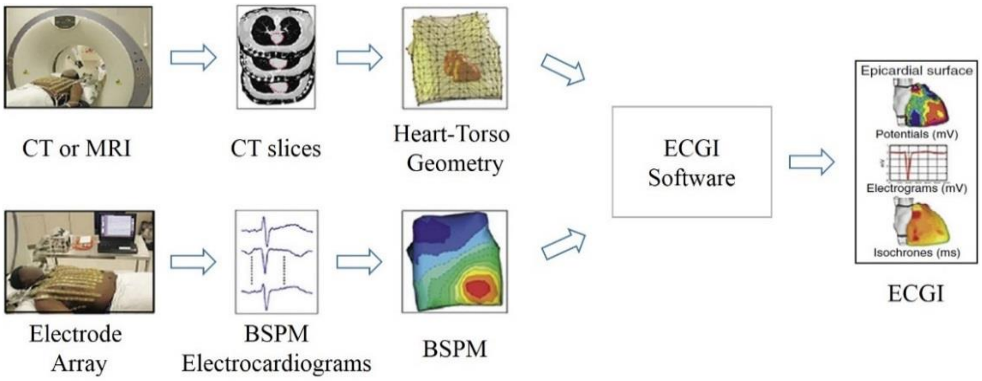
CT or MRI
CT slices
Heart-Torso Geometry
Electrode Array
BSPM Electrocardiograms
BSPM
ECGI Software
Epicardial surface
Potentials (mV)
Electrograms (mV)
Isochrones (ms)
ECGI

Figure 2- 6: ECGI Procedure [9]

As it can be seen in Figure 2-4, the procedure consists of three main stages: (1) electrocardiogram data acquisition, (2) geometry construction, and (3) forward and inverse problem solutions (via ECGI software). Signal acquisition is done by BSPM through an electrode array. Various numbers of electrodes are reported from different groups, ranging from 224 to 256. All the signals are recorded simultaneously and the process is monitored to ensure correct acquisition procedure, such as proper contact of electrodes [26], [27], [28], [29], [30].

The next step is to extract geometry including heart-torso model, and electrode positions using conventional imaging modalities such as Computed Tomography (CT), and Magnetic Resonance Imaging (MRI). Both CT and MRI can be used to obtain the slices containing volumetric data of the torso and the organs inside, including the heart itself. By using techniques such as Region Growing [31], Guide Point Fitting of Hedley [32], and Voxel Classification of Budgett [33], the slices are segmented and similar surfaces are extracted. Finally surface or volume elements are extracted representing different surfaces or volumes such as trunk, lung, heart, etc. Ultimate result contains accurate, realistic patient specific 2D or 3D geometric model of the heart-torso [34]. Using numerical methods such as Boundary Element Method (BEM) or Finite Element Method (FEM), forward problem of ECG is solved to obtain a relationship between the cardiac sources and the BSPMs.

Finally, using the forward problem solution and the body surface potentials, electrical sources in the heart are estimated. This process is known as the Inverse Problem of ECG. Regularization methods such as Truncated Singular Value Decomposition (TSVD), Tikhonov regularization method, etc., are required to overcome the ill-posed nature of the inverse problem and obtain stable solutions [35]. Standard regularization techniques employ only spatial information without the temporal information, so they are not so much useful to solve the inverse problem of the electrocardiography [36]. There are methods capable of providing both spatial and temporal regularization, such as Greensite method [37]. These methods can be more useful than the standard ones for obtaining temporally more stable inverse solutions. For instance, using the method developed by Greensite and Huiskamp, reconstruction of myocardial time-activation and tracking activation sequences would be possible. Another important point about the regularization methods is determination of proper regularization parameter for the solution. Too much regularization may cause over-smoothing of the solution while inadequate regularization leads to noisy solution [35], [34].

In conclusion, ECGI combines BSPM measurements and anatomical imaging modalities (CT and MRI) to generate more functional imaging modality capable of reconstructing cardiac sources. It employs numerical methods (BEM and FEM) together with regularization techniques (Tikhonov, SVD, Greensite, etc) to solve the inverse problem of ECG. The obtained data have higher spatial resolution compared to the conventional 12-lead ECG and BSPM. For example, it can locate initiation site of focal arrhythmia with spatial accuracy of 6mm [38], [39].

2.7 Amplifier for ECG Measurement

Designing analog front end for ECG is strongly depends on the resolution of the ADC used in signal trace. Depending on resolution of ADC, two approaches are possible for analog paths feeding the ADC [40], [41]. In both approaches, it is assumed that the system is designed to be powered by battery, so 50Hz notch filter is not included in the analog paths. However, as described in the following, it is possible to implement digital 50Hz notch filter if proper approach is selected [40], [41].

First approach is when ADC has resolution less than 16-bit. If the resolution is less than 16-bit, low noise amplifier with high gain should be used. As it is obvious from Figure 2-7a, the amplifier noise is amplified by high gain together with desired signal. Because of high amplification factor, the noise introduced by amplifier has to be as low as possible. Therefore, care must be taken when choosing an amplifier [40].

The other approach, given in Figure 2-7b is based on low gain amplification. As a result the noise introduced by the amplifier would be always less than the total noise introduced by the whole system. In this case, ADC with high resolution, greater than 16-bit, is essential [40].

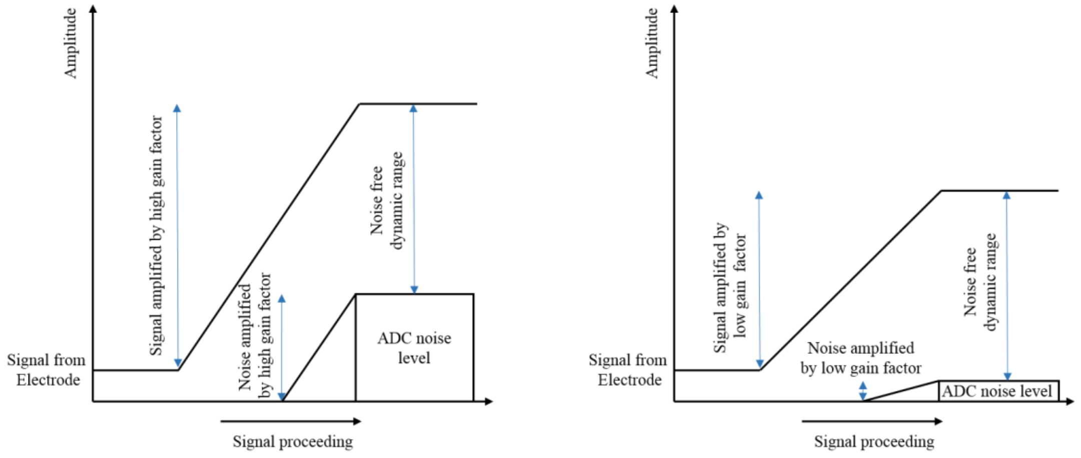
Amplitude
Signal amplified by high gain factor
Noise free dynamic range
Noise amplified by high gain factor
ADC noise level
Signal from Electrode
Signal proceeding
Amplitude
Signal amplified by low gain factor
Noise free dynamic range
Noise amplified by low gain factor
ADC noise level
Signal from Electrode
Signal proceeding

(a) (b)

Figure 2-7: Two ECG front end design approaches, (a) Low noise amplifier with high gain. (b) low gain approach [40]

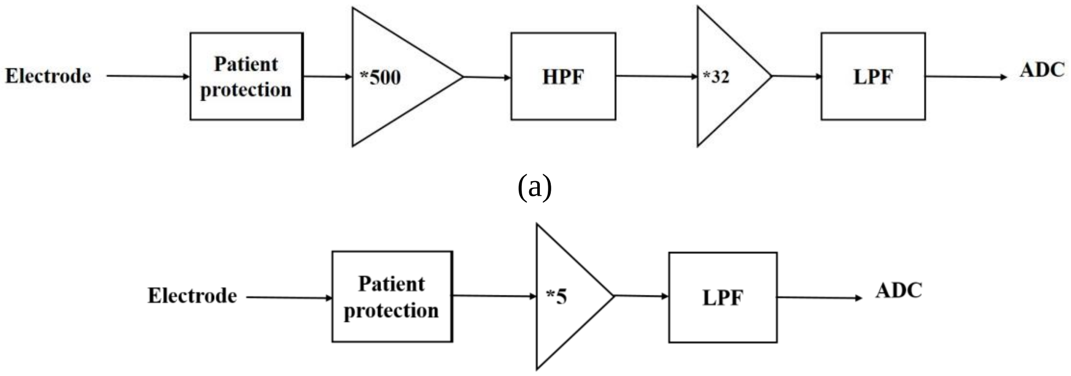
Electrode
Patient protection
*500
HPF
*32
LPF
ADC
Electrode
Patient protection
*5
LPF
ADC

(a)

(b)

Figure 2-8: Signal chain for high gain and low gain approaches, (a) typical signal chain for low noise amplifier high gain approach, (b) typical signal chain for low gain approach [40], [41]

Although in both approaches the signal quality is retained, the selected method would affect the analog paths prior to ADC significantly in terms of simplicity and cost. Figure 2-8a and 2-8b show the candidate configurations for these two approaches. If ADC with resolution less than 16-bit is used in signal chain, then both high pass and low pass filters have to be included prior to ADC input. Amplification is done in two steps, pre-amplification with low gain to increase the signal amplitude before noise interference and main amplification after removing

DC components to prevent the saturation of pre-amplifier. This approach increases the complexity and number of components used in the analog paths [41]. In contrast, low gain approach, Figure 2-8b, uses fewer numbers of components to feed the detected analog signals toward the ADC. Since the noise level is kept as low as possible, the DC information also preserved. Therefore, high pass filter can be eliminated from the signal chain. Moreover, the flexibility of the system would be increased by implementing digital signal conditioning algorithms, such as adaptive high pass filter, 50Hz notch filter and optimized baseline wondering removal.

2.8 Other Systems

Recently, with the advance in the CMOS technology and abilities to make smaller integrated circuits, commercial ECG analog front end circuits are introduced by prominent companies, such as Texas Instrument (TI), Analog Devices (AD), and ST microelectronics (ST). In this section, four commercial bio-potential front ends, ADS119x, ADS129x from TI, ADAS1000-x from AD, and HM301D from ST, will be explained and discussed. Each of these front end circuits contains analog circuitry supported by Sigma Delta analog to digital converter. Table 2-1 summarizes the general properties of these devices.

Table 2- 1: General properties of commercial ECG front ends[2]

Device	# Of Channels	EMI	ADC	Resolution (Bit)	Applications	Manufacturer
ADS1294	4	Yes	2nd order ∑Δ	24	ECG & AED	TI
ADS1296	6	Yes	2nd order ∑Δ	24	ECG & AED	TI
ADS1298	8	Yes	2nd order ∑Δ	24	ECG & AED	TI
ADS1299	8	Yes	2nd order ∑Δ	24	ECG & AED	TI
ADS1194	4	Yes	2nd order ∑Δ	16	ECG & AED	TI
ADS1196	6	Yes	2nd order ∑Δ	16	ECG & AED	TI
ADS1198	8	Yes	2nd order ∑Δ	16	ECG & AED	TI
ADAS1000	5	No	SAR	14	ECG & AED	AD
ADAS1000-1	5	No	SAR	14	ECG & AED	AD
ADAS1000-2	5	No	SAR	14	ECG & AED	AD
ADAS1000-3	3	No	SAR	14	ECG & AED	AD
ADAS1000-4	3	No	SAR	14	ECG & AED	AD
HM301D	3	No	2nd order ∑Δ	16	ECG & AED EMG EEG	ST

2.8.1 ADS129x

ADS129x is a family of ECG analog front end consisting of ADS1294, ADS1296, ADS1298, and ADS1299[3] from TI. The last digit states the number of channels supported by each one of these devices; for example ADS1298 contains 8 channels and ADS1294 contains just four. ADS1299 also supports 8 channels but it is designed specifically for EEG applications. In these devices, each channel is digitized by a dedicated 24-bit ∑-Δ converter with a maximum sampling rate of 32ksps. All of the channels are simultaneously digitized by its dedicated converter. In addition to 8-channels, there are built in RLD, lead off detection, WCT, pace detection and test signal in these devices.

2.8.2 ADS119x

ADS119x is also an analog front end family from TI again. It is similar to ADS129x series except the resolution of its analog to digital converter and maximum sampling rate are different. Each channel in ADS119x is digitized by a dedicated 16-bit ∑-Δ converter with a maximum sampling rate of 8ksps. Except the resolution and maximum sampling rate, there are no major other differences between ADS129x and ADS119x.

---

[2] None of devices in the list includes defibrillator protection, so external circuitry is required for each channel

2.8.3 ADAS1000-x

ADAS1000-x is a family of ECG analog front ends from Analog Devices. According to Table 2-1, maximum number of supported input channels is 5 for ADAS1000-1 and ADAS1000-2. Maximum sampling rate is 128ksps. Programmable internal low pass filter can be configured optionally to 40Hz, 150Hz, 250Hz, and 450Hz for data rate of 2 kHz. Digital high pass filter is also either 0.5Hz or 0.05Hz. Despite the advantage of simultaneous dedicated converter to each channel, the limitation in the number of channels and the resolution of the device are serious restrictions of this series compared to the ADS series of TI.

2.8.4 HM301D

This device from ST, supports up to 3 analog channels plus one impedance measurement channel (2 and 4 wires). Compared to previous devices, it has more limitations. Most importantly, the resolution of the device is restricted to 14-bits, which seems insufficient for modern ECG data acquisition systems. However, it includes built in RLD, WCT, and respiration impedance measurement circuitries, which are standard features for ECG applications.

2.8.5 Design Characteristics and Comparison of Commercial Front End Circuits

Table 2-2 summarizes some specifications of the devices reviewed above with respect to the values in the data sheets.

Table 2- 2: Summarized features of commercial analog front ends discussed

Device	**CMRR(dB)**	**SNR(dB)**	**Gain**	**Z_{in} (Ω)**	**Power dissipation (max)**
ADS119x	105dB	97	1, 2, 3, 4, 6, 8, 12	1G	17.5 mW
ADS129x	115	112	1, 2, 3, 4, 6, 8, 12	1G	17.5 mW
ADAS1000-	110	100	-	10G	41 mW
HM301D	100	72	8, 16, 32, 64	50M	NA

CHAPTER 3

DESIGN OF THE ECG FRONT END CIRCUIT

In this chapter, first standard and recommended requirements of ECG front-end circuit will be presented. Then according to these requirements, component selection criteria and brief explanation of the selected components will be stated. Important issues about ECG front-end will be given, such as Wilson Central Terminal (WCT), right leg drive (RLD), and noise discussion. And finally, based on the requirements, design details and block diagrams will be will be presented.

3.1 Introduction

The basic requirement for recoding electrical activity of the heart from surface of the body, is the ability to sense voltages smaller than 4mV within the bandwidth of at least 250Hz [6]. The working bandwidth is one of the parameters that determine the feasibility of the device for specific applications; therefore, when selecting bandwidth, it is important to make sure to select the lower and upper cut-off frequencies correctly. For example, to be able to make ST segment analysis or sleep apnea detection, it is required to have the ability to set the lower cut-off frequency to 0.05Hz or even lower [42] [43]. This value is also recommended by American Heart Association (AHA), American National Standard Institute (ANSI), and Association for the Advancement of Medical Instrumentation (AAMI). However, lower cutoff frequency equal to 0.67Hz is also affirmed as a relaxed limit by the AHA [10], [44]. On the other hand, upper limit equal to 500Hz is required for the applications such as Heart Rate Variability (HRV) and PR interval variability analysis. The recommended upper cutoff frequency for adults by AHA and ANSI/AAMI is 150Hz with sampling rate of two or three times the theoretical minimum [44]. Therefore, with respect to the spectrum requirements, it seems that high cutoff frequency of 500Hz with sampling rate of 1 kHz would be sufficient for most of the applications. Nevertheless, for some applications such as pacemaker detection for which at least 1 kHz sampling rate is recommended, these specifications stand at the boundary [10][3].

During designing procedure, great attention was paid to cover wide range of possible applications for the device. The capability for global measurement gives the flexibility for interval measurements with accurate earliest onset and latest offset identification. Simultaneous temporally aligned measurements between QT-interval, PR-interval, and QRS duration of spatially different leads result in more information than those collected from a single lead. In addition, simultaneous recording of all channels would be suitable in terms of being capable of making comparison between different leads. In conclusion, simultaneous recording of data increases the spatio-temporal aspects of the gathered data which have diagnostic value.

A summary of recommended requirements has been given in Table 3-1. It has to be mentioned here that this table just gives some of the performance requirements in ANSI/AAMI/EC13:2002 standard. There are other parameters such as presented in section 4.2.8 of the AAMI document, about alarm system requirements, that are out of the scope of this thesis. However, for a complete performance test, it is essential to meet the conditions appropriately [45].

---

[3] The bandwidth between 1Hz and 30Hz is capable of giving stable ECG record, but at the same time it causes loss of valuable data at low and higher frequencies [10].

Table 3- 1: Summary of ECG performance requirements [45]

Section	**Requirement**	**min**	**max**	**Unit**
4.2.2	Overload protection			
4.2.2.1	Minimum applicable differential AC voltage with line frequency	min	1	Vp-p
4.2.2.2	Defibrillation overload protection			
	Over voltage		5000	V
	Recovery time		5	sec
	Energy reduction		10	%
4.2.3	Risk current (Isolated patient connection)		10	µA
4.2.4.2	Risk current (Isolated patient connection) with auxiliary device attached		10	µA
4.2.9.1	Input Dynamic Range			
	Input signal		±5	mV
	Rate		320	mV/sec
	DC offset voltage		±300	mV
4.2.9.3	System noise		30	µVp-p
4.2.9.5	Gain			
	Gain factors	5		mm/mV
	Gain error		5	%
	Gain variation per minute		±0.66	%
	Gain variation per hour		±10	%
4.2.9.8	Frequency response			
	Sinusoidal		0.67-40 (-3dB)	Hz
4.2.9.11	Base Control and stability			
	Return time after reset		3	sec
	Drift rate in 10 sec		10	µV
	Baseline drift rate in an hour		500	µV
	Drift over temperature		50	µV/°C

3.2 Bio-potential Electrodes

Electrodes are used as actuator in biomedical devices. They are responsible to detect the potentials generated by sources inside the body such as brain and heart. In fact, because of the nature of the current flow inside the body bio-potential electrodes are transducers that transform ionic flow into electrical current. The electrode used to detect the electrical activity of the heart can either be attached on the surface of the body, known as body surface electrodes, or be inserted inside the body at the desired location, known as internal electrodes. There are many types of internal electrodes used to make in-vivo measurements from epicardial, myocardial, and endocardial regions of the heart. Brief description together with their application is given in section 2.3.

In many applications, Ag/AgCl electrodes are preferred. These are metal plate electrodes with silver plate at the center. The central Ag plate is generally covered with AgCl [6]. In comparison with polarizable electrodes, in which current in the electrode cables are induced by the charge displacement on the sides of the electrode, Ag/AgCl electrodes are non-polarizable. In non-polarizable electrodes, current can pass through the interface. Therefore unlike polarizable electrodes that show strong capacitive behavior, non-polarizable electrodes have the advantage of having no capacitive behavior ideally [6]. As a result, large overpotential in the electrode is not expected. Because of this behavior, non-polarized electrodes have better performance in terms of motion artifact. Working principle of Ag/AgCl electrode consists of two steps: (1) oxidation of central silver plate and producing cation of silver (Ag^+) and an electron (e^-). The cation is discharged to the electrolyte while electron travelling through the wires toward the readout device. (2) At the same time the Ag+ goes into reaction with anion Cl- forming AgCl. The generated AgCl contribute to the AgCl layer of the electrode.[4] This procedure leads to construction of half-cell potential across the interface. As mentioned, this electrode is non-polarizable and it has very low half-cell potential approximately 0.220V [6].

---

[4] $Ag \leftrightarrow Ag^+ + e^-$
$Ag^+ + Cl^- \leftrightarrow AgCl$

The type of electrode is important because the characteristics of the components used to construct the analog path depend on the electrode, such as input impedance and input bias current. Usually, commercial companies recommend an electrode from a specific company for their devices. This is because of the influence that electrodes can have on the analog path of the design. There are two important factors about the electrodes that have an impact on the design architecture. Half-cell potential (overpotential) is one of them. It appears as a DC offset at the readout device. For ECG, DC offset can reach values up to ± 300mV. If high gain amplification is aimed, this level of DC offset would be problematic for operational and instrumentation amplifiers. For example, DC offset of ±300mV in a system with gain factor of 100, would increase to ±30V. This value is beyond the rails of the operational and instrumentation amplifiers with the rails of ±7.5V. Thus, the larger the amplification, the more problems with DC offset value would come up.

The second fact is the poor contact between the electrode and skin, which is a common problem during ECG recordings. In case of poor contact, the input bias current of the front-end amplification stage can polarize the electrode [6]. Therefore, when selecting amplifiers, the amplifiers with lower input bias current and higher input impedance are preferred. Amplifiers with inconvenient input impedance sinks higher amount of current from electrode and causes further polarization of it.

For BSPM applications, series of electrodes implemented on flexible plastic string are preferred. These electrodes are attached to the body in columns, and several strings of electrodes beside each other make the rows. So we have group of electrodes in columns and rows. Figure 3-1 illustrates network of 67-electrode used in a BSPM system [8], [14], [16], [46].

In conclusion, half-cell potential and fine interface contact are the parameters about the electrodes that determine some design factors about the readout circuit, such as amplification gain and input bias current, As a result, Ag/AgCl electrode is preferable because of their lower half-cell potential (220mV) and non-polarizable nature which would be helpful to minimize the potential problems originated by electrode network.

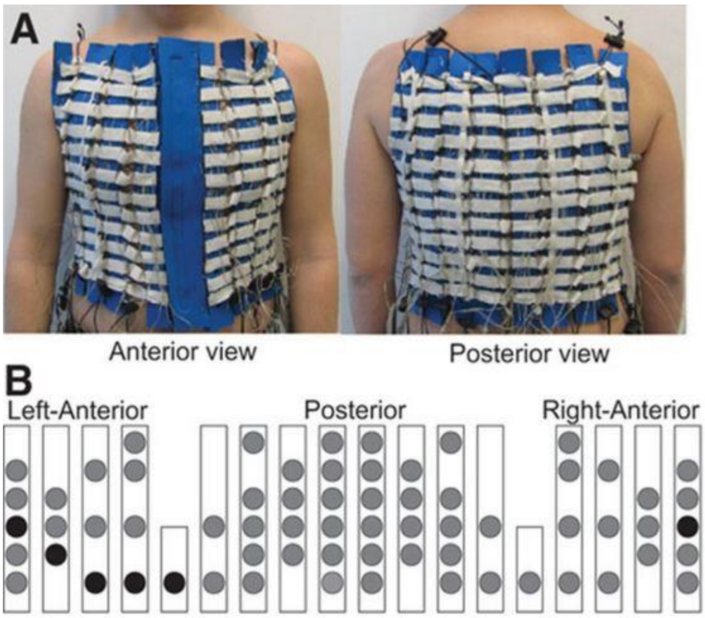

Figure 3- 1: Electrode array used for BSPM. (A) Anterior and posterior views of the electrode array attached on the blue string. (B) Location of electrode on the surface of the body [46]

3.3 Unipolar vs. Bipolar Measurement

Recognizing direction of propagation and extracting timing of the electrical events from invasive and non-invasive mapping are important in terms of constructing electrical map and activation sequence of electrical activity of the heart. Both unipolar and bipolar measurements provide useful information to achieve this goal. The points such as maximum amplitude, zero crossing, maximum first derivative, etc. of electrocardiogram can be used to catch on the underlying electrical activity. For example, maximum negative first derivative indicates the depolarization wave front coming closer to the electrode [46]. Bipolar measurement detects activations from multiple points which cause impurity in the desired signal; therefore, for these requirements, unipolar measurement is preferred. On the other hand, better SNR performance of the bipolar method can be helpful in some cases such as local depolarization detection. Unlike the bipolar measurement, unipolar measurement suffers from low SNR, which may cause difficulties in separating local activity from distance activities [46].

To sum up, each of these measurement methods has its own advantages and disadvantages. The capability to have both of them in a single device would be significantly useful since they supplement each other. In our front-end design, chest electrodes (V1~V6) that are recorded with respect to WCT result in unipolar measurements, whereas two of the recordings lead I and II, are bipolar measurements.

3.4 DC Coupling vs. AC Coupling

The general strategy of a design of electronic systems is defined by physical characteristics of signal of interest, such as bandwidth, amplitude, phase, etc. As described in section 3-1, the biological signals are usually low frequency, and low amplitude signals. To meet our initial objectives, bandwidth between 0.05Hz and 500Hz will be adequate for most of the ECG applications including the ones with low time variance behavior such sleep apnea and also the ones with higher frequency characteristics such as late ventricular potentials. It is obvious that the lower band is extremely close to zero. This fact will affect some design criteria from couplings between stages to device selection.

To interconnect several stages together, two completely different ways are possible. The first one is AC coupling. This kind of coupling uses capacitors installed in series between stages to filter out the DC component of the signal. Thus, this coupling would be useful for the signals with higher frequency characteristics in which lower frequencies are undesired. In fact, the capacitor behaves as open circuit at low frequencies and eliminates them. On the other hand, DC coupling permits both AC and DC signals to pass through. The connection in DC coupling can be done just by using wires. Advantage of AC coupling is the separate biasing for each state, so there would be no loading effect between stages. In this way, several stages can be cascaded easily without worry about loading problem. But at the same time, several problems arise when operating at lower frequencies. The first one is to find appropriate capacitors capable of passing the intended lower band. Second one is the tolerance of capacitors. Finding the appropriate capacitors to meet the restrictions narrowly would be difficult. In addition, in systems with multiple channels with the same parameters, such as ours, the capacitor values would be different; therefore, each signal would experience a different filtering path. As a result, the coordination between channels may be lost. Another problem with AC coupling is the latency because of time constant introduced by the capacitor and the load. In comparison, DC components of the signal can easily pass through DC coupling. Making a choice between AC and DC couplings is in compromise with selecting operational amplifiers, instrumentation amplifiers, and analog to digital converter (ADC). Since filtering is decided to be done digitally and this analog front-end is supposed to feed signals to ∑-Δ ADC, DC coupling is preferred over AC coupling in this study. As a result, to reduce loading effect of stages, in stage 1 and 2 the op-amps and instrumentation amplifiers with the possible highest input impedance are selected.[5]

In conclusion, with respect to design strategy, DC coupling between stages is preferred over AC coupling. The analog front end output will be fed to a 24-bit ∑-Δ ADC in future studies. For this type of ADC, usually high pass filter is not included in the preceding analog signal path. This is possible because of the acceptable performance of these converters in frequencies close to zero. Therefore, high pass filter can be implemented in the software running on the computer.

3.5 Noise in the ECG Analog Front-End Unit

There are three potential noise sources in ECG analog path. The first one is skin electrode surface interface. AAMI standard recommends the model in Figure 3-2 for representing this interface. The electrode skin contact interface is modeled by 51kΩ in shunt with 47nF, and 100kΩ resistor in series is used as patient protection[6].

---

[5] As explained in section 3.2, the type of the electrode is one of the critical parameters that play role in selecting the amplifier.

[6] The value recommended by IEC 60601-2 is 50kΩ.

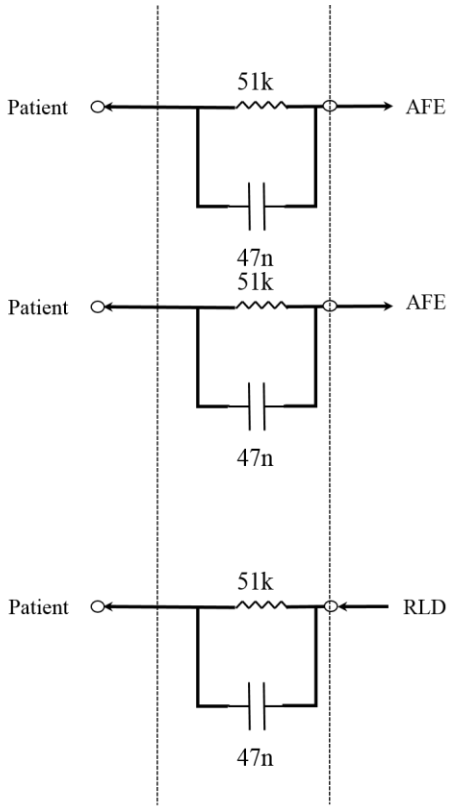

Figure 3- 2: Electrode skin contact interface recommended by AAMI

The RMS noise for a resistor R can be obtained as:

$$e^2 = 4kTR\Delta f \tag{3-1}$$

where:

- T: Temperature in Kelvin (298 K at room temperature),
- K: Boltzmann's constant ($1.3806*10^{-23}$),
- R: Resistor,
- Δf: frequency,

For the RC network, noise voltage can be extracted as:

$$Z = R||\left(\frac{1}{j\omega RC}\right) = \frac{R}{1+(j\omega RC)} = \frac{R}{1+(\omega RC)^2} - \frac{j\omega RC}{1+(\omega RC)^2} \tag{3-2}$$

$$\overline{V_t^2} = \int_0^\infty 4kTRe(Z)df = 4kT\int_0^\infty \frac{R}{1+(2\pi fRC)^2}df \tag{3-3}$$

$$\xRightarrow[x\leftarrow 2\pi fRC]{} dx \leftarrow 2\pi RCdf \tag{3-4}$$

then:

$$\overline{V_t^2} = \frac{2kT}{\pi C}\int_0^\infty \frac{1}{1+x^2}dx = \frac{2kT}{\pi C}[tan^{-1}(x)]_0^\infty = \frac{2kT}{\pi C}\left(\frac{\pi}{2}-0\right)$$

$$\overline{V_t^2} = \frac{kT}{C} \tag{3-5}$$

In addition to electrode-skin interface, protection circuit shown in Figure 3-2 also adds noise to the circuit. Noise voltage can be calculated from equation (3-1) for 50kΩ as 28.68 nV/√Hz.

Other noise sources in the ECG analog path are the op-amps, instrumentation amplifiers and active filters. To decrease the internal noise contribution of these elements, their noise voltage values are taken into account for component selections as given in Table 3-3 and Table 3-4. In conclusion, the total system noise contribution of the designed ECG analog front-end is expected to be below 30µVp-p that is recommended by AAMI (Table 3-1).

3.6 Common Mode Rejection and RLD

According to the definition given by Winter and Webster, the common mode voltage (V_C) is defined as the voltage of the patient with respect to the differential amplifier's common [47]. This common mode voltage appears as a differential signal at the input of the differential amplifier (common mode to differential signal conversion) therefore, it is desirable to minimize V_C as much as possible in the circuit using circuit design techniques.

Electromagnetic interferences (EMI) are the main source of the common mode signals in the ECG systems. A typical measurement situation shown in Figure 3-3 illustrates the potential EMI sources in the ECG system. These potential interferences can occur in the interactions of electromagnetic fields with the patient's body through the C_C and C_T capacitances, signal measuring cables (C_{CB}), and ECG system by power coupling capacitance C_C. The main frequency of interest in the EMI is the 50Hz that comes from the AC power network[7].

---

[7] In US standard power line frequency is 60Hz. Occasional regional frequencies such as 162/3 Eastern European and 25Hz Austrian railway traction power line frequencies may also have to be considered.

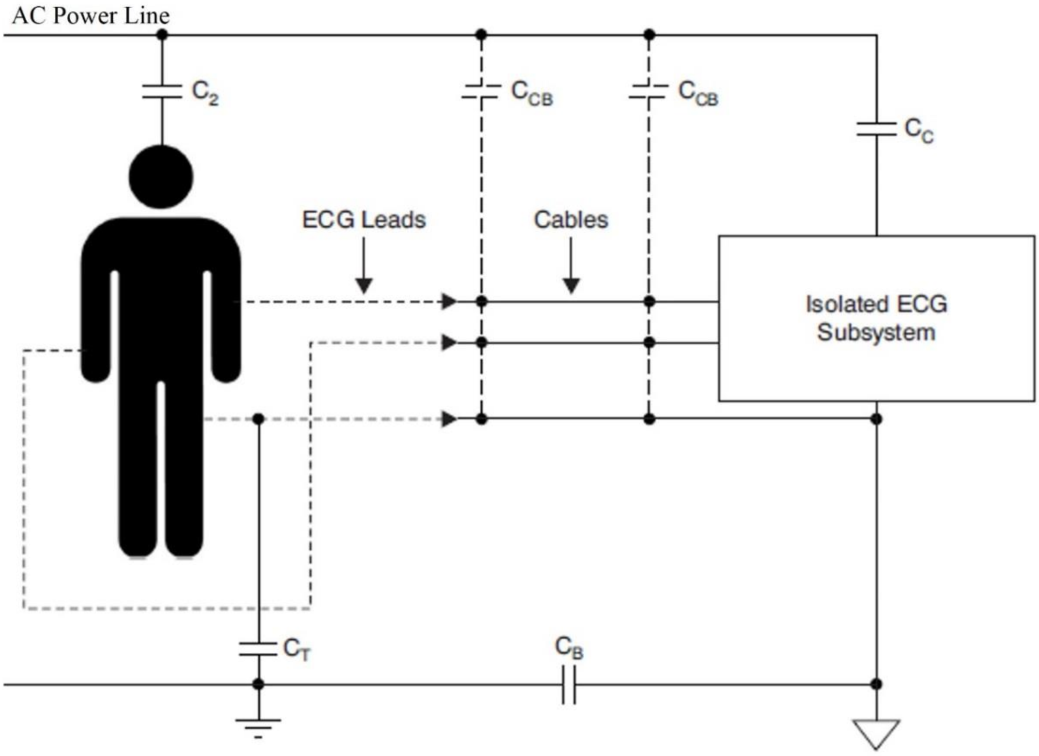

Figure 3- 3: ECG system and EMI interference [48]

There are several methods to compensate for EMI and improve common mode rejection capability of the ECG systems. These techniques are summarized in the following.

- Faraday Shield: Faraday shield protects the ECG front-end from various interference points such as C_{CB} and C_C.
- Insulation capacitances: Proper capacitance between the ground of the patient and ECG device ground may help to improve the overall CMR of the system. For devices that use battery as power supply, this is not a problem.
- Filtering: This technique is simply removing 50Hz or 60Hz frequencies using analog notch filters (pre-conversion processing) or digital filters after analog to digital conversion (post-conversion processing).
- Right Leg Drive: This technique is used as a standard method in ECG systems. In this method, common mode voltage is sampled, amplified, inverted and fed back to the right leg via the RLD electrode. The major concern about the RLD is the stability of the circuitry. Stability

of RLD depends on pole added by the op-amp used in construction and the cutoff frequency of the RLD circuitry. Optimal RLD circuit may help increase the overall CMRR of the system; however according to Winter and Webster, non-optimal design also works since other sources create more interference than the patient.

3.7 Safety Standards and Requirements

In every medical device, safety is the first concern that designers have to think about. Both the patient and the readout device have to be protected from electric shocks and high voltages. There are several commonly accepted standards for medical applications, such as AAMI, IEC60601 series, federal regulations (FDA standards) and also country specific ones. In this analog front-end we disregard these sections since it is not designed to be used together with a defibrillator.

ECG devices are used in direct contact with the patient, so patient has to be protected from electric shocks. The maximum permitted leakage current (either sink or source) in the frequency range of 1 kHz is 10μA. This restriction is obeyed using resistance in the signal path [45], [6]. In addition, in the selection of amplifiers, input bias currents have to be considered. The operational and instrumentation amplifiers with minimum input bias current are preferred.

In addition to the patient, device itself has to be protected. One of these protections is defibrillation protection. In addition to clearance[8] that is defined by standards, differential protection[9] is the most important safety issue about defibrillation. Generally it is complied using set of shunt arrangements at the input after the electrode. The arrangement contains voltage clamping components such as gas tube (Neon lamps), or varistor placed parallel with the leads. These calming devices show high resistance at low voltages, and low resistance at high voltages. The typical V/I characteristic curve for varistor is shown in Figure 3-4. The typical clamping voltage of these devices is about 50-100V which lets current pass for lower voltages without clamping [49]. To prevent this current, a series resistor together with shunt clamping diodes is used. By this way, supply rails counteract the extra current preventing damage to the device. The point about the clamping diodes is their operating voltage which must be comparable with the maximum voltage supply in the circuit. Zener diodes can be used to establish the desired voltage.

---

[8] Clearance is a spacing rule that defines the distance between two conductive planes.

[9] Differential protection is the protection against the potential high voltage shocks through the positive and negative input of the circuit.

The clamping components placed directly between leads would cause energy loss that is incompatible with energy consumption criteria. (“Energy reduction test” IEC 60601-2-49). To overcome this problem, series resistor, with typical value of 50kΩ, is used before clamping device. As a conclusion, the protection circuit in Figure 3-5 can be used as protection circuitry for both patient and ECG recording device.

Since this analog front is not supposed to be used together with a defibrillator and it is powered by a battery, the safety circuit is disregarded for the sake of simplicity. However, the power isolation is done by isolated DC to DC converter, Traco Power, which meets the AAMI/ANSI ES 60601-1:2005(R) and IEC/EN 60601-1 3rd edition medical safety standards.

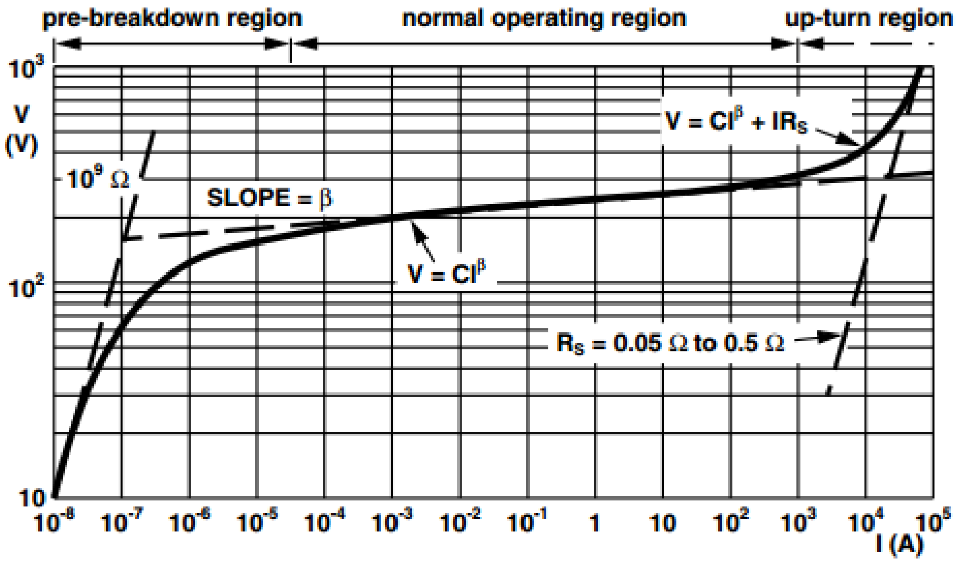

Figure 3- 4: Typical V/I curve of varistor [50].

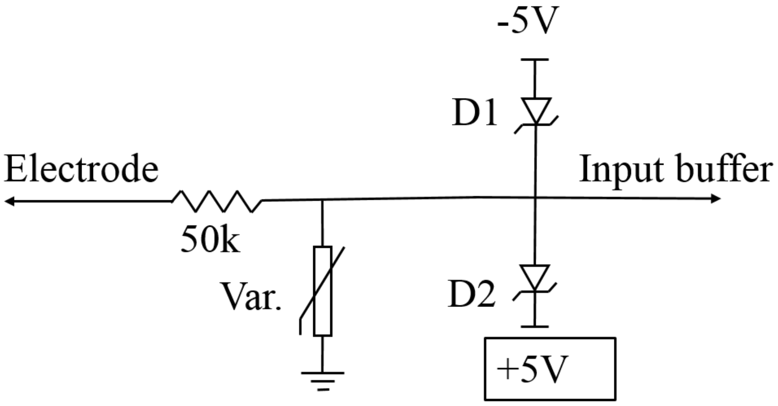

Figure 3- 5: Protection circuit.

3.8 General Topology of the Design

Designed analog unit consists of two parts: (1) power unit, and (2) ECG analog front-end. As shown in Figure 3-6a, +5V can be applied from USB jack either from computer or battery. In this case, jumpers must be shorted to use on-board power unit which generates ±5V, +1.8V, +3.3V, and +1.2V. It is also possible to apply the required power rails from an external power supply. In this case, jumper must be open and the pin connected (P2s) to the AFE, ADC, and MCU must be fed by proper voltages.

ECG analog front-end includes WCT, RLD, six unipolar channels, V1 to V6, and two bipolar channels (Lead I and Lead II). In Figure 3-6b simplified schematic of electrode and lead configuration for ECG front-end is given.

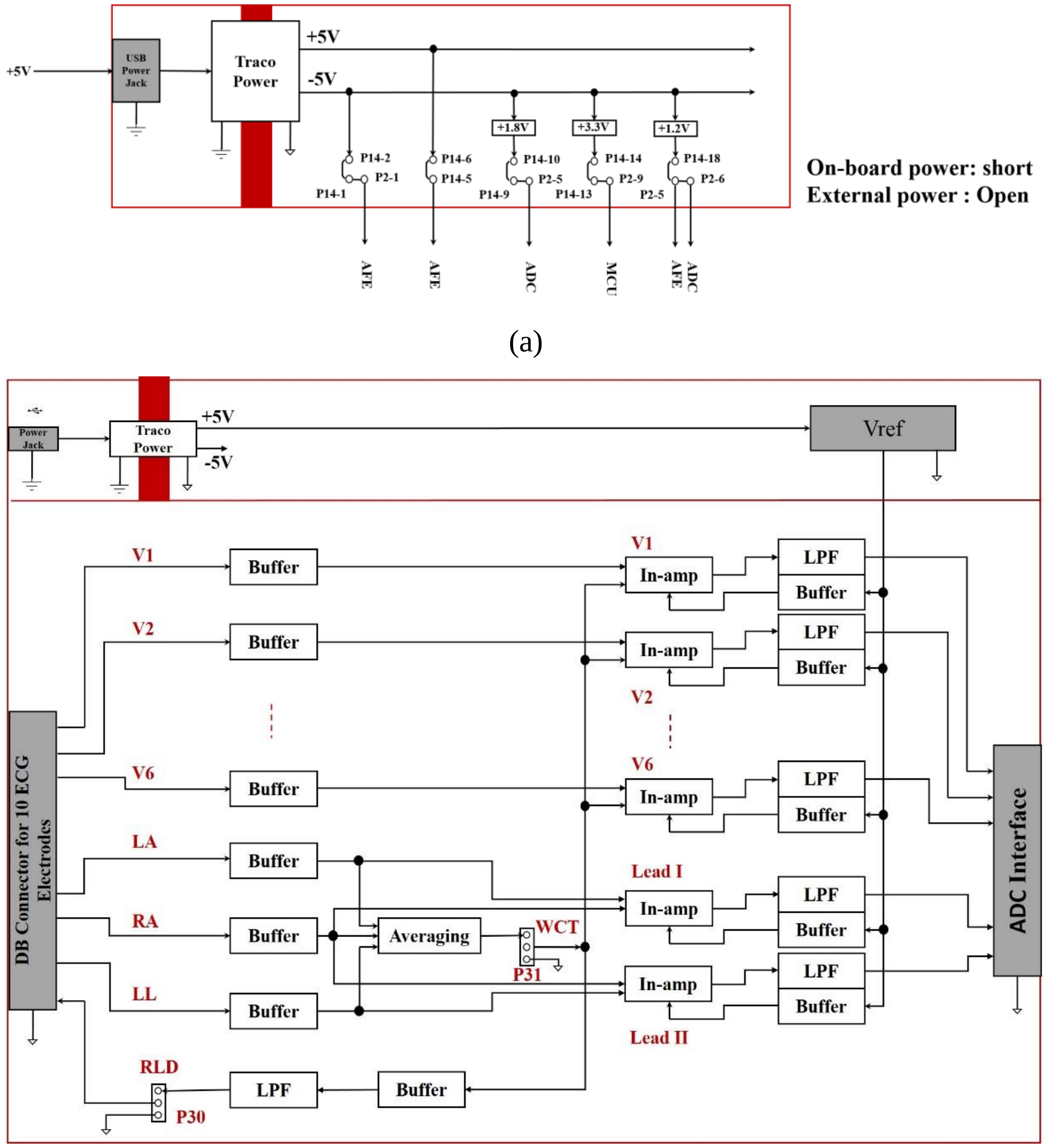
+5V
USB Power Jack
Traco Power
+5V
-5V
+1.8V
+3.3V
+1.2V
P14-2
P2-1
P14-1
P14-6
P14-5
P14-10
P2-5
P14-9
P14-14
P2-9
P14-13
P14-18
P2-6
P2-5
AFE
AFE
ADC
MCU
AFE
ADC
On-board power: short
External power : Open
(a)
Power Jack
Traco Power
+5V
-5V
Vref
DB Connector for 10 ECG Electrodes
V1
V2
V6
LA
RA
LL
Buffer
Buffer
Buffer
Buffer
Buffer
Buffer
Averaging
WCT
P31
RLD
P30
LPF
Buffer
V1
V2
V6
Lead I
Lead II
In-amp
In-amp
In-amp
In-amp
In-amp
LPF
Buffer
LPF
Buffer
LPF
Buffer
LPF
Buffer
LPF
Buffer
ADC Interface

Figure 3- 6: Block diagram of the analog unit, (a) power unit, (b) ECG front-end

3.9 Design Approach

3.9.1 Analog Path Design

As illustrated in Figure 3-6b, analog front-end domain includes six unipolar and two bipolar channels. Each channel consists of three stages: (1) input buffer, (2) amplifier, and (3) low pass filter stages. In this section each of these blocks and the components used in the design will be discussed in details. Figure 3-7a and Figure 3-7b depict the schematics of unipolar and bipolar channels, respectively.

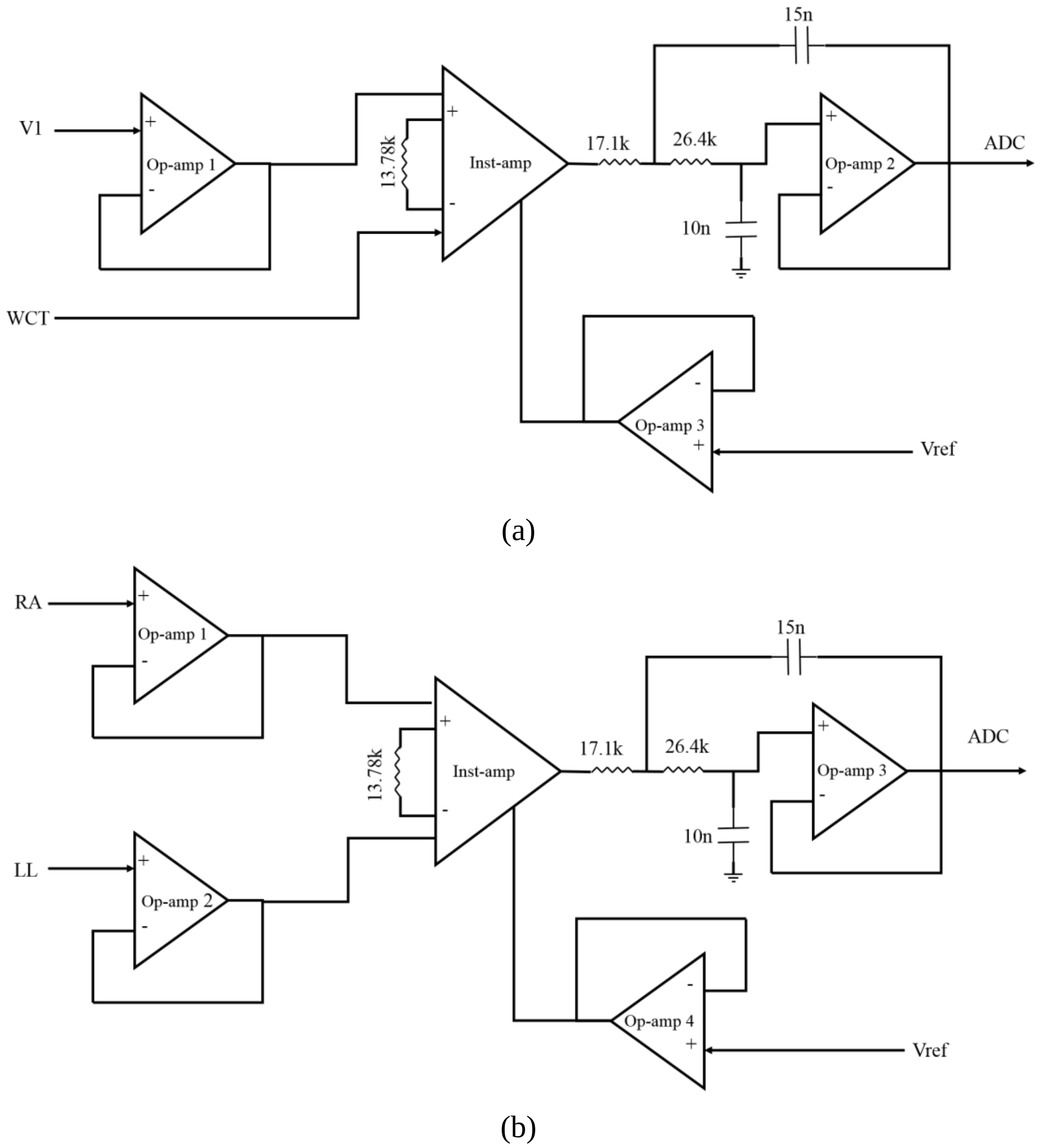
15n
V1
Op-amp 1
13.78k
Inst-amp
17.1k
26.4k
Op-amp 2
ADC
10n
WCT
Op-amp 3
Vref
(a)
RA
Op-amp 1
15n
13.78k
Inst-amp
17.1k
26.4k
Op-amp 3
ADC
10n
LL
Op-amp 2
Op-amp 4
Vref
(b)

Figure 3- 7: ECG analog front-end signal paths, (a) unipolar channels V1 to V6, (b) bipolar Leads I and II.

The first stage of each path is a voltage buffer. Input voltage buffer can be useful for reaching CMRR as fine as possible. The difference in series impedance of instrumentation amplifier affects the CMRR adversely. This happens because a portion of the common voltage appears as differential voltage as a result of the impedance mismatch at the inputs of the instrumentation amplifier. Simple voltage buffer can solve the problem by balancing the impedance at the inputs of the amplifier. Of course special attention is required during designing PCB to take the length of wiring as equal as possible for the channels[10].

To select the right op-amp for the input stage, all the topics discussed in sections 3.1, 3.2, and 3.5 have to be considered. As discussed previously in these sections, because of safety and over potential issues, input bias current of the amplifier stage is one of the critical parameters that require attention. Another important issue that has to be reckoned is the input impedance of the amplifier stages. This is important especially in the input stage which is in direct contact with the electrode network. Therefore, the operational amplifier used in the input stage should have the highest possible input impedance.

Input impedance and subsequently input bias current of the operational amplifiers strongly depend on the technology used in fabrication. There are two commonly used technologies in integrated circuits: (1) BJT, and (2) CMOS[11]. The main difference between these technologies lies at the input transistor stage, which determines the input characteristics including input impedance and input bias current. CMOS amplifier has lower impedance and lower input bias current than BJT amplifiers. However, electrostatic diodes (ESD) at the input of the CMOS op-amps are potential sources of error for biasing. As a result of low input impedance, CMOS amplifiers have better input current noise cancelation capability. On the other hand, BJT amplifiers are better in offset voltage handling and common mode rejection ratio (CMRR) [41]. The merits and drawbacks of two technologies are summarized in Table 3-2.

As a conclusion, CMOS amplifiers are preferred because of their higher input impedance and lower input bias current. They also have better gain stability over a wide range of frequency. In addition to characteristics described above, other parameters such as gain bandwidth product (GBP), CMRR, and power supply rejection ratio (PSRR) are considered for proper op-amp selection. When components were selected, we made sure that these factors were in the desired range and the main focus was on parameters such as offset voltage and offset drift. Table 3-3 provides comparison of some of the op-amps considered for this design.

---

[10] . In fact, since we are using instrumentation amplifier for amplification and it involves voltage buffers inside, there is no need for additional input buffer. However, to ensure high input impedance, input signals are buffered using high input impedance op-amps.

[11] BiFET is an integration of these two technologies which serves advantages of both up to portion.

Table 3- 2: CMOS vs. BJT

CMOS	**BJT**
• High input impedance	• High CMRR
• Low input bias current	• High output drive
• Low input current noise	• Low offset voltage
• low input offset current	• Lowe offset voltage drift
• High voltage gain	• Low input voltage noise
• Low gain error	
• Low power consumption	

As it is highlighted in green in Table 3-3, the best choice from this set is the OPA4140 from Texas Instrument Inc. This is a quad, high precision op-amp appropriate for medical instrumentation and data acquisition systems. It has an acceptable flat CMRR about 130dB in a bandwidth of 1 kHz. Extremely high input impedance (10TΩ) and very low input bias current (10pA) make it attractive to be used as input buffer for our ECG analog front-end. In addition, its low noise (5.1nV/√Hz) is far below the desired value.

The next stage in analog domain is amplification stage. This stage consists of the instrumentation amplifier responsible to amplify the signal by a factor of 14.068[12]. It is directly fed by the output of the input stage buffer via DC coupling. The criteria to select the right instrumentation amplifiers are similar to the op-amp. The main expectation from instrumentation amplifier can be summarized as: very low DC offset, low drift, low noise, very high open-loop gain, and very high CMRR [51][13]. In addition to the routine points paid attention in the selection of instrumentation amplifier, the amount of gain resistor is tried to be kept as small as possible. Resistors are sources of thermal noise in the circuit, so special effort is taken to keep the resistors small in all of the design including gain resistor of instrumentation amplifier [41].

---

[12] Since this analog front-end is planned to be used together with ∑Δ analog to digital converter and because of the noise shaping characteristics of this type of converter, the gain factor is selected very small.

[13] Both the op-amp in the input stage and instrumentation amplifier in this stage support the expected bandwidth. Minimum bandwidth of the amplifiers has to be 100 times of the bandwidth of the system; for the current system is greater than $100 * 500Hz = 50kHz$ [49].

Table 3- 3: Op-amp selection criteria[14]

TL084 **Texas Instrument**	**AD8624** **Analog Devices**	**OPA1654** **Texas Instrument**	**OPA4140** **Texas Instrument**	**OP37** **Analog Devices**	
3	0.56	18	11	63	**GBP (MHz)**
3000	10	±500	30	30	**Vos (µV)**
18	0.5	2	0.35	0.2	**TCVos (µV/°C)**
18	11	5.4	5.1	3.8	**en (nV/√Hz)**
70	137	114	126	125	**Aol (db)**
1T	1G	100M	10T	4M	**Zin (Ω)**
86(±15V)	135 (±15V)	110 (±15V)	140 (±18V)	120	**CMRR (dB)**
13	0.48	10	20	17	**SR (V/µs)**
0.03	< 0.2	±0.01	< ±0.01	±15	**ib (nA)**
1.4	0.215	2	2		**Iq (mA)**
±18	±18	±15	±20	±22	**Dual (v)**
SOIC14, PDIP14, SO14, CDIP14, TSSOP14, LCCC20	16-Lead LFCSP, 14-Lead TSSOP	TSSOP, SO14	TSSOP, SO14		**Package**

---

[14] All the op-amps excluding OP37, are quad.

As the stage for signal amplification, the accuracy of amplification in this stage is important. For this reason, gain resistors with highest accuracy (<1%) are preferred.

Table 3-4 summarizes the process of choosing an instrumentation amplifier. This table contains the comparisons which are important for the circuit aimed in this work. For devices compared, other parameters such PSSR, and GBP are within the range, so all the devices meet the general requirements.

All the devices compared in Table 3-4 are dual channel except INA333. As it is obvious, INA2128 and LT1167 meet most of the requirements appropriately. INA2128 is a dual-channel low power instrumentation amplifier with excellent accuracy and acceptable common mode rejection performance. In contrast, LT1167 is a single channel instrumentation amplifier with a better CMRR. Since in our design CMRR is the dominant parameter, LT1167 is preferred over INA2128.

As seen from Figure 3-3, to be compatible with full scale input range of the analog to digital evaluation board, +1.2V is applied to the reference pin of LT1167 after buffering. Reference pin of LT1167 is recommended to be grounded properly to avoid negative effects such as CMRR reduction. To overcome this impedance mismatch, +1.2V is buffered with the same op-amp used in input stage (OPA4140) and applied to reference pin of the LT1167.

The last stage of analog domain is the low pass filter and ADC driver stage. Every analog signal has to be low pass filtered to eliminate high frequency elements of the signal. With respect to Nyquist theorem, the cut-off frequency of the filter must be at most $\mathbf{1/2}$ of the sampling frequency. The frequencies above $(\mathbf{1/2})\boldsymbol{BW}$ would fold over the frequencies below this value and make it impossible to recover the original signal from the sampled signal.

Table 3- 4: Instrumentation amplifier selection criteria

INA333 **Texas Instruments**	**AD8426** **Analog Devices**	**INA2141** **Texas Instruments**	**INA2128** **Texas Instruments**	**LT1167** **Linear Technology**	
0.035(G=10)	0.160	1	1.3	0.8 (Av = 10)	**GBW (MHz)**
±32.5(max)	100 (max)	50	=±20	50	**Vos (µV)**
±0.15(max)	0.5	0.5	±0.2±2/(G=10) =±0.4	0.7	**TCVos (µV/°C)**
50	24	13	8	67	**en (nV/√Hz)**
100G	0.8G	100G	100G	1T	**Zin (Ω)**
110	110	106	106	115 (Av = 10)	**CMRR (dB)**
±0.25(max)	0.1	±0.03	±0.02	0.01 (Av = 10)	**GR (%)**
0.16	0.4	4	20	0.75	**SR (V/µs)**
±0.2(max)	20	±2	±2	0.08	**ib (nA)**
0.05	0.350	0.750	0.700	0.9	**Iq (mA)**
±3.5	±18	±18	±18	±20	**Dual (v)**
1	2	2	2	1	**# of channels**
MSOP-8, DFN-8	16-Lead LFCSP	16-PIN PDIP, SOL-16	16-PIN PDIP, SOL-16	8-Pin DIP, SO-8	**Package**

2^{nd} order linear phase 0.05° Sallen-Key low pass filter with cutoff frequency of 500Hz is designed as shown in Figure 3-8a using FilterPro[15]. Linear phase 0.05° low pass filter is selected because of linear phase and minimum group delay characteristics. Equation (3-6) defines the transfer function of the LPF, and the Bode plot is given in Figure 3-8b.

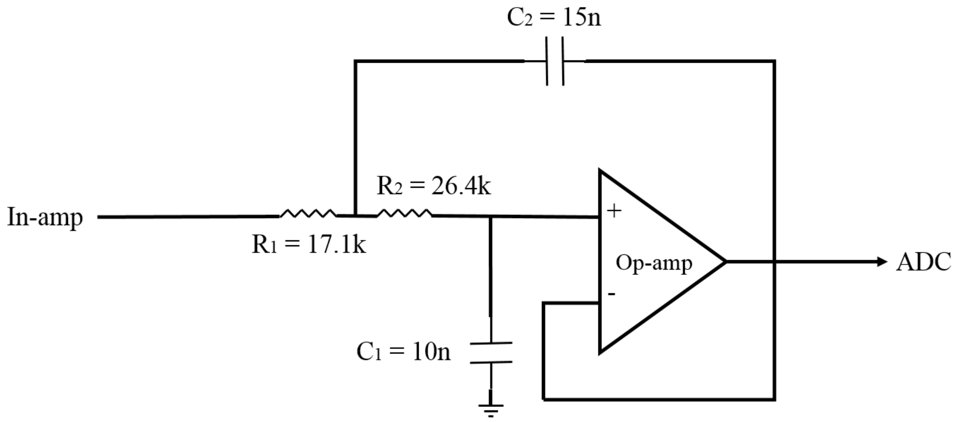

(a)

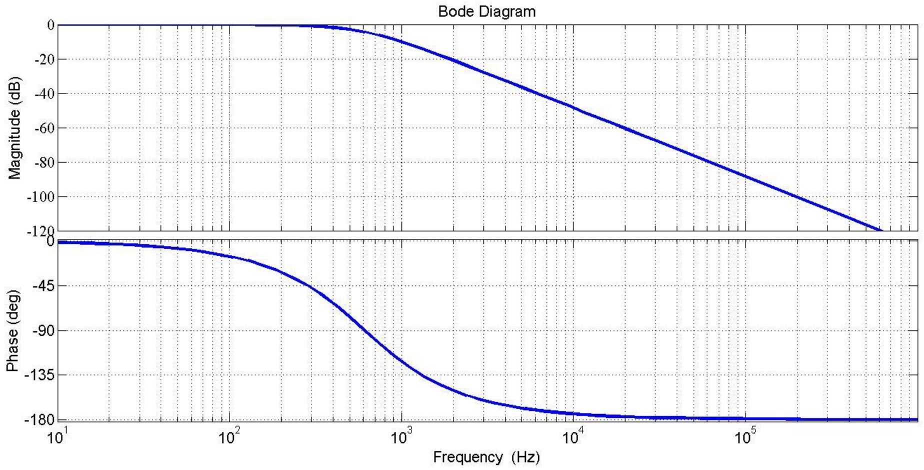

(b)

Figure 3- 8: Low pass filter, (a) 2nd order linear phase 0.05 Sallen-Key Low pass filter, (b) Bode plot of the low pass filter with transfer function given in Equation (3-6)

$$H(s) = \frac{\frac{1}{R_1 R_2 C_1 C_2}}{s^2 + s\left(\frac{1}{R_1}+\frac{1}{R_2}\right)\frac{1}{C_2}+\frac{1}{R_1 R_2 C_1 C_2}} = \frac{14.6797*10^6}{s^2 + s6.3856*10^3 + 14.6797*10^6} \qquad (3\text{-}6)$$

---

[15] FilterPro is open source software from TI for filter deign.

From these three stages (input protection stage, amplification stage, and ADC driver stage), two main goals are aimed: (1) designing the stages in a way that meets the ECG recording requirements, and (2) retaining analog signal quality as best as possible. This is important because it is impossible to compensate any loss of dynamic range in the digital domain due to loss in the analog domain. Therefore, in all of the three stages, potential sources of noise were tried to be limited by appropriate selections of the resistors, and integrated devices.

3.9.2 Wilson Central Terminal

Wilson central terminal is used as reference for unipolar measurements of chest electrodes V1 to V6. As shown in Figure 3-9, WCT is constructed by obtaining the average of the potentials at right arm (RA), left arm (LA), and left leg (LL) using equal valued resistors. Each lead is buffered to minimize loading effects on the leads. Since the impedance mismatch at the inputs of the instrumentation amplifier leads to common mode to differential signal conversion, additional buffer (Op-amp 4) is used to provide impedance matching between the differential inputs of the instrumentation amplifier.

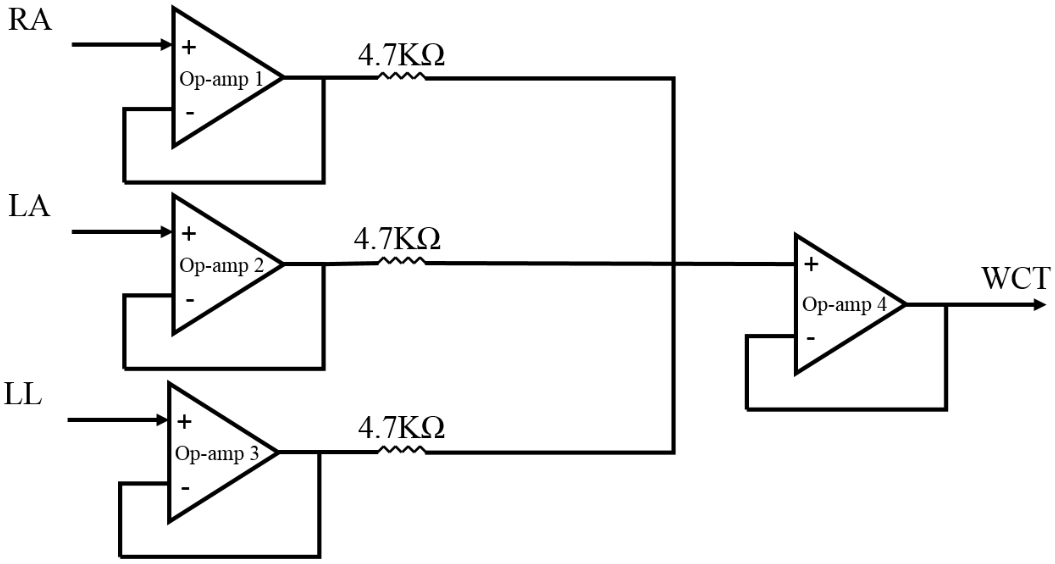

Figure 3- 9: Wilson Central Terminal (WCT)

3.9.3 Right Leg Drive

As explained in section 3.6, right leg drive is the standard method to reduce the common mode voltage caused by the patient. Winter and Webster recommends optimization for the RLD circuit; however, in many cases non-optimal one also works properly because of two reasons: (1) reduced common mode voltage is below the sensitivity of the circuit, (2) common mode voltage from other sources are larger than the common mode voltage that comes from patient's body. Figure 3-10 shows the RLD circuit designed for this circuit.

The gain of the RLD circuit and the ratio of the current limiting resistor to electrode resistance are:

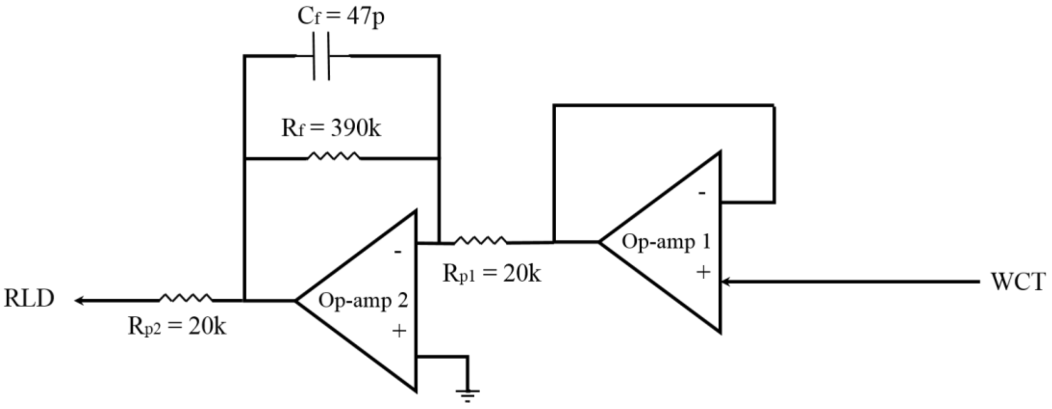

Figure 3- 10: RLD

$$G = -\frac{R_f}{R_{p1}} = -\frac{390k\Omega}{20k\Omega} = 19.5 \quad (3\text{-}7)$$

$$\frac{R_{p2}}{R_e} = \frac{20k\Omega}{2k\Omega} = 10 \quad (3\text{-}8)$$

then, the effective resistance will be obtained as:

$$R_c = \frac{R_{p2}+R_e}{G+1} = 1.46k\Omega \quad (3\text{-}9)$$

As a result of a reduction in the effective resistance R_C, V_C will be decreased.

The bandwidth of the RLD can be calculated as:

$$f_{BW} = \frac{1}{2\pi R_f C_f} = 8.68kHz \quad (3\text{-}10)$$

3.10 Conclusion and Improvements

In this chapter, the criteria that should be met by standard ECG analog front-end were discussed. Different standards were explained. Unipolar and bipolar measurements were explained. DC and AC couplings were compared. Finally, general infrastructure of the design was given and with respect to all these explanations, the ECG analog front-end designed in this study was presented.

In sections 3.1 and 3.2, safety parameters that are recommended by well-known standards were explained in detail and a typical design was developed. However, in this study we did not aim to use the device together with a defibrillator and in surgical conditions. Therefore, in the developed ECG analog front-end, these sections are disregarded and left to future works.

CHAPTER 4

EXPERIMENTAL RESULTS

In this chapter, performance evaluations of the designed analog front end are presented. These performance tests include frequency response, differential mode and common mode gains and linearity, noise, cross talk. In addition, methods and circuits used to make the measurements to apply these tests are explained in detail in corresponding sections.

The circuit implemented on a PCB is shown in Figure 4-1.

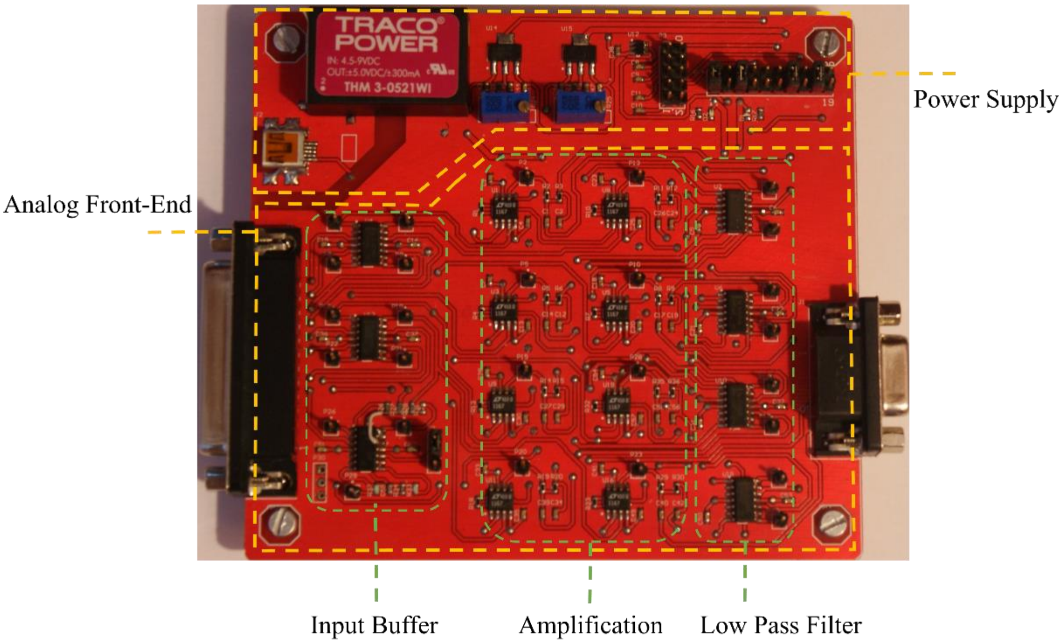
Power Supply
Analog Front-End
Input Buffer
Amplification
Low Pass Filter

Figure 4- 1: Analog front end and Power supply.

The following equipments are used for the experiments in this thesis.

- Function generator: Agilent 33120A (Sections 4.1, 4.2, 4.3, 4.4, 4.5, 4.6)

- Oscilloscope 1: Rigol DS1104Z (Sections 4.1, 4.2, 4.3, 4.4, 4.5, 4.6)
- Oscilloscope 2: Analog Discovery (Sections 4.7, 4.8)
- Power supply: Agilent E3631A (Sections 4.1, 4.2, 4.3, 4.4, 4.5, 4.6, 4.7, 4.8)
- ECG simulator: ST Electromedicina (Section 4.7)

4.1 Input Impedance

The setup in Figure 4-2 is used to measure the input impedance for each channel. Sinusoidal inputs with amplitude 200mVp-p and frequencies 100Hz and 500Hz are applied to each channel and outputs of the corresponding channel are measured in the presence of $\boldsymbol{Z_{test}}$. According to Table 3-3, input buffer op-amps have high input impedance as much as 10TΩ. Therefore, very high input impedances are expected to be observed. Since the output is equal to $\boldsymbol{V_{in}}$ multiplied by the gain factor of the amplifier, $\boldsymbol{V_{in}}$ can be calculated by dividing the measured output by the channel gain, which is 14, according to theory (which will also be measured and evaluated in Section 4.2).

$$G = \frac{V_{out}}{V_{in}} = 14 \tag{4-1}$$

Using the measured output voltages in Equation (4-1), $\boldsymbol{V_{in}}$ for each channel are calculated. By neglecting source impedance and using Equation (4-2), the input impedances of the channels are calculated for the two different values of input frequency as given in Table 4-1.

$$Z_{in} = Z_{test}\frac{V_{in}}{V_s - V_{in}} \tag{4-2}$$

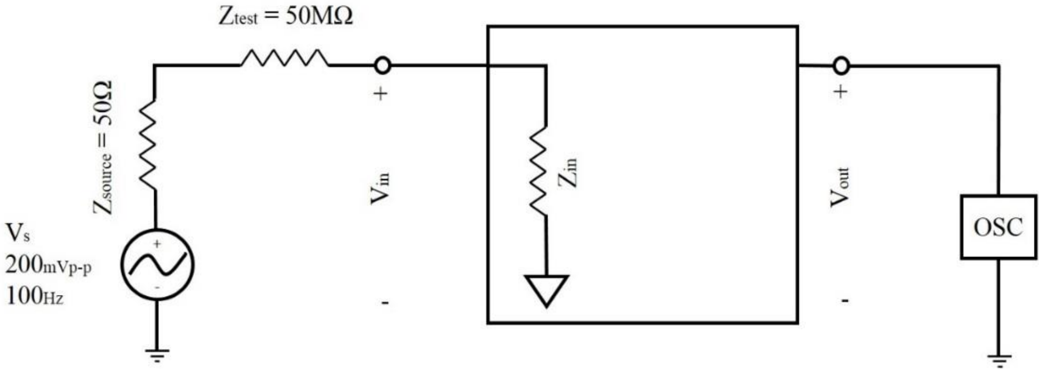

Figure 4- 2: Setup used for input impedance measurement

Table 4- 1: Measured input impedance

Frequency (Hz)	**V1 (GΩ)**	**V2 (GΩ)**	**V3 (GΩ)**	**V4 (GΩ)**	**V5 (GΩ)**	**V6 (GΩ)**	**Lead I (GΩ)**	**Lead II (GΩ)**
100	1.95	1.95	1.9	1.95	1.95	1.8	1.95	1.95
500	0.0666	0.0666	0.0666	0.0442	0.0442	0.0442	0.0442	0.0442

4.2 Differential Mode Gain

Each channel of the analog front end is examined to determine their individual frequency responses. Figure 4-3(a) and Figure 4-3(b) show the configurations used to measure the frequency responses of unipolar and bipolar channels, respectively. For unipolar channels, 100mVp-p sinusoidal signal is applied to channels V1 to V6, while the reference electrode is connected to the analog front end ground using jumper P31. Because the differential input is sinusoidal, we need to connect the reference electrode to make the differential measurement with respect to reference value. This is done by P31 by connecting reference electrode to ground of the ECG front end. For bipolar channels, as shown in Figure 4-3(b), one of the inputs is connected to the 100mVp-p sinusoidal differential signal.

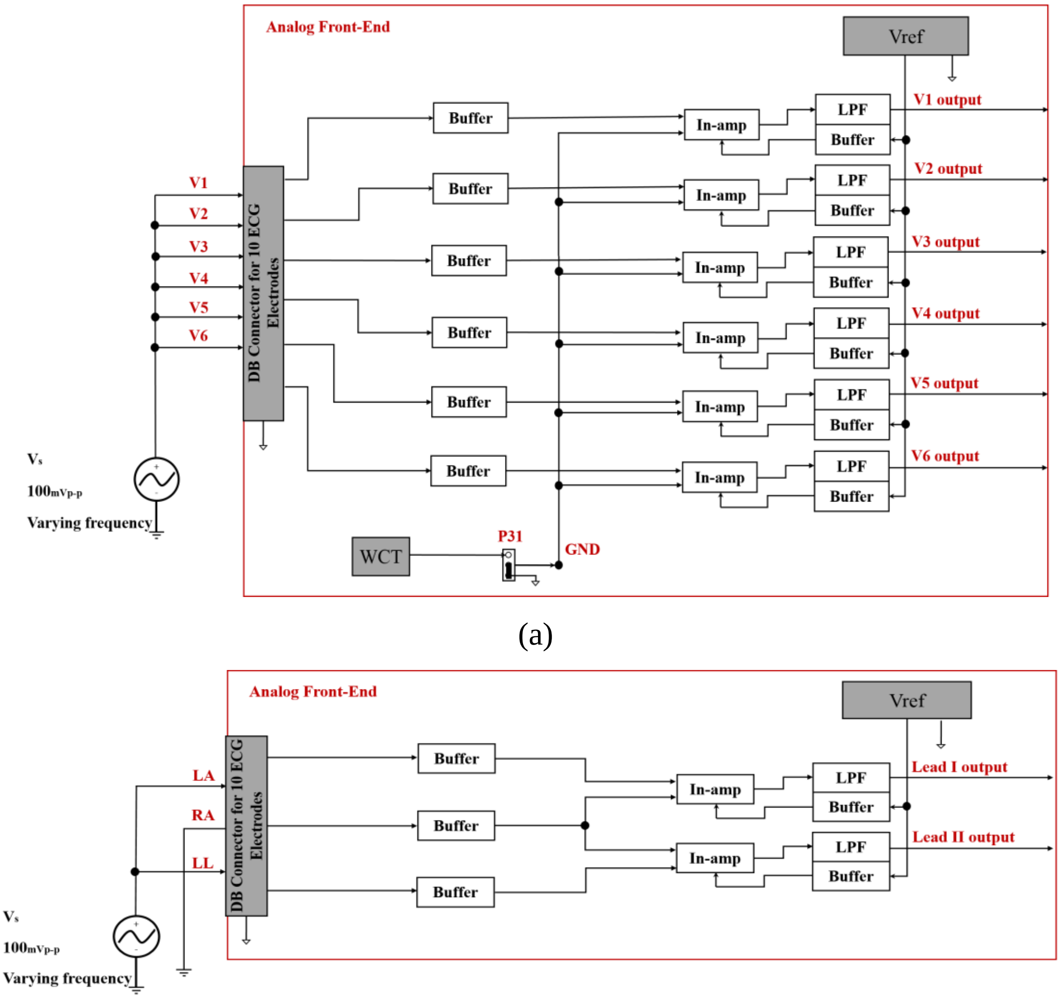
Analog Front-End
Vref
V1
V2
V3
V4
V5
V6
DB Connector for 10 ECG Electrodes
Buffer
In-amp
LPF
V1 output
V2 output
V3 output
V4 output
V5 output
V6 output
Vs
100mVp-p
Varying frequency
WCT
P31
GND
LA
RA
LL
Lead I output
Lead II output

(a)

(b)

Figure 4-3: Configurations used for differential mode frequency response, (a) setup to measure frequency response of unipolar channels, (b) setup used to measure frequency response of bipolar channels

To record the frequency responses of the channels, the frequency of the differential input signal is altered between 0.01Hz and 1kHz. For each frequency, amplitudes and phases of the outputs of the low pass filters are measured as it is demonstrated in Figure 4.4. Figure 4-4a and Figure 4-4b illustrate the print screens of the outputs of the unipolar channels V1 and V4 at 10Hz and 500Hz, respectively. Figure 4-4c and Figure 4-4d also show the outputs of the bipolar Lead I and Lead II at 50Hz and 1kHz, respectively.

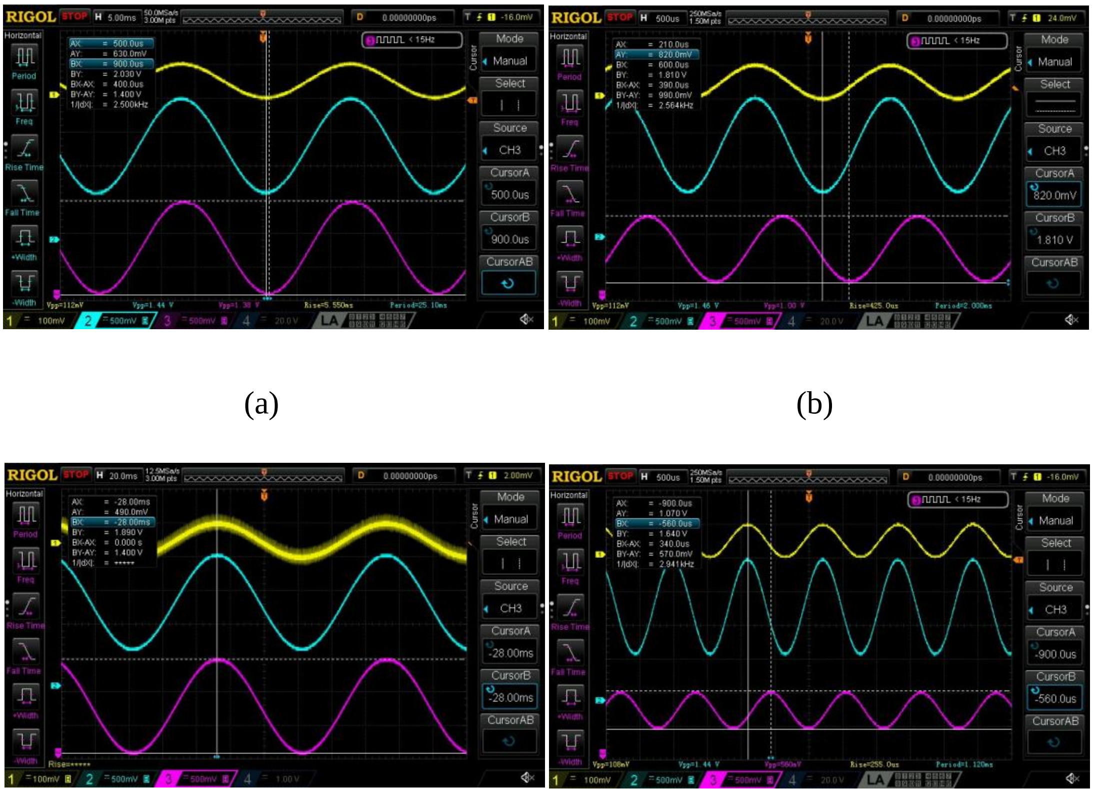

(a) (b)

(c) (d)

Figure 4- 4: The oscillogram of differential mode gain responses. Yellow signal is the differential 100mVp-p input signal, turquoise is the signal amplified by factor of 14 by instrumentation amplifier, and the pink signal is the output of the low pass filter, (a) channel V1 responses for 10Hz input, (b) channel V4 responses for 500Hz input, (c) bipolar Lead I responses for 50Hz input, (d) bipolar Lead II responses for 1000Hz input

Table 4-2 lists the amplitude and phase measurements for each channel at different input frequencies. Figure 4-5 also represents bode diagram of the frequency responses (gain response, in panel (a) and phase response, in panel (b)) of the unipolar channels V1 to V6 and bipolar Lead I and Lead II. Both the gain and phase responses are in coordination with transfer function given in Equation (3-6) and its plot in Figure 3-8.

Table 4- 2: Differential mode amplitude and phase measurements

Frequency (Hz)	V1		V2		V3		V4	
	Amplitude (V)	Phase (deg)	Amplitude (V)	Phase (deg)	Amplitude (V)	Phase (deg)	Amplitude (V)	Phase (deg)
0.01	1.4	0.00	1.4	0.00	1.4	0.00	1.4	0.00
0.05	1.4	0.00	1.4	0.00	1.4	0.00	1.4	0.00
0.1	1.4	0.00	1.4	0.00	1.4	0.00	1.4	0.00
0.5	1.4	0.00	1.4	0.00	1.4	0.00	1.4	0.00
1	1.4	0.00	1.4	0.00	1.4	0.00	1.4	0.00
2	1.4	0.00	1.4	0.00	1.4	0.00	1.4	0.00
3	1.4	0.00	1.4	0.00	1.4	0.00	1.4	0.00
4	1.4	0.00	1.4	0.00	1.4	0.00	1.4	0.00
5	1.4	0.00	1.4	0.00	1.4	0.00	1.4	0.00
6	1.4	0.00	1.4	0.00	1.4	0.00	1.4	0.00
7	1.4	0.00	1.4	0.00	1.4	0.00	1.4	0.00
8	1.4	0.00	1.4	0.00	1.4	0.00	1.4	0.00
9	1.4	0.00	1.4	0.00	1.4	0.00	1.4	0.00
10	1.4	0.00	1.4	0.00	1.4	0.00	1.4	0.00
20	1.4	-2.88	1.4	-1.44	1.4	-2.88	1.4	-2.88
30	1.4	-4.32	1.4	-4.32	1.4	-4.32	1.4	-4.32
40	1.4	-5.76	1.4	-5.76	1.4	-5.76	1.4	-5.76
50	1.4	-7.20	1.4	-5.40	1.4	-7.20	1.4	-7.20
60	1.4	-10.80	1.4	-8.64	1.4	-8.64	1.4	-8.64
70	1.4	-10.08	1.4	-10.08	1.4	-10.08	1.4	-10.08
80	1.4	-11.52	1.4	-11.52	1.4	-11.52	1.4	-11.52
90	1.4	-12.96	1.4	-12.96	1.4	-12.96	1.4	-12.96
100	1.4	-14.40	1.4	-14.40	1.4	-14.40	1.4	-14.40
200	1.32	-31.68	1.31	-28.80	1.35	-27.36	1.31	-28.80
300	1.27	-49.68	1.27	-43.20	1.24	-46.44	1.24	-43.20
400	1.14	-66.24	1.14	-57.60	1.14	-61.92	1.12	-56.16
500	0.99	-72.80	0.99	-70.20	0.99	-71.40	0.99	-70.20
600	0.90	-84.24	0.89	-84.24	0.89	-82.08	0.09	-77.76
700	0.78	-98.28	0.77	-97.78	0.78	-93.24	0.77	-90.72
800	0.644	-106.56	0.66	-104.83	0.66	-102.53	0.66	-97.92
900	0.556	-112.75	0.56	-110.16	0.57	-110.16	0.548	-110.16
1000	0.476	-118.08	0.50	-122.40	0.48	-116.64	0.472	-115.20

Table 4- 2 (continued)

Frequency (Hz)	**V5**		**V6**		**Lead I**		**Lead II**	
	Amplitude (V)	**Phase (deg)**	**Amplitude (V)**	**Phase (deg)**	**Amplitude (V)**	**Phase (deg)**	**Amplitude (V)**	**Phase (deg)**
0.01	1.4	0.00	1.4	0.00	1.4	0.00	1.4	0.00
0.05	1.4	0.00	1.4	0.00	1.4	0.00	1.4	0.00
0.1	1.4	0.00	1.4	0.00	1.4	0.00	1.4	0.00
0.5	1.4	0.00	1.4	0.00	1.4	0.00	1.4	0.00
1	1.4	0.00	1.4	0.00	1.4	0.00	1.4	0.00
2	1.4	0.00	1.4	0.00	1.4	0.00	1.4	0.00
3	1.4	0.00	1.4	0.00	1.4	0.00	1.4	0.00
4	1.4	0.00	1.4	0.00	1.4	0.00	1.4	0.00
5	1.4	0.00	1.4	0.00	1.4	0.00	1.4	0.00
6	1.4	0.00	1.4	0.00	1.4	0.00	1.4	0.00
7	1.4	0.00	1.4	0.00	1.4	0.00	1.4	0.00
8	1.4	0.00	1.4	0.00	1.4	0.00	1.4	0.00
9	1.4	0.00	1.4	0.00	1.4	0.00	1.4	0.00
10	1.4	0.00	1.4	0.00	1.4	0.00	1.4	0.00
20	1.4	-2.88	1.4	-2.88	1.4	-2.88	1.4	-2.88
30	1.4	-4.32	1.4	-4.32	1.4	-4.32	1.4	-4.32
40	1.4	-5.76	1.4	-5.76	1.4	-5.76	1.4	-5.76
50	1.4	-7.20	1.4	-7.20	1.4	-7.20	1.4	-7.20
60	1.4	-8.64	1.4	-8.64	1.4	-8.64	1.4	-8.64
70	1.4	-10.08	1.4	-10.08	1.4	-10.08	1.4	-10.08
80	1.4	-11.52	1.4	-11.52	1.4	-11.52	1.4	-11.52
90	1.4	-12.96	1.4	-12.96	1.4	-12.96	1.4	-12.96
100	1.4	-14.40	1.4	-14.40	1.4	-14.40	1.4	-14.40
200	1.33	-28.80	1.33	-28.80	1.32	-28.80	1.32	-28.80
300	1.25	-43.20	1.25	-43.20	1.25	-43.20	1.25	-43.20
400	1.13	-57.60	1.13	-57.60	1.16	-57.60	1.16	-57.60
500	0.99	-71.60	0.99	-70.20	0.99	-72.00	0.99	-72.00
600	0.88	-79.92	0.88	-92.88	0.88	-86.40	0.87	-84.24
700	0.75	-93.24	0.75	-95.76	0.76	-95.76	0.76	-95.76
800	0.66	-100.80	0.66	-103.68	0.65	-106.56	0.66	-106.56
900	0.57	-110.16	0.57	-110.16	0.56	-113.40	0.56	-116.64
1000	0.49	-118.80	0.49	-118.80	0.48	-118.80	0.49	-118.80

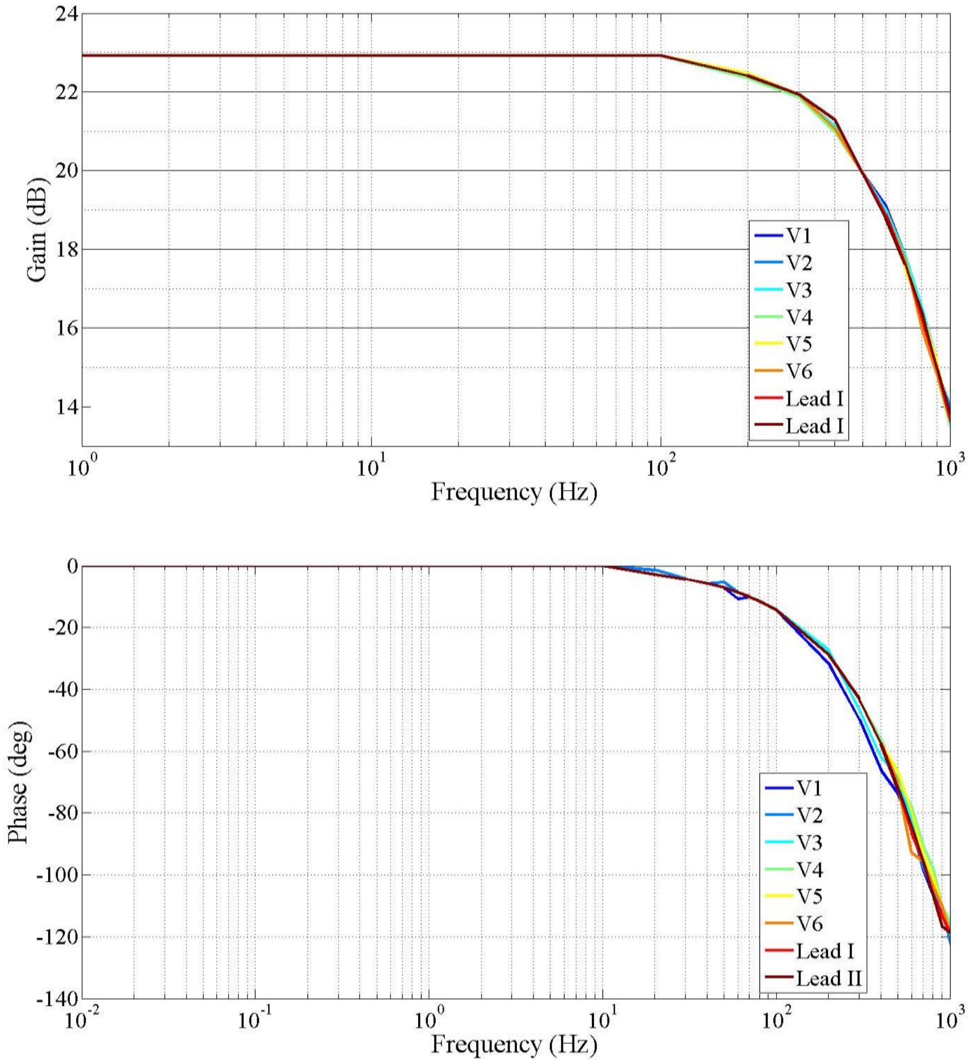

Figure 4- 5: Bode plot of the frequency response of the unipolar channels V1 to V6 plus bipolar Lead I and Lead II

In addition, -3dB cutoff frequencies of channels are measured by sweeping frequencies close to central 500Hz with accuracy ± 2Hz as given in Table 4-3. Since all the components used in the channels are chosen with attention to be same as much as possible, it is expected that the frequency responses of the channels to be very close to each other. With respect to gain of the instrumentation amplifier and also the transfer function of the LPF, at cutoff frequency expected gain and phase are 19.96 dB and -76°. Therefore, for a given differential input, 100mVp-p, it is predicted to measure 0.994Vp-p at the output of the LPF. As given in Table 4-2, 0.99Vp-p is measured in the output of the LPF stages that show 4mVp-p deviation from theoretical value. This deviation comes from the gain of the instrumentation amplifier that is measured as 14 instead of 14.068.

Table 4- 3: Measured -3dB cutoff frequencies

Channel	Expected -3dB Cutoff (Hz)	Measured -3dB Cutoff (Hz)
Channel V1	500	500 ± 2
Channel V2	500	500 ± 2
Channel V3	500	500 ± 2
Channel V4	500	500 ± 2
Channel V5	500	500 ± 2
Channel V6	500	500 ± 2
Lead I	500	500 ± 2
Lead II	500	500 ± 2

In conclusion, deviations from intended 500Hz cutoff frequency are resulted by: (1) imperfect resistors R1 and R2 (Figure 3-8(a)), (2) the paths from instrumentation amplifier to LPF stages which should be kept as short as possible.

Last experiment on differential mode behavior of the designed ECG analog front end is the differential gain linearity. Gain linearity is an important parameter in the ECG data acquisition systems. Signals with different amplitudes have to be amplified with the same magnitude. In addition, the maximum gain error recommended for the recorded signals by AHA is 25μV. Therefore, it is important to keep track of the gain and resulting output level.

To check the linearity of the gain, sinusoidal signals with frequency of 10Hz and 500Hz, but varying amplitudes are applied to the inputs of the ECG front end. With respect to the LT1167 datasheet, theoretical amplification factor is equal to:

$$G = \frac{49.4k\Omega}{R_g} + 1 = \frac{49.4k\Omega}{3.78k\Omega} + 1 = 14.068 \qquad (4\text{-}3)$$

Figure 4-6 and Figure 4-7 plot the output vs. input at 10Hz and 500Hz respectively. The related error are calculated and represented for 10Hz and 500Hz in Table 4-4 and Table 4-5.

From Figures 4-6 can be interpreted that the gain remains linear following closely the expected gain given in Equation (4-3) up to 300mVp-p. DC offset led from electrode skin contact interface can reach to ±300V [6]. Therefore, with respect to the gain of 14, even for ±300mV DC offset, these ECG front end channels behave linear. The maximum error remains less than 2% for the inputs equal to 300mVp-p; however, for inputs larger than 300mVp-p the output buffer of low pass filter is saturated and causes non-linearity.

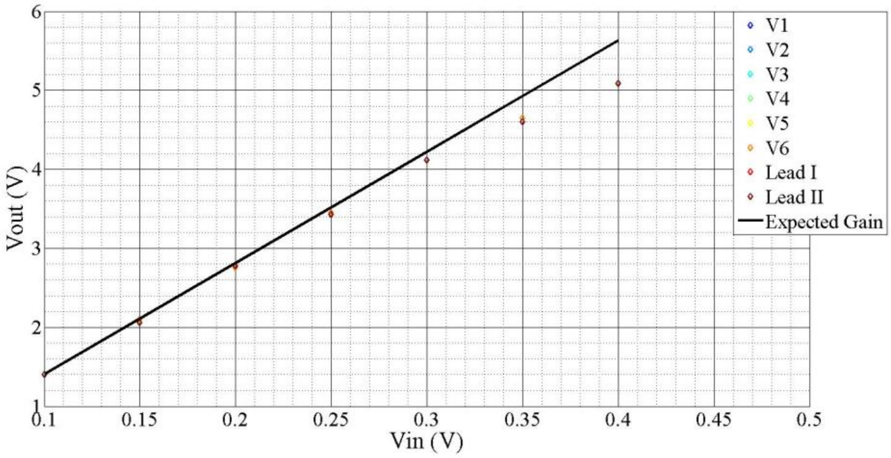

Figure 4- 6: Differential gain linearity at 10Hz

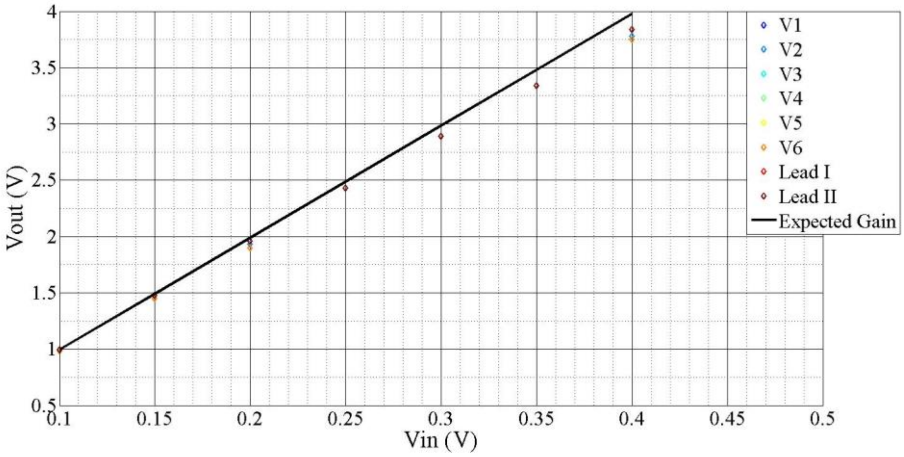

Figure 4- 7: Differential gain linearity at 500Hz

4.3 Common Mode Gain

Common mode rejection is one of the key performance criteria of the ECG analog front end. As discussed in Section 3.6, common mode signal can influence the analog front end in different ways; however, the patient body is the main source of the interference in the bio-applications.

Since the common mode signal would be attenuated by the instrumentation amplifier in the second stage of the designed analog front end (Refer to Figure 3-7a and Figure 3-7b), it is expected that the output corresponding to the common input signal to be very small, in the μV range. Therefore, special experimental setup is required to measure the response of the circuit to common mode input signal. For this purpose, post-amplifiers in Figure 4-8a and Figure 4-8b are recommended by Texas Instrument and Analog Devices. If we assume that the maximum sensitivity of the oscilloscope is 1mV/div and if we adjust the gain of the configurations in Figure 4-8 to 1000, then the working sensitivity would increase to 1μV/div which will be sufficient to measure the common mode signals attenuated by the CMRR larger than 100dB.

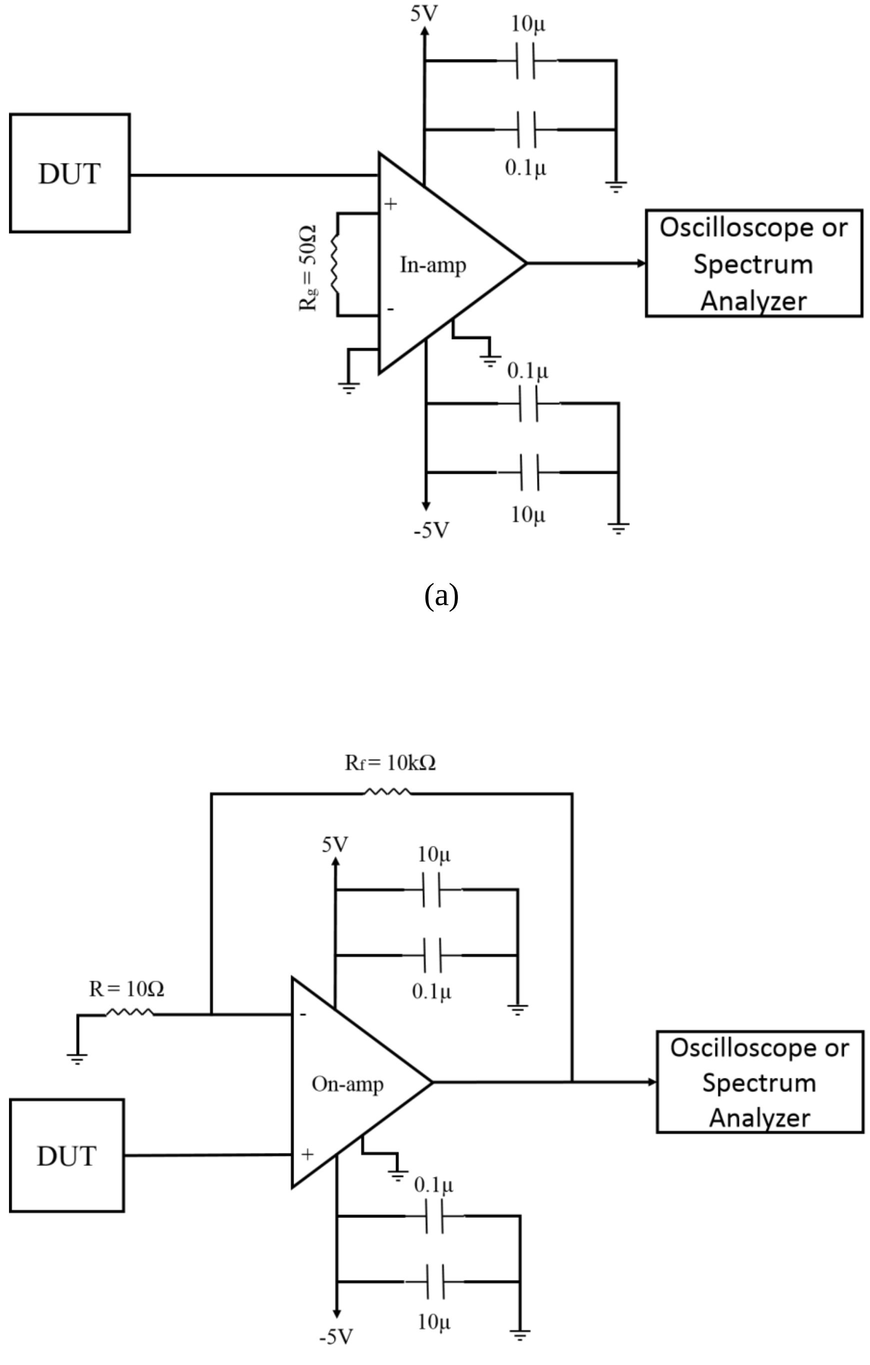
5V
10μ
0.1μ
DUT
+
In-amp
-
$R_g = 50\Omega$
Oscilloscope or Spectrum Analyzer
0.1μ
10μ
-5V
$R_f = 10k\Omega$
5V
10μ
0.1μ
R = 10Ω
-
On-amp
+
DUT
Oscilloscope or Spectrum Analyzer
0.1μ
10μ
-5V

(a)

(b)

.

Figure 4- 8: Post-amplifiers for high CMRR measurement using (a) non-inverter configuration using op-amp, (b) instrumentation amplifier

One important factor about using post amplifiers shown in Figure 4-6 is the noise level of the component and equipment used in the measurement setups. TI recommends that the noise floor of the device under test (DUT) should be greater than the three times of the noise floor of the equipment, either the oscilloscope or the spectrum analyzer used in the measurements [52]. Another important parameter is the noise contribution of the post amplifier used in the measurement configuration. To ignore the noise impact of the post amplifier, TI recommends that noise floor of the post-amplifier must be at least three times less than noise floor of the DUT [52]. Finally, post-amplifier used in any of the configurations must support the bandwidth requirements of the amplification. The feasibility of both recommendations is tested by increasing the power rails to ±15V and applying 100mVp-p, 100Hz sinusoidal input signal. To measure the common mode gain in our ECG front end, we used the configuration in Figure 4-6a. LT1167 is used as the post-stage instrumentation amplifier. With noise floor of $7.5\mathrm{nV}/\sqrt{\mathrm{Hz}}$ and bandwidth of 12kHz at the gain of 1000, it seems appropriate for our requirements.

With respect to AAMI standards, to measure the common mode gain and common mode rejection ratio, all the inputs have to be connected to the common mode signal. Therefore, to measure the common mode gain in our ECG analog front end, the configuration in Figure 4-9 is used. With respect to datasheet of the LT1167, the maximum common mode voltage range is restricted to +Vs−1.3V and –Vs+2.1. For this setup, 3.3Vp-p common mode voltage is applied to the DUT while the RLD and WCT are configured as shown in Figure 4-9 using P30 and P31. By configuring P31 to WCT, WCT is used as a reference electrode for the common mode gain measurements of unipolar channels. P30 also connects the RLD to common mode voltage enlivening the actual common mode voltage on the body surface. Post-amplifier in Figure 4-8a is used to increase the working sensitivity of the setup. The frequency of the common mode voltage is altered between 0.1Hz and 500Hz and for frequency values within this range, the common mode output of all channels are measured and listed in Table 4-6. The bandwidth filter of the oscilloscope used for the measurements (Rigol DSO1174) is restricted to the minimum possible amount, i.e., 20MHz. Maximum measurement error for the common mode gain caused by bandwidth is approximately 8µVp-p which happens in low frequencies. With respect to Table4-6, this amount of measurement error leads to approximately 10% error in common mode gains.

Although post amplifier with large gain is used to measure the common mode gain of both unipolar and bipolar channels, the common mode gain was impossible to measure for the bipolar channels. Unipolar channels sense the same signal in the presence of WCT circuitry on the negative inputs of the instrumentation amplifiers. Therefore, any asymmetry in the averaging block of WCT may lead to common mode to differential mode conversion in the inputs of the instrumentation amplifiers. In contrast, exactly same signal is applied to both inputs of the instrumentation amplifiers in bipolar Lead I and Lead II for common mode measurements. Therefore, higher common mode rejection is expected from bipolar leads compared to unipolar channels. This may explain why we could not measure the common mode gain for bipolar leads Lead I and Lead II even with post amplification.

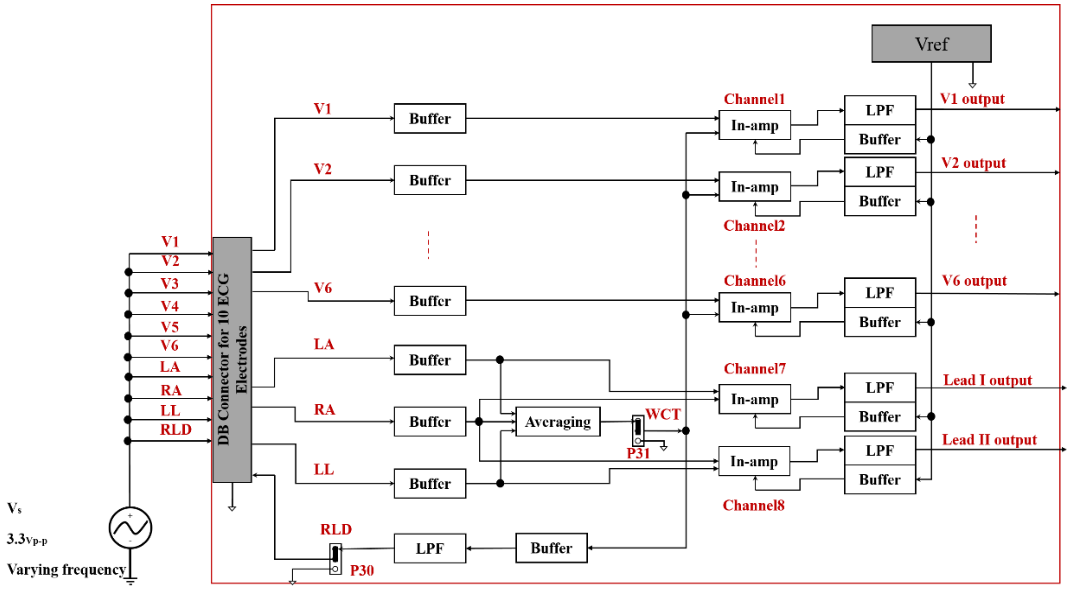
Vref
V1
V2
V6
LA
RA
LL
Buffer
Channel1
In-amp
LPF
V1 output
V2 output
Channel2
Channel6
V6 output
Channel7
Lead I output
Lead II output
Channel8
Averaging
WCT
P31
RLD
P30
DB Connector for 10 ECG Electrodes
V1
V2
V3
V4
V5
V6
LA
RA
LL
RLD
Vs
3.3Vp-p
Varying frequency

Figure 4- 9: Configurations used for common mode gain measurement

Table 4- 4: Common mode output voltage amplitude measurements for unipolar channels V1 to V6

Frequency	V1	V2	V3	V4	V5	V6
	Amplitude (µV)	Amplitude (µV)	Amplitude (µV)	Amplitude (µV)	Amplitude (µV)	Amplitude (µV)
0.5	74.00 ± 10%	74.00 ± 10%	106.00 ± 10%	92.00 ± 10%	80.00 ± 10%	104.00 ± 10%
1	74.00 ± 10%	74.00 ± 10%	106.00 ± 10%	92.00 ± 10%	80.00 ± 10%	104.00 ± 10%
2	74.00 ± 10%	74.00 ± 10%	106.00 ± 10%	92.00 ± 10%	92.00 ± 10%	104.00 ± 10%
3	74.00 ± 10%	74.00 ± 10%	110.00 ± 10%	92.00 ± 10%	92.00 ± 10%	104.00 ± 10%
4	74.00 ± 10%	74.00 ± 10%	110.00 ± 10%	92.00 ± 10%	92.00 ± 10%	98.00 ± 10%
5	74.00 ± 10%	74.00 ± 10%	110.00 ± 10%	100.00 ± 10%	98.00 ± 10%	98.00 ± 10%
6	74.00 ± 10%	74.00 ± 10%	110.00 ± 10%	100.00 ± 10%	102.00 ± 10%	102.00 ± 10%
7	96.00 ± 10%	74.00 ± 10%	116.00 ± 10%	104.00 ± 10%	106.00 ± 10%	106.00 ± 10%
8	96.00 ± 10%	98.00 ±10%	120.00 ± 10%	114.00 ± 10%	108.00 ± 10%	108.00 ± 10%
9	96.00 ± 10%	98.00 ± 10%	124.00 ± 10%	114.00 ± 10%	110.00 ± 10%	110.00 ± 10%
10	96.00 ± 10%	98.00 ±10%	126.00 ± 10%	114.00 ± 10%	118.00 ± 10%	118.00 ± 10%
20	190.00 ± 5%	184.00 ± 5%	190.00 ± 5%	182.00 ± 5%	192.00 ± 5%	192.00 ± 5%
30	264.00	268.00	268.00	286.00	262.00	256.00
40	352.00	348.00	348.00	344.00	340.00	336.00
50	412.00	430.00	424.00	412.00	416.00	420.00
60	504.00	520.00	500.00	480.00	500.00	496.00
70	590.00	600.00	580.00	570.00	570.00	560.00
80	660.00	670.00	670.00	650.00	650.00	660.00
90	740.00	760.00	730.00	720.00	720.00	730.00
100	820.00	840.00	840.00	810.00	800.00	790.00
200	1580	1580	1540	1500	1580	1580
300	2160	2200	2160	224\	2160	2160
400	2720	2760	2600	2600	2620	2620
500	2880	2880	2880	2880	2680	2880

Figure 4-10 illustrates measurements from channel V1, and channel V5 at 10Hz. and 500Hz. As shown in the Figure 4-10a and Figure 4-10b, for each measurement, 3.3Vp-p input common mode signal, WCT, RLD, and the output of the low pass filter are evaluated. At each one, the amplitude of the output response are measured. In these figures, yellow signal is the 3.3Vp-p common input signal, the turquoise is the WCT which have to be same as the input signal. The pink signal is the RLD which also has to be the same as the input signals. The blue signal is the response to the common mode signal from which the amplitude is measured. In Figure 4-11, the common mode behavior of the channels are plotted vs. frequency. This behavior is expected with respect to the Figure 4-12 which shows the CMRR vs. frequency in LT1167 [53]. As it is shown in Figure 4-12, with $\boldsymbol{Vs = \pm 15V}$ and $\boldsymbol{G = 10}$, CMRR begins to fall slightly before 100Hz which means that the common mode gain starts to increase from that point on.

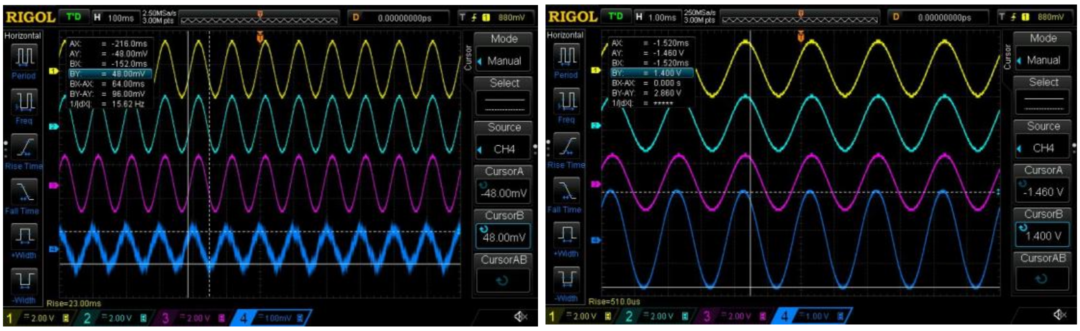

```
AX:     =  -216.0ms
AY:     =  -48.00mV
BX:     =  -152.0ms
BY:     =  48.00mV
BX-AX:  =  64.00ms
BY-AY:  =  96.00mV
1/|dX|: =  15.62 Hz
```

```
AX:     =  -1.520ms
AY:     =  -1.460 V
BX:     =  -1.520ms
BY:     =  1.400 V
BX-AX:  =  0.000 s
BY-AY:  =  2.860 V
1/|dX|: =  *****
```

RIGOL
T'D
H 100ms
2.50MSa/s
3.00M pts
D 0.00000000ps
T 880mV
Horizontal
Period
Freq
Rise Time
Fall Time
+Width
-Width
Cursor
Mode
Manual
Select
Source
CH4
CursorA
-48.00mV
CursorB
48.00mV
CursorAB
Rise=23.00ms
1 2.00 V
2 2.00 V
3 2.00 V
4 100mV
RIGOL
T'D
H 1.00ms
250MSa/s
3.00M pts
D 0.00000000ps
T 880mV
Horizontal
Period
Freq
Rise Time
Fall Time
+Width
-Width
Cursor
Mode
Manual
Select
Source
CH4
CursorA
-1.460 V
CursorB
1.400 V
CursorAB
Rise=510.0us
1 2.00 V
2 2.00 V
3 2.00 V
4 1.00 V

(a) (b)

Figure 4- 10: Common mode gain measurements. Yellow signal is the common mode 3.3V input signal, turquoise signal the signal reference electrode WCT, pink signal shows the voltage on RLD electrode, and the blue signal is the output of the low pass filter

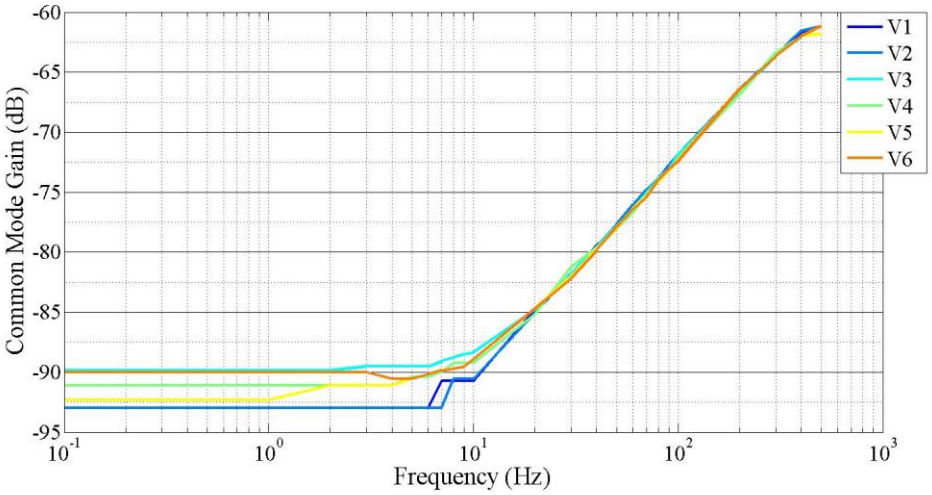

Figure 4- 11: Common mode gain vs. frequency

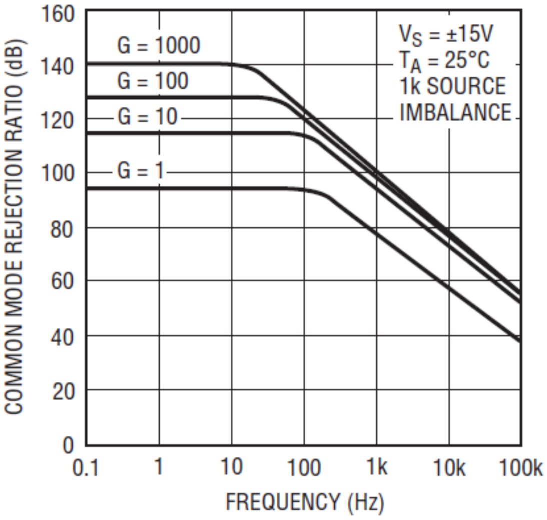

Figure 4- 12: CMRR vs. frequency characteristics of LT1167[54]

4.4 Common Mode Rejection Ratio

According to differential mode and common mode gains obtained in Section 4-2 and Section 4-3, respectively, common mode rejection ration (CMRR) can be calculated from Equation (4-4). With respect to common mode gain measurement errors given in Table 4-6, the maximum error in CMRR would be less than 1.1dB.

$$CMRR\ (dB) = 20\log_{10}\frac{A_{dm}}{A_{cm}} \qquad (4\text{-}4)$$

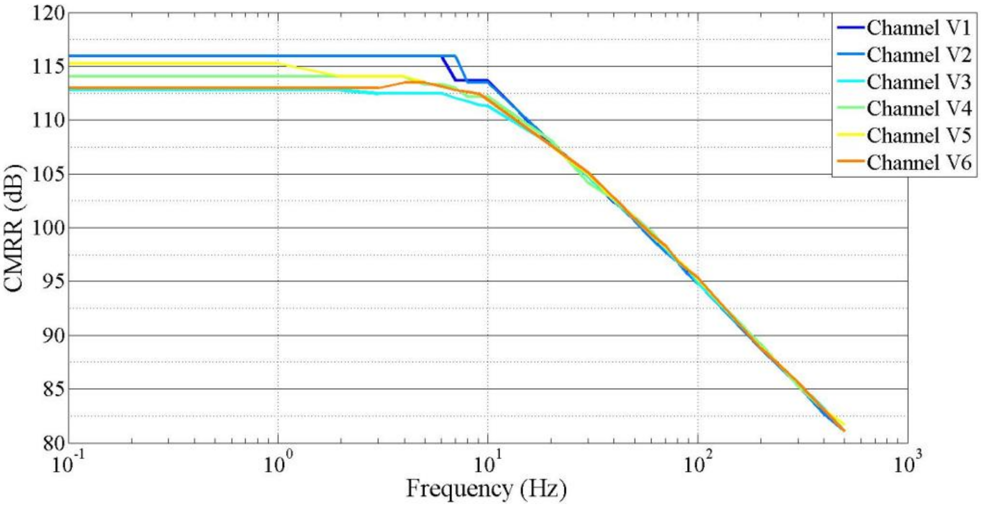

Figure 4- 13: Common mode rejection ratio

As observed from Figure 4-11, CMRR can be as high as 115 dB at low frequencies. However, it starts to decrease rapidly as frequency increases. This is because of the increase in common mode gain of the instrumentation amplifier described in the previous section. Nevertheless, within most portions of the pass-band, CMRR is above 90dB and it never drops below 82dB within the 500Hz pass-band. In comparison to CMRR characteristics of LT1167, according to Figure 4-12, CMRR starts to decrease approximately around 10Hz rather than 100Hz. This may be caused by the unequal value of resistors in WCT block. Although we tried to select resistors with values as close as possible, there is still a slight difference between them, which may be due to PCB mounting process. The most important CMRR component in ECG recordings is at 50Hz. AAMI recommended that the CMRR at 50Hz to be greater than 92dB. In our measurements as summarized in Table 4.7, CMRR remains above 100dB.

Table 4-5: CMRR measured at 50Hz

Channel	CMRR at 50Hz (dB)
V1	101
V2	100.6
V3	100.7
V4	101
V5	100.9
V6	100.8

4.5 ECG Analog Front End Noise Floor

Noise level in the ECG analog front end is another important parameter that has to be considered. According to AAMI standards, the maximum allowable peak to peak noise voltage for ECG recording devices is 30µVp-p during 10sec recordings. Hence, selecting the right components, either active or passive, would be very helpful to meet the expectations. In addition to components used in ECG analog front end, test setup is another key factor that can influence the measured noise level significantly. TI recommends the setup used for common mode gain measurements for noise measurements too. For this purpose, the configuration illustrated in Figure 4-10 is used to determine the noise floor of the designed ECG analog front end. This configuration is similar to the one used for common mode gain measurements except: (1) all inputs are connected to the analog front end common ground, (2) the reference pin of the instrumentation amplifiers are connected to the analog front end common ground to limit the noise contribution from outside of the analog front end.

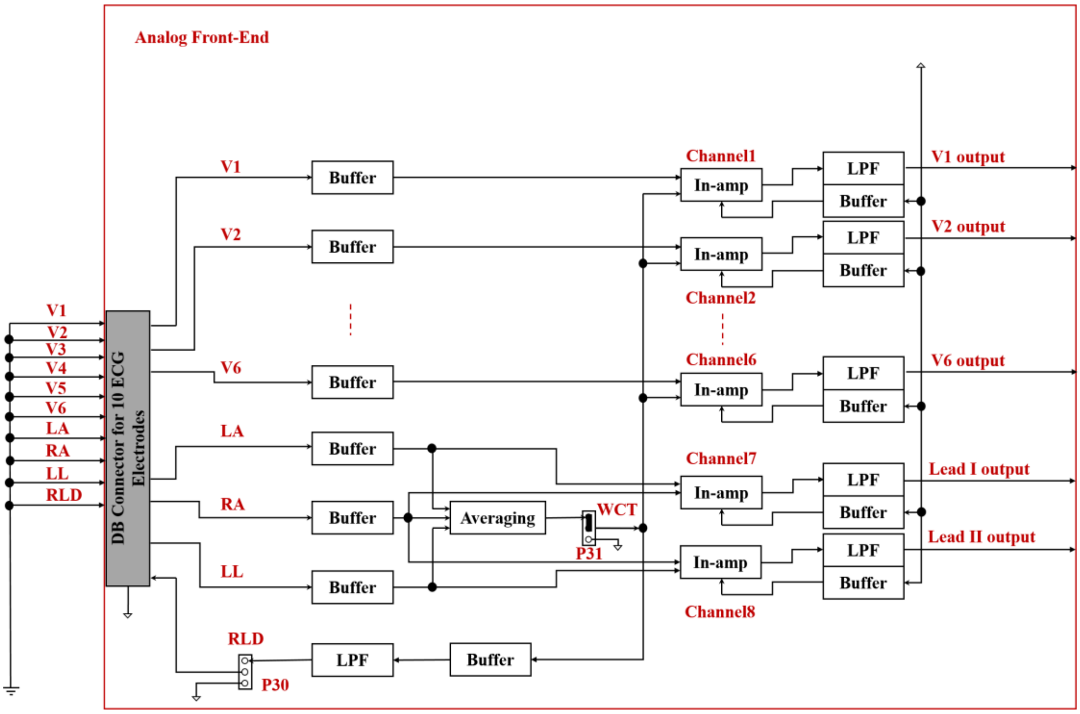
Analog Front-End
V1
V2
V3
V4
V5
V6
LA
RA
LL
RLD
DB Connector for 10 ECG Electrodes
V1
V2
V6
LA
RA
LL
RLD
Buffer
Buffer
Buffer
Buffer
Buffer
Buffer
Averaging
WCT
P31
LPF
Buffer
P30
Channel1
In-amp
Channel2
In-amp
Channel6
In-amp
Channel7
In-amp
In-amp
Channel8
LPF
Buffer
V1 output
V2 output
V6 output
Lead I output
Lead II output

Figure 4- 14: Configuration used for noise level measurement of ECG analog front end

The same post-amplifier used in the common mode gain measurements is used here again. The gain of the instrumentation amplifier is adjusted to 1000 using two parallel 100Ω resistors. The result is captured for 12sec, as recommended by AAMI, in time domain from oscilloscope to determine the peak to peak noise. The data are transferred to the computer for plotting and also further signal processing. Figure 4-11 shows the time domain plot of the measured noise level using MATLAB.

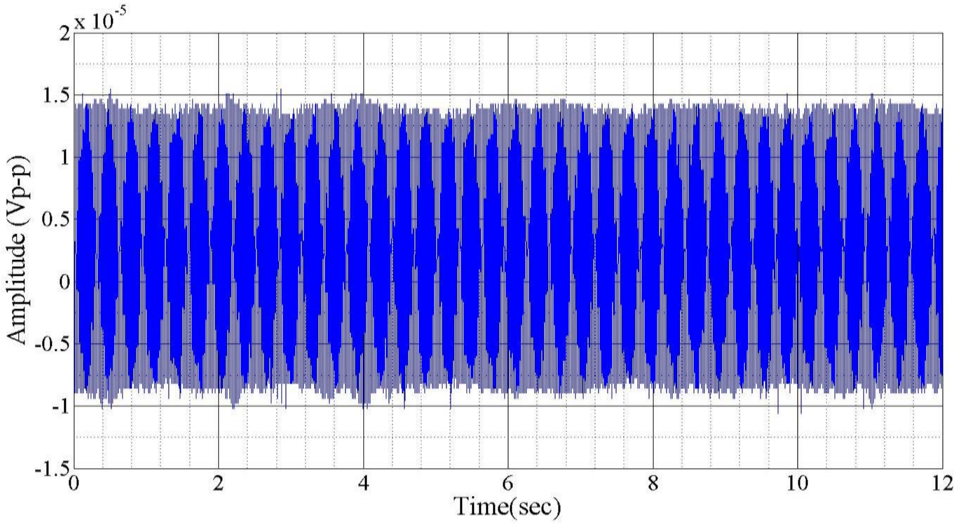

Figure 4- 15: Measured peak to peak noise floor for ECG analog front end

25µVp-p noise voltage is measured during the 12sec recording. This is less than the 30µVp-p required for AAMI standard. To determine the frequency components of the noise, Fast Fourier Transform (FFT) of the noise is calculated in MATLAB and the magnitude of this FFT is shown in Figure 4-16. 50Hz and its harmonics are obvious in this figure. This 50Hz and its harmonics come from the oscilloscope 1 (Rigol DSO1174), since it is connected to the main city network ground. In real measurements, in which ECG front end ground is isolated completely from the network ground, 50Hz and its harmonic effects are expected to be restricted to environmental interference that would be negligible.

In conclusion, LT1167, which is the same instrumentation amplifier used in the analog front end, is also used in the post-amplifier circuitry. Therefore, both ECG analog front end and post-amplifier have the same noise level. It is expected that the measured noise floor to be less than the one measured in Figure 4-15, if instrumentation amplifier with noise contribution less than 3 times of the ECG front noise level is used. Furthermore, the size of the designed PCB can be reduced significantly to decrease the area open for environmental interferences. In this way, less noise is expected to be measured.

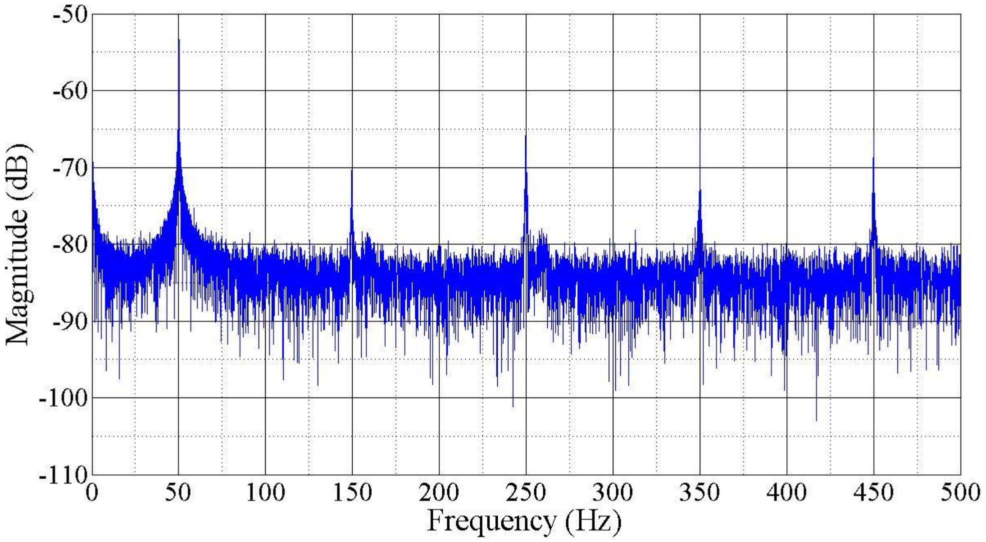

Figure 4- 16: FFT of the measured ECG analog front end noise floor. 50Hz network frequency and its harmonics are obvious in the noise spectrum

4.6 Crosstalk between Channels

Crosstalk occurs as a result of mutual inductive and capacitive couplings in the circuit [55]. As illustrated in figure 4-17, the signal propagates in aggressor trace from A to B causes coupling in the victim trace C-D via inductive and capacitive impacts. This coupling propagates both backward toward the near end point C and also forward toward far end point D. Backward crosstalk appears in the near end point C is called near end crosstalk, and forward crosstalk appears in the far end point D is called far end crosstalk [55].

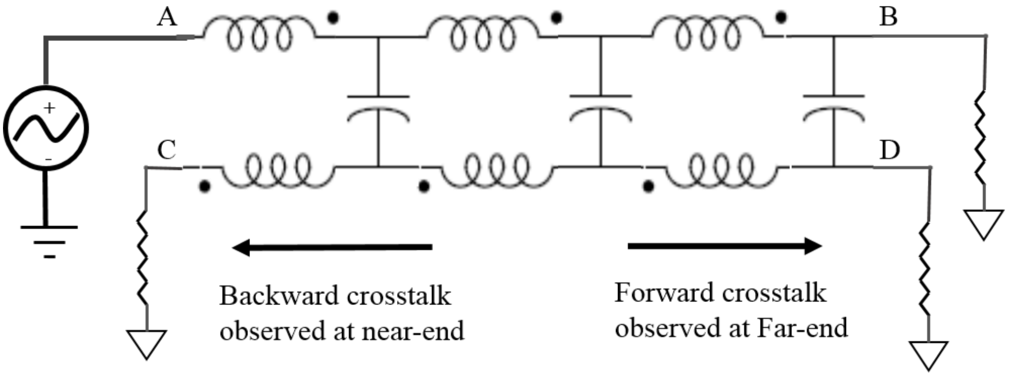

Figure 4- 17: Crosstalk as result of mutual inductive and capacitive couplings of propagating signal in aggressor trace (A-B) on victim trace (C_D)

To measure the crosstalk between channels in our ECG, 700mVp-p, 100Hz, sinusoidal signal is applied to channel V1 as aggressor trace while the other end is terminated. The remaining channels are also terminated at both ends. This configuration is shown in Figure 4-18. In Figure 4-19, the results measured from near end and far end for a given input are given. The blue signal is the signal propagating at aggressor trace, channel V1, and red signals are the measurements taken from near end and far end. As it is obvious, no crosstalk is observed either in near end or far end at 100Hz. To sweep all working bandwidth, the frequencies is increased up to 500Hz but again no crosstalk is noticed in the victim channels. This result is predictable because crosstalk usually happens at much higher frequencies in which fast rising and fallings are presented [55].

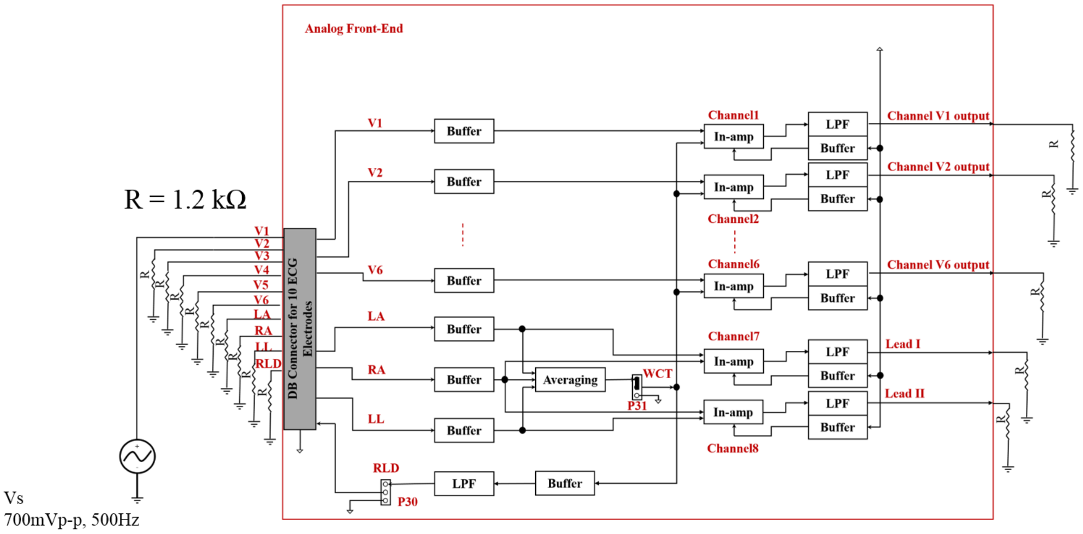
Analog Front-End
R = 1.2 kΩ
V1
V2
V3
V4
V5
V6
LA
RA
LL
RLD
R
DB Connector for 10 ECG Electrodes
Buffer
Averaging
WCT
P31
P30
LPF
In-amp
Channel1
Channel2
Channel6
Channel7
Channel8
Channel V1 output
Channel V2 output
Channel V6 output
Lead I
Lead II
Vs
700mVp-p, 500Hz

Figure 4-18: Configuration used to measure crosstalk. Channel V1 is aggressor trace carrying 700mVp-p sinusoidal signal while terminated at the other end. Remaining channels are terminated at the both end acting as victim channels

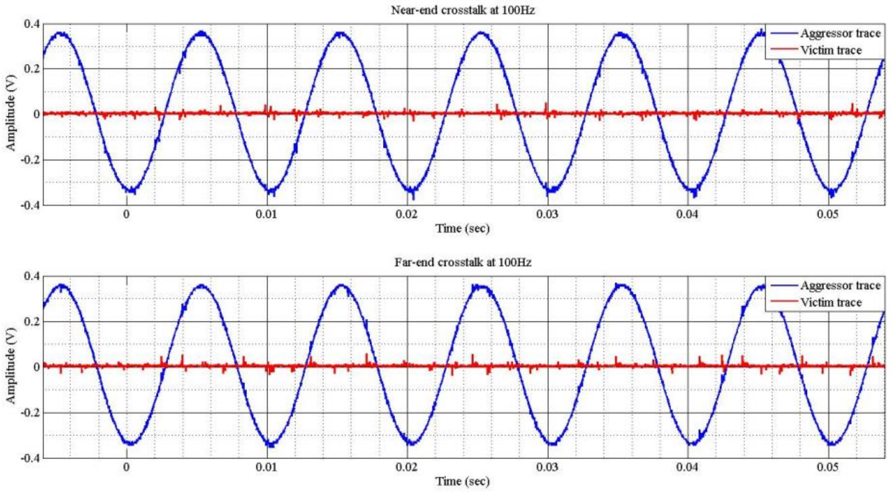

Figure 4-19: Crosstalk measured from near end and far end for a given sinusoidal input with peak value of 700mV and frequency of 100Hz. The figure at the top shows the measurement taken from near end and the one below illustrates the far end measurement

4.7 Experimental Results from ECG Simulator

In this section, the experimental results recorded from an ECG simulator are reported. For this purpose, ST-Electromedicina ECG simulator is used and the output is recorded PC-based Analog Discovery oscilloscope. ST-Electromedicina ECG simulator generates each of the chest signals, V1 to V6, RA, LA, LL and RLD separately. Figure 4-20 shows the setup used for measurements for the ECG signals generated by the simulator.

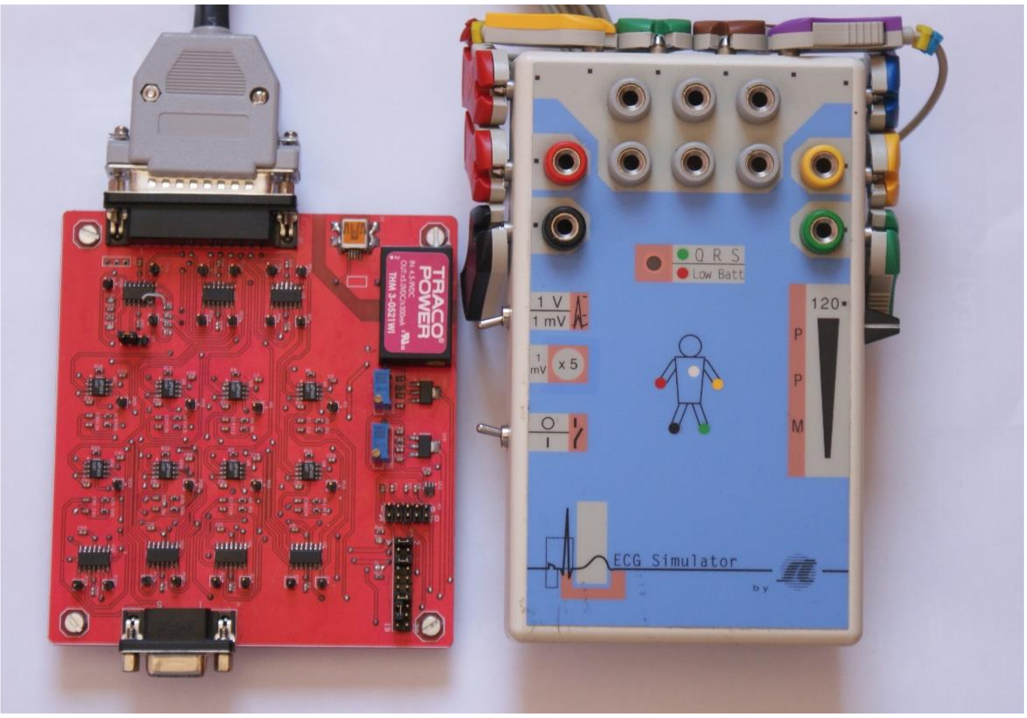

Figure 4- 20: Setup used for recordings from ECG Simulator

The simulator used in this study gives outputs for RA, LA, LL, RLD, and V1 to V6 signals separately. However, V1 to V6 signals are the same signals so at the corresponding channel outputs the same results are expected. The output amplitude of the simulator is adjusted to 1mV to enliven the actual measurement from the real person. The measurements have been done by Analog Discovery PC-based oscilloscope and numerical measurements are transferred to computer from Analog Discovery and plotted in MATLAB. Figure 4-21 shows the results of the measurements from simulator for channels V1 to V6 and leads I and II. As it is obvious from this figure, Lead II is upside down because of a mistake we made during the design of our PCB. In fact, RA electrode is connected to non-inverter input and LL electrode is connected to inverter input of instrumentation amplifier which must to be vice versa.

Figure 4- 21: ECG measurements from simulator

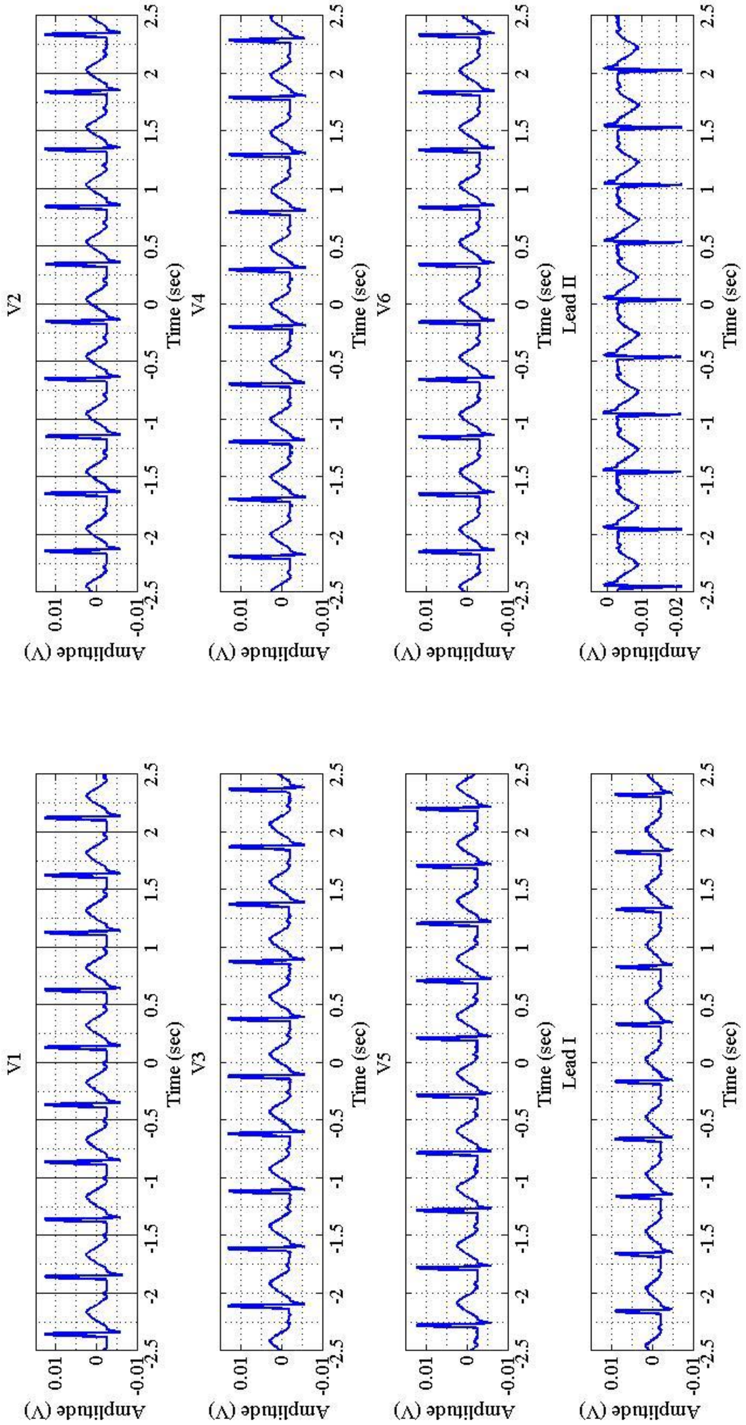

4.8 Measurement from Human Subject

In this section, experimental results measured from the human subject using 10 electrodes are represented as shown in Figure 4-22.

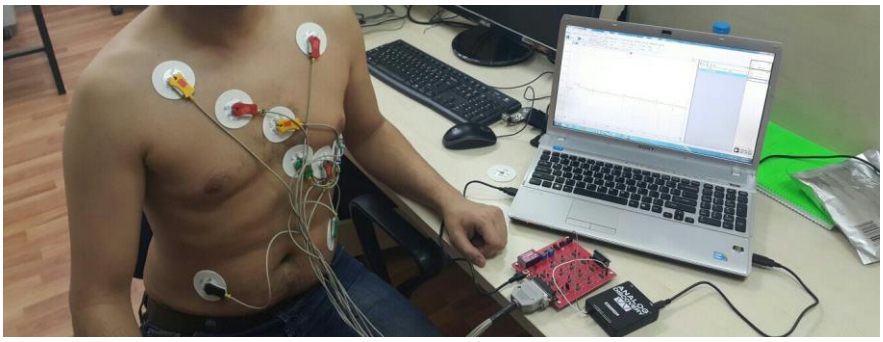

Figure 4- 22: ECG recording from real person using 10 electrodes

The measurements have been done by Analog Discovery PC-based oscilloscope and numerical measurements are transferred to computer from Analog Discovery and plotted in MATLAB. Figure 4-23 shows the unipolar channels V1 to V6 and bipolar Lead I and Lead II measured from body. Here also, Lead II is vice versa because of the mistakes have been done in PCB design. As it can be seen from Figure 4-23, there are DC offsets at each measurement. These DC values are led by two reasons: (1) electrode-skin contact interface, (2) operational amplifiers and instrumentation amplifiers. According to datasheets of OPA4140 and LT1167, we can neglect the DC offset contributions of operational amplifiers and instrumentation amplifiers; therefore, electrode-skin contact surface can be counted as the prominent source of the DC levels observed in measurements in Figure 4-23. Finally, no 50Hz interference is observed during measurements. This is because of: (1) isolation between city network ground and ECG front end ground accomplished by TracoPower, (2) optimized RLD circuit which filters the common mode interferences comes from the body [47].

Figure 4- 23: ECG measurements from human subject

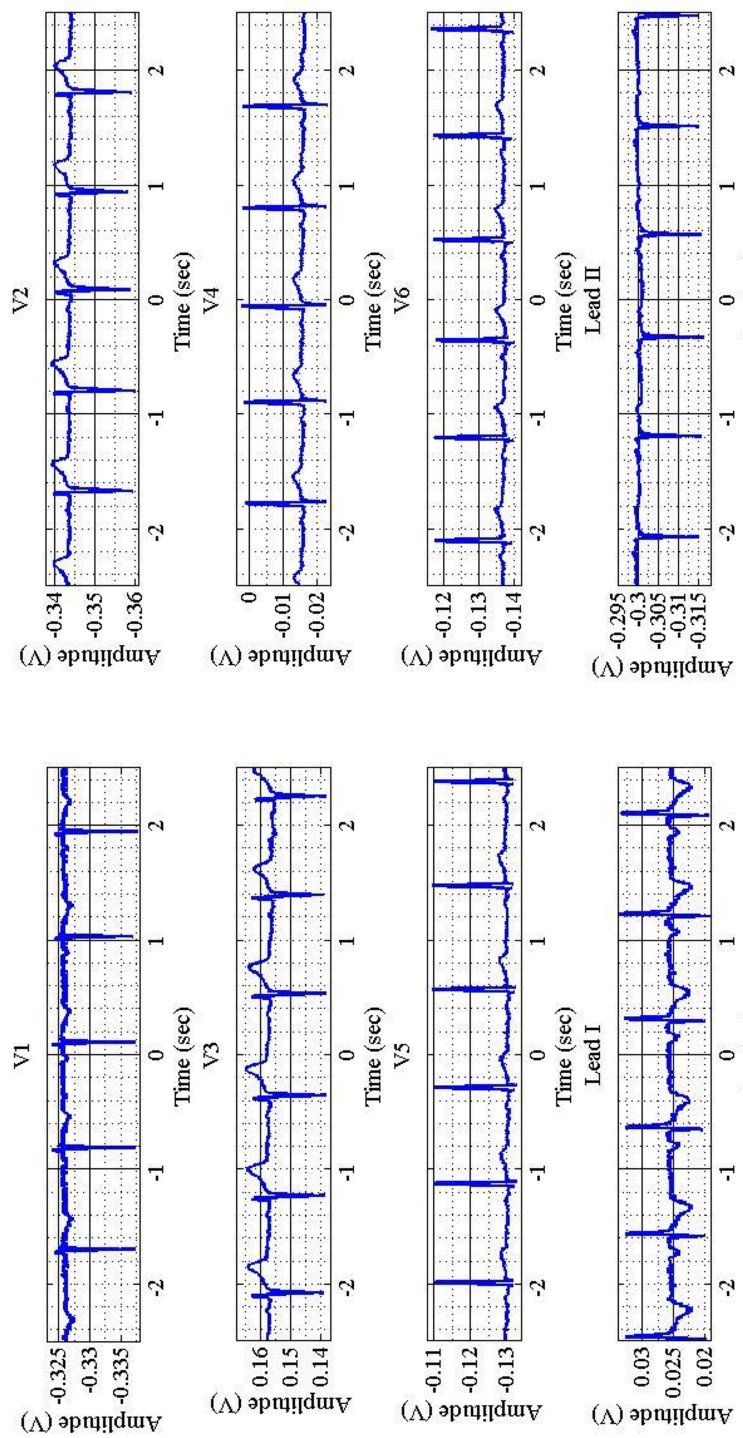

CHAPTER 5

CONCLUSION

This thesis represents and documents a design and implementation of an ECG front end circuit and its evaluations. The summary of the work is given and results are discussed. At the end, future works and potential improvements are represented.

5.1 Summary of the Thesis

In this thesis, design and implementation of ECG front end circuit is aimed. The designed power unit consists of two parts: onboard power unit, and ECG front end. It is possible to supply the required powers for ECG front end and proceeding potential digital circuitry using the onboard power unit. Traca Power DC-to-DC converter is used in the input of this unit to generate ±5V from +5V input and capable of sourcing ±300mA. ECG front end works with ±5V. Using LM317 voltage regulators, +3.3V and +1.8V are generated from +5V for potential digital circuitry. Finally 1.2V reference voltage is generated to be used both for DC shift for analog signals by applying to reference pin of instrumentation amplifier and also as a reference for ADC. Traca Power DC-to-DC converter used in the input is compatible with IEC/EN 60601-1 and AAMI/ANSI ES 60601-1:2005(R) standards for Means of Patient Protection (MOPP). It provides $5000VAC_{RMS}$ Input/Output isolation rated for $250VAC_{RMS}$ working voltage.

ECG front end designed in this thesis supports total 8 channels, six unipolar channels V1 to V6, and two bipolar channels Lead I and Lead II. Unipolar channels make the measurements with respect to WCT as a reference electrode that is built by averaging of RA, LA, and LL electrodes. To prevent electrode loading that can cause DC offset at the input, each channel is buffered using OPA4140 that has input impedance typically 10TΩ. All the channels are amplified with same gain of 14 using instrumentation amplifier and filtered using 2nd order Sallen-Key low pass filter with 500Hz cutoff frequency. RLD is also designed and optimized to gain of 19.5 (V/V) and bandwidth of 8.68kHz for common mode voltage cancellation of the noise coming from patient’s body. This ECG front end is planned to be used together with 24-bit Sigma-Delta analog digital converters. Therefore, two important issues are considered during the design to benefit the privilege of using 24-bit Sigma-Delta analog digital converters: (1), the gain is retained low because of the noise shaping characteristic of the ADC, (2) no high pass filter is used because of the high resolution of the ADC. Finally, battery is the main power source for this ECG front end. Thus, no significant 50Hz interference is expected. As a result, for the sake of simplicity, analog 50Hz notch filter is not used in any of the channels. Instead, digital 50Hz notch filter is recommended to be used to remove any 50Hz interference; this filter can be implemented either in the digital signal processor or in the user interface designed on the computer.

In the first performance experiment, input impedances of all channels are measured. Although the input impedance of the input buffers are 10TΩ, the input impedances are measured to be about 1.95GΩ. This can be caused by solder joints, even though care is taken during component mounting. However, it is still far below the 5MΩ recommended by AHA and 2.5MΩ recommended by IEC and AAMI standards.

At the second experiment, differential mode characteristics of the channels are examined. Differential gain is measured as 14(V/V). The frequency response is measured over a range of 10mHz and 1kHz and bode diagram is plotted. Cutoff frequencies are measured as approximately 500Hz for all channels. Since the resistances and capacitances used in LPFs are the same with tolerance of 1% and 5%, measuring 500Hz cutoff at channels is seems to be an acceptable result. Finally, gain linearity is considered for all channels. It is expected that the channels to be able to handle ±300mV DC offset embedded on the ECG signal. Therefore, at 10Hz we have increased the sinusoidal input amplitude up to 300mVp-p without significant loss of linearity. The measurements show the errors remain less than 2% for all channels that confirms the expectation.

At the third experiment, common mode gain is evaluated for all channels in the range of 100mHz and 500Hz. Based on the measurements, common mode gain is plotted in dB vs. frequency. From the corresponding plot, it is spotted that the common mode begins to increase at about 10Hz. With respect to LT1167 datasheet, this behavior is predicted but at about 80Hz. The difference in measurement conditions between the datasheet and our setup, such as supplies and source impedance, may be the reasons for the rise in common mode gain at lower frequencies. This would not be problem if CMRR meets the expectations over the bandwidth, especially at 50Hz.

After differential and common mode gain considerations, based on the results CMRR is calculated. As a result of common mode gain rising at about 10Hz while differential mode gain lasts constant at 22.92dB, CMRR also starts to fall at the same frequency, 10Hz. The important CMRR component in ECG recording is related to 50Hz. AAMI recommends that CMRR must be at least 92dB at 50Hz. In our design, all channels have CMRR about 101dB that meet the recommendation very well.

Measuring the noise floor is another experiment that we have done. According to AAMI standard, in 10sec of ECG recording, the measured p-p noise floor must be less than 30μV. In this study, it is measured as 25μVp-p in the designed ECG front end.

At the next experiment, crosstalk between channels is considered. By applying 700mVp-p and terminating the victim channels, frequency is swept over the working bandwidth up to 500Hz but no crosstalk is observed, neither in the near end nor in far end.

Finally to confirm the operation of the designed ECG front end with ECG data, recordings are done from an ECG simulator and from a human test subject. Both results confirm the capability of the designed ECG front end in retaining of the high quality analog recordings from electrodes.

In conclusion, with respect to performance measurements and experimental results from simulator and human body, the designed ECG front end is capable of making high quality ECG measurements from electrodes attached to the surface of the body. Therefore it can be used as front end for a high quality ECG recording device that contains digital circuitry and can transmit data to a computer for further digital signal processing.

5.2 Future Works

The design in this thesis can be used for standard 12-lead system since it contains both unipolar and bipolar measurements. It also can be a part of a larger BSPM system. Moreover, the designed ECG front end can be used for other bio-applications such as EEG and EMG recording with some modifications. Gain factor of 14 seems to be sufficient for both ECG, EEG and EMG with respect to the low gain approach discussed in section 2.7. However modification is required in the bandwidth. It can be done either by replacing resistors and capacitors of LPF by appropriate value or just doing it by code in the user interface of the computer.

There are additional features that can be added to this ECG front end. One of them is temperature measurement that is standard option in most commercial devices such as ADS1298. Pace detection can also be added to the design, however, digital algorithms to detect pace seem to be more efficient.

The ECG front end in this thesis is designed to be compatible with the 24-Sigma-Delta analog digital converters. Specifically, ADS1278 as simultaneous octal 24-Sigma-Delta is recommended as ADC. Therefore, there are works remained in digitization of data and transferring to computer. Further signal processing functions can be done on the digitized signals such as digital 50Hz notch filter.

REFERENCES

[1] "The World Health Report 2013," World Health Organization, Luxembourg, 2013.

[2] D. Jenkins, "http://www.ecglibrary.com/ecghist.html," 2009.

[3] B. He and R. J. Cohen, "Body Surface Laplacian ECG Mapping," *IEEE Transactions Biomedical Eng*, vol. 39, no. 11, pp. 1179-1191, 1992.

[4] J. Malmivuo and R. Plonsey, Bioelectromagnetism: Principle and applications of bioelectric and biomagnetic fields, New York: Oxford University Press, 1995.

[5] A. C. Guyton and J. E. Hall, Text book of medical physiology, Philadelphia: Elsevier Inc, 2006.

[6] J. G. Webster, in *Medical Instrumentation: Application and Design*, New York, John Wiley & Sons, Inc, 1998, p. 10.

[7] [Online]. Available: http://www.medic.ukm.my/ecg/trigle.html.

[8] R. Hoekema, G. J. H. Uijen, D. Stilli, and A. Van Oosterom, "Lead System Transformation of Body Surface Map Data," *Journal of Electrocardiology,* vol. 31, no. 2, pp. 71-82, 1998.

[9] Y. Wang, P. S. Cuculich and et al., "Focal atrial tachycardia after pulmonary vein isolation: Noninvasive mapping with electrocardiographic imaging (ECGI).," *Heart Rhythm*, p. 1081, 2007.

[10] P. Kligfield, R. Childers and et al., "Recommendations for the Standardization and Interpretation of the Electrocardiogram Part I: The Electrocardiogram and Its Technology: A Scientific Statement From the American Heart Association Electrocardiography and Arrhythmias Committee, Council on ...," *Journal of the American College of Cardiology,* vol. 49, no. 10, pp. 1109-1127, 2007.

[11] P. G. Postema, J. A. Korse and et al., "Local depolarization abnormalities

are the dominant pathophysiological mechanism for Type 1 electrocardiogram in Brugada Syndrome," *JACC,* pp. 789-797, 2010.

[12] A. Sippensgroenewegen, H. Spekhorst and et al., "Value of Body Surface Potential Mapping in localizing the site of origin of Ventricular Tachycardia in patients with previous Myocardial Infraction," *JACC,* pp. 1708-1724, 1994.

[13] D. M. Mirvis, "Detection of experimnetal right ventricular infraction by isopotential body surface potential mapping during sinus rythm and during ectopic ventricular pacing," *JACC,* pp. 157-163, 1987.

[14] B. Taccardi and B. Punske, "Body Surface Potential Mapping.," in *Cardiac Electrophysiology: From Cell to Bedside.*, Philadelphia, WB Saunders, 2004, pp. 803-811.

[15] D. H. Brooks and R. S. MAcLeod, "Imaging the electrical activity of the heart: direct and inverse approach.," *IEEE,* pp. 548-552, 1994.

[16] D. D. Finaly, C. D. Nugent and e. al., "Mining for diagnostic information in body surface potential maps: a comparison of feature selection techniques," *Biomed Eng. Online,* 2005.

[17] Y. Rudy, Interviewee, *Stepping Beyond ECG: Electrocardiographic Imaging.* [Interview]. Friday, 01 June 2012.

[18] B. Taccardi, P. R. Lux, R. S. Ershler and R. S. Macleod, "Potential Distributions and Excitation Time Maps Recorded with High Spatial Resolution from the Entire Ventricular Surface of Exposed Dog Hearts," *IEEE Computers in Cardiology,* pp. 1-4, 1992.

[19] M. P. Nash, C. P. Bradley, L. K. Cheng and et al., "An Experimental-Computational Framework for Validating in-vivo ECG Inverse Algorithms," *FASEB J.,* vol. 2, no. 2, p. IJBEM, 2000.

[20] D. M. Langrill and B. J. Roth, "The effect of plunge electrodes during electrical stimulation of cardiac tissue," *IEEEBME,* vol. 48, no. 10, pp. 1207-1211, 2001.

[21] L. J. Smeet, S. A. Ben-Haim and et al., "New method for nonfluoroscopic

endocardial mapping in humans: Accuracy assessment and first clinical results," *Circulation*, pp. 2426-2432, 1997.

[22] M. Eldar, A. Fitzpatrick, J. Smeet and et al., "Percutaneous multielectrode endocardial mapping during ventricular tachycardia in the swine model," *Circulation*, vol. 94, pp. 1125-1130, 1996.

[23] D. S. Khoury, B. Taccardi, L. R. Lux and et al., "Reconstruction of endocardial potentials and activation sequences from intracavitary probe measurements," *Circulation*, vol. 91, pp. 845-863, 1995.

[24] R. J. Schilling , N. S. Peters and D. W. Davies , "Simultaneous endocardial mapping in the human left ventricle using a non-contact catheter: Comparison of contact and reconstructed electrograms during sinus rhythm," *Circulation*, vol. 9, p. 887–898, 1998.

[25] C. C. Gornick, S. W. Adler, B. Pederson and et al., "Validation of a new noncontact catheter system for electroanatomic mapping of left ventricular endocardium," *Circulation*, vol. 6, pp. 829-835, 1999.

[26] R. N. Ghanem , C. Ramanathan and et al., "Noninvasive electrocardiographic imaging," *Heart Rhythm*, pp. 339-354, 2005.

[27] C. Ramanathan, R. N. Ghanem, P. Jia and et al., "Noninvasive electrocardiographic imaging for cardiac electrophysiology and arrhythmia.," *Nat Med.*, p. 422, 2004.

[28] X. Zhang, I. Ramachandra and et al., "Noninvasive three-dimensional electrocardiographic imaging of ventricular activation sequence.," *Am. J. Physiol Heart CircPhysiol*, p. 289:H2724, 2005.

[29] A. Intini, R. N. Goldstein and et al., "Electrocardiographic imaging (ECGI), a novel diagnostic modality used for mapping of focal left ventricular tachycardia in a young athlete.," *Heart Rhythm*, p. 1250, 2005.

[30] P. Jia, C. Ramanathan, R. N. Ghanem and et al., "Electrocardiographic imaging of cardiac resynchronization therapy in heart failure: Observation of variable electrophysiologic responses.," *Heart Rhythm*, p. 296, 2006.

[31] N. Sapidis and P. Besl, "Direct construction of polynomial surfaces from

dense range images through region growing.," *ACM: Transactions on Graphics,* pp. 171-200, 1995.

[32] W. J. Hedley, Finite element modelling of the left ventricle using magnetic resonance image data., The University of Auckland, New Zealand: Master's thesis, Department of Engineering Science, 1998.

[33] D. M. Budgett, Remote sensing of the epicardium, University of London: PhD thesis, Imperial Collage of Science, Technology and Medicine, 1995.

[34] L. Cheng, Non-invasive electrical imaging of the heart, The University of Auckland, New Zealand: Department of Engineering Science, School of Engineering, 2001.

[35] R. M. Gulrajani, "The Forward and Inverse Problems of Electrocardiography.," *IEEE Eng.,* pp. 84-101, 1998.

[36] D. H. Brooks, G. F. Ahmad, R. S. MacLeod and e. al., "Inverse Eectrocardiography by Simultaneous Imposition of Multiple Constraints.," *IEEE Trans. Biomed. Eng.,* vol. 46, no. 1, pp. 3-18, 1999.

[37] F. Greensite and G. Huiskamp, "An Improved Method for Estimating Epicardial Potentials from the Body Surface.," *IEEE Trans. Biomed. Eng.,* pp. 98-104, 1998.

[38] Y. Wang, P. S. Cuculich, J. Zhang and et al., "Noninvasive Electroanatomic Mapping of Human Ventricular Arrhythmias with Electrocardiographic Imaging.," *Sci Transl Med.,* p. 98ra84, 2011.

[39] P. S. Cuculich, Y. Wang, D. L. Bruce and et al., "Noninvasive Characterization of Epicardial Activation in Humans With Diverse Atrial Fibrillation Patterns," *Circulation,* pp. 1364-1372, 2010.

[40] K. Soundarapandian and M. Berarducci, "Analog Front End Design for ECG Systems Using Delta-Sigma ADCs," *Application Report,* April 2010.

[41] B. Baker, A Baker's Dozen: Real Analog Solutions for Digital Designers, Burlington: Newnes, 2005.

[42] A. Taddaei and e. al., "The European ST-T database: standard for evaluating systems for the analysis of ST-T changes in ambulatory

electrocadiography," *European Heart Journal,* vol. 13, pp. 1164-1172, 1992.

[43] M. R. Jarvis and P. P. Mitra, "Apnea patients characterized by 0.02Hz peak in the mutitaper spectrogram of electrocardiogram signals," *Computer in Cardiology,* vol. 27, pp. 769-772, 2000.

[44] A. N. S. Institute and A. f. t. a. o. M. Instrumation, "Diagnostic electrocardiographic devices," ANSI, AAMI, Arlington, 2000.

[45] Anonymous, "Cardiac Monitors, Heart Rate Meters, and Alarms," Association for the Advancement of Medical Instrumentation, Arlington, 2002.

[46] I. M. Zipes, Clinical Arrhytmology and Electrocardiography: A Comapnion to Braunwald's Heart Dsease., Philadelphia: Saunders Elsevier, 2006.

[47] B. B. Winter and J. G. Webster, "Driven-Right-Leg Circuit Design," *IEEE Transactions on Biomedical Engineering,* pp. 62-66, 1983.

[48] V. Acharya , "Improving Common-Mode Rejection Using the Right-Leg Derive Amplifier," *Application Report,* July 2011.

[49] MEDTEQ, "IEC60601 series: Defibrillator Testing," [Online]. Available: http://www.medteq.info/med/DefibTests.

[50] VISHAY, "Varistor Introduction," Sep 2013. [Online]. Available: www.vishay.com/doc?91000.

[51] C. Kitchin and L. Counts, A Designer's Guide to Instrumentation Amplifiers, Analog Devices Inc., 2006.

[52] A. Kay, "TI Precision Designs: Reference Design," *TI Precision Designs,* December 2013.

[53] ANSI/IEEE, "IEEE Standard Digital Interface for Programming Instrumentation," An American National Standard, New York, 1988.

[54] "Single Resistor Gain Programmable, Precision Instrumentation Amplifier.," [Online]. Available: http://www.linear.com/.

[55] H. W. Johnson and M. Graham, High Speed Digital Design - A handbook of Black Magic, Englewood Cliffs, New Jersey: Prentice Hall, 1993.

APPENDIX A

SCHEMATIC

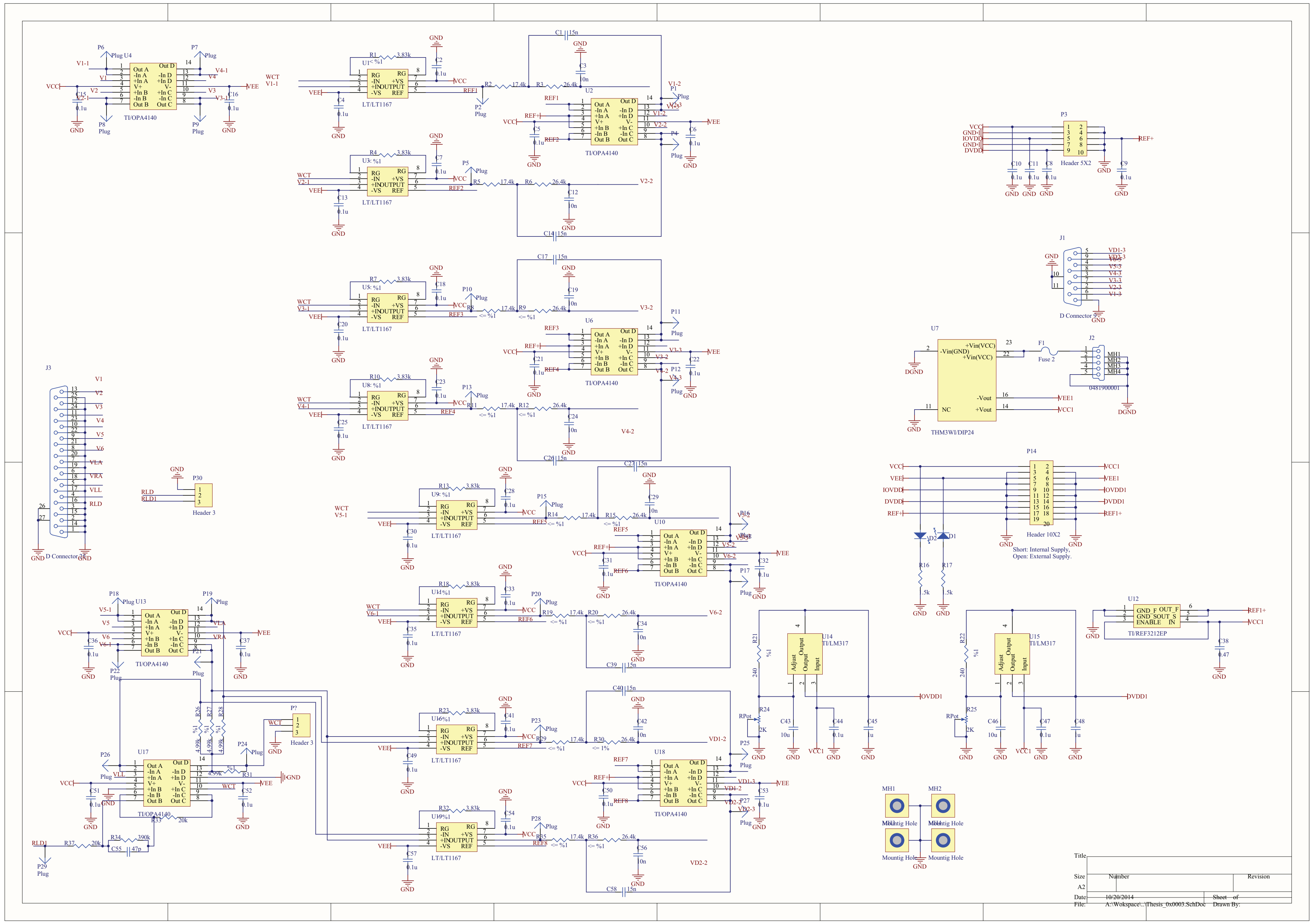
TI/OPA4140
LT/LT1167
TI/LM317
TI/REF3212EP
THM3WI/DIP24
Header 5X2
Header 10X2
Header 3
D Connector
Fuse 2
Mountig Hole
Short: Internal Supply.
Open: External Supply.
VCC
VEE
GND
DGND
WCT
REF1
OVDD1
DVDD1
Title
Size
A2
Number
Revision
Date:
10/20/2014
File:
A:\Wokspace...\Thesis_0x0003.SchDoc
Sheet of
Drawn By:

Figure A- 1: Schematics of the power unit and ECG front end

APPENDIX B

LAYOUTS

In Figures B-1 and B-2, top and bottom layers of the PCB are shown.

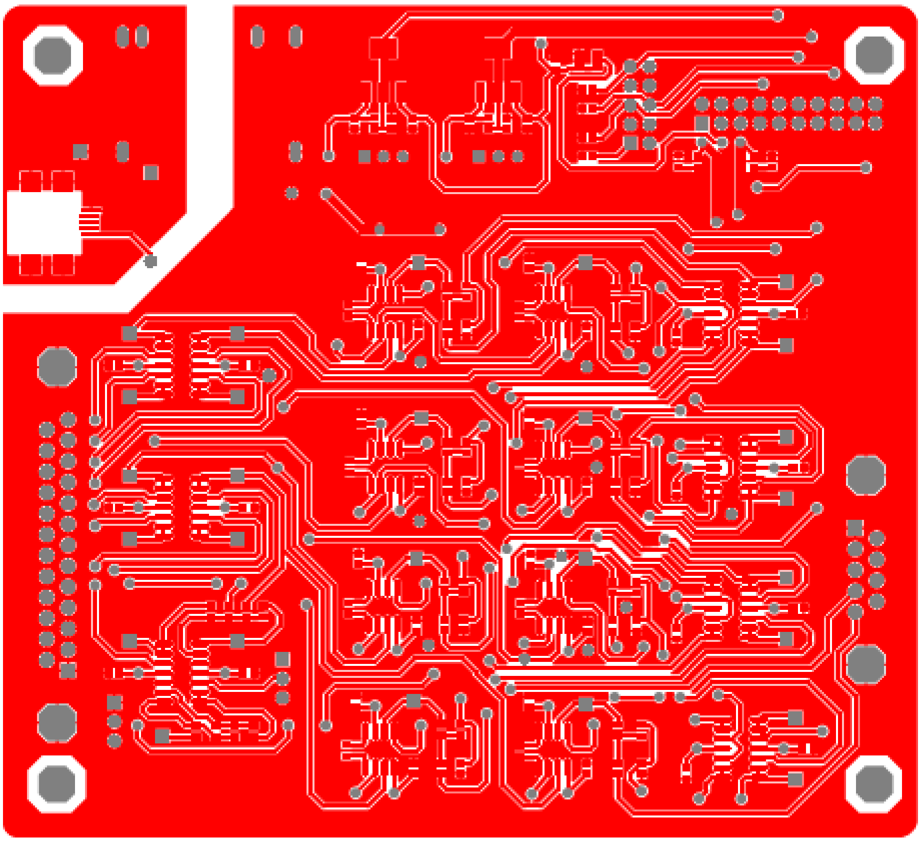

Figure B- 1: Top layer layout

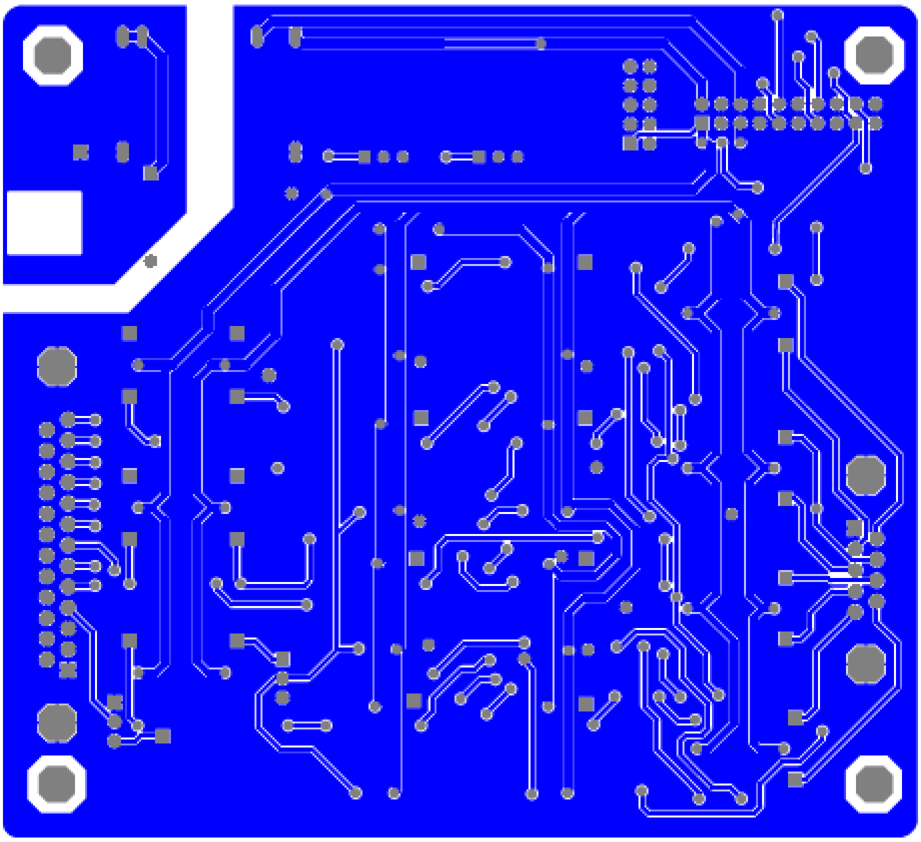

Figure B- 2: Bottom layer layout